Characterisation of the Platinum Group Minerals in the Ombuku North intrusion peripheral to the Kunene Complex: Insights into its PGE potential

By

Lorraine Masoko Mothobekhi

Student Number 783056

Research Report

Submitted in partial fulfilment of the requirements for the degree of Master of Science

In

Economic Geology

In the Faculty of Science, University of the Witwatersrand, Johannesburg, South Africa

Supervisor: Dr Ben Hayes

Co-Supervisor: Dr Lorenzo Milani

March 2024

Declaration

I, Lorraine Masoko Mothobekhi, hereby declare the following:

- This research project is entirely my own work, and I have diligently acknowledged and credited all authors whose work has been utilised in this project.
- I understand the importance of avoiding plagiarism, defined as the unauthorised utilisation of another individual's work without proper attribution, is unethical and against academic integrity.
- I affirm that the work presented for assessment in the aforementioned course is solely my original, and I have not received any unauthorised assistance except where explicitly stated otherwise.
- Throughout this project, I have adhered to the prescribed requirements for referencing and citing the thoughts and ideas of others, ensuring transparency and integrity in academic.

Signed: Lorraine Masoko Mothobekhi

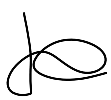

Date: 31 October 2024

Acknowledgement

I am conveying my utmost appreciation and thankfulness to my supervisors, Dr Ben Hayes, and Dr Lorenzo Milani, throughout the entire research process, their assistance, guidance, and support have been truly invaluable. Their expertise, patience, and steadfast dedication and commitment have been instrumental in shaping this work.

Special thanks go to Dr Nonkuselo Madlakana at Wits University Automated Mineralogy Laboratory for providing the necessary resources and facilities for conducting research. I am grateful to Anglo American Group Discovery Geoscience, whose academic and technical support made it possible for me to pursue my master's degree and complete this thesis.

I am extremely thankful to my ever-supportive family for their continuous support and love, encouragement, and understanding throughout my academic and career journey. Their unwavering support has been my pillar of strength. Special thanks to those who laid a foundation that made this MSc study possible. Finally, thank you to my career mentor, friends, classmates, and colleagues who have supported me along the way, offering encouragement, motivation, and a listening ear when needed.

Without the support and encouragement of the individuals and organisations mentioned above, this thesis would not have been possible. Thank you all for your contributions and support.

Through it all, it is God who made it possible!

Abstract

The Kunene AMCG (Anorthosite-Mangerite-Charnockite-Granite) Complex, located in the southern part of Angola and northern part of Namibia, is known as one of the most extensive Proterozoic anorthosite complexes worldwide, with an extent of the area ≥ 18 000 km^2, and positioned along the southwest margins of the Congo craton. The mafic-ultramafic intrusions within the vicinity of the Kunene Complex are mineralised with nickel, copper, and platinum group elements (PGEs). The area has not been extensively explored, and only minor exploration work has been conducted to search for magmatic sulphide deposits, particularly nickel deposits. The PGE potential of the mafic-ultramafic intrusions in the area and their potential mineral system has not previously been extensively studied. The available geochemical assay data of the Ombuku North intrusion in northern Namibia was sourced from African Nickel Limited (ANL) and was used in this study to assess its PGE potential and to better understand its potential mineral system. Petrographic work demonstrated Ombuku North intrusion was commonly associated with magmatic sulphides (pentlandite, pyrrhotite, chalcopyrite), formed from a Mono Sulphide Solution, and magnetite. Samples were selected for further detailed platinum group mineral (PGM) investigations on the basis of their PGE contents. Ombuku North is characterised by slightly anomalous PGE values and the available thin sections from Ombuku North with corresponding bulk rock PGE values of >80 parts per billion (ppb) were selected for the identification and characterisation of the PGMs, and for detailed petrographic analyses.

In this study, PGM mineral analyses were done using a Tescan Integrated Mineral Analyser (TIMA) which is a fully automated instrument, whereas previous mineral analyses for PGMs in Ombuku North and some of the other mafic-ultramafic intrusions in this region were collected using Scanning Electron Microscopy-Energy Dispersive Xray Spectroscopy (SEM-EDS) method, which is only partially automated. TIMA could identify the PGM in the selected samples from Ombuku North. The identified PGMs included sperrylite, michenerite, stibiopalladinite, and vincentite, all associated with serpentinised rocks. The platinum arsenides (sperrylite) are mainly hosted in magnetite and in pyrrhotite.

The palladium bismuthotellurides (michenerite and vincentite) and a platinum antimonide (stibiopalladinite) are hosted in pentlandite. The origin of these PGMs can be associated with both magmatic and hydrothermal processes. Magmatic processes are primarily responsible for the initial formation and crystallisation of silicate minerals within the mafic-ultramafic intrusions, including primary magmatic sulphide assemblage. Late hydrothermal processes are related to the alteration of these rocks, where fluids circulated through the rock leading to the formation of secondary minerals such as serpentine, talc, and the redistribution of PGE. Although PGE data are also provided also for other intrusions, this study mainly focused on Ombuku North intrusion due to the limited availability of assay data. We infer that amongst all the mineralised mafic-ultramafic intrusions related to the Kunene Complex, the most prospective for PGE anomalies are the altered ultramafic lithologies at Ombuku North.

Contents

List of Figures

List of Tables

CHAPTER 1: INTRODUCTION

The Kunene AMCG Complex (KC) stands as one of the largest Proterozoic massif-type anorthosite complexes worldwide, situated in southern Angola and northern Namibia (Ashwal and Twist, 1994). It is positioned at the southwestern edge of the Congo craton on the Angolan Shield (Bybee et al., 2019; Hayes et al., 2022; Lehmann et al., 2020; Milani et al., 2022; Rey-Moral et al., 2022), (**Fig. 1a**). It covers an extensive area exceeding 18 000 km^2 (Ashwal and Twist, 1994) and it stretches approximately 200 kilometers from northern Namibia into Angola (Menge et al., 1998). A general overview of the Kunene Complex is shown in **Fig. 1b**. The KC primarily comprises anorthosite, with mafic to ultramafic intrusions concentrated along its western margins (Maier et al., 2013; Milani et al., 2024).

These mafic-ultramafic (MUM) intrusions are mostly found at the southwestern and western periphery of the KC, forming elongated bodies (Drüppel et al., 2001), and each covering less than 10 km^2 (Maier et al., 2013). They are comprised of anorthosite, gabbro, troctolite, peridotite, and pyroxenite, and some of these MUM intrusions are mineralised with Nickel-Copper-Platinum Group Elements (Ni-Cu-PGE), with thin chromitite layers locally present (Maier et al., 2013). Kalahari sediments overlie the eastern part of the KC, increasing the potential for discovering other MUM intrusions mineralised with Ni-Cu-PGE sulphides, as well as with Iron-Titanium-Vanadium-Phosphorus (Fe-Ti-V-P) which are commonly associated with Proterozoic massif-type anorthosites (Mayer et al., 2004). Due to prolonged wars from 1975 to 2001 in Namibia and Angola, the area has not been extensively studied, although numerous exploration projects aimed at discovering magmatic sulphides, particularly nickel-rich ones, have been undertaken (Maier et al., 2013). The Nickel Copper (Ni-Cu) magmatic sulphide ore deposit of the Voisey's Bay intrusion, discovered in 1994 in Canada, is a significant example of a world-class nickel sulphide deposit associated with an AMCG Complex (Naldrett et al., 1997).

Magmatic PGE occurrences are widespread globally, but the deposits of economically viable PGE are relatively scarce. Countries like South Africa (Bushveld Complex) and Russia (Norilsk-Talnakh) contribute over 90 % of the world's PGM production. Additional economically viable deposits occur within layered mafic-ultramafic intrusions such as the Great Dyke in Zimbabwe, the Stillwater Complex in the United States of America, and the Sudbury Complex in Canada (Mudd et al., 2018).

The platinum group elements are considered globally as critical metals, because of their demand in different industries for modern technological applications and for the green economy. The need for platinum has been increasing rapidly because of the automotive industry and the need for green energy as it is used as a catalytic converter in hydrogen-powered fuel cell electric vehicles (FCEVs). This study focuses on characterising the spatial distribution of PGMs in the Ombuku North intrusion at the periphery of the KC in northern Namibia to better understand the magmatic PGE potential of the intrusion (**Fig. 1a**).

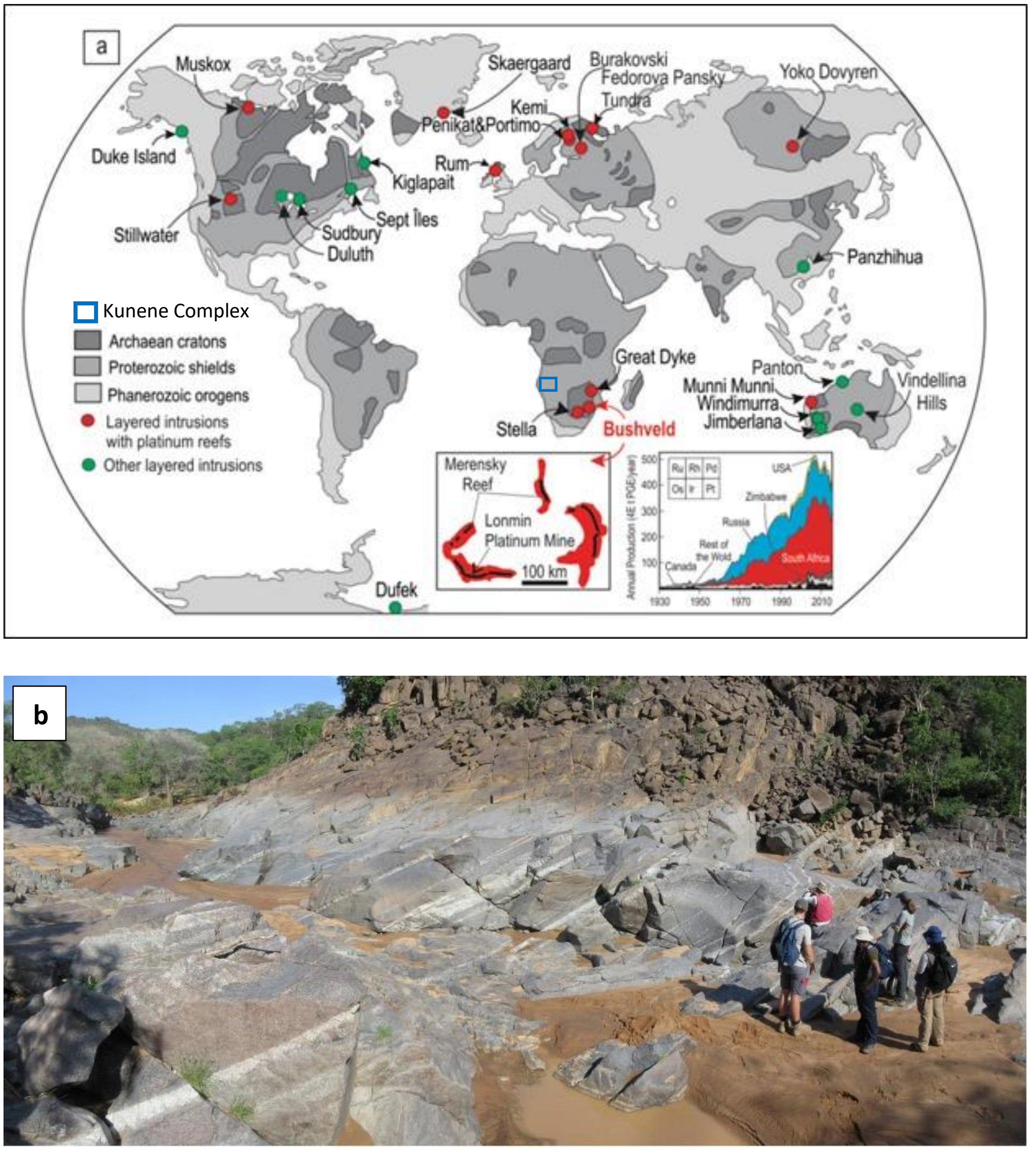

Fig. 1: (**a**) Global location of layered intrusions and different PGE deposits in the world (Burlakovs et al., 2020). The insert map illustrates the annual PGE production from the leading producing countries (Chistyakova et al., 2019), (**b**) shows the typical anorthosite outcrop of the Kunene Complex (https://cimera.co.za/kunene-complex/).

Thin sections with assays showing anomalous PGE contents were identified and used for image analysis utilising TIMA (Tescan Integrated Mineral Analyser). The aim was to determine the presence, distribution, and composition of PGMs within these rocks. Additionally, samples containing well-characterised sulphide mineralisation were targeted, given the close association of PGMs with sulphide (and oxide phases).

Identifying PGM types within the Ombuku North intrusion will provide insights into the nature and characteristics of PGE mineralisation in the area.

African Nickel Limited (ANL), Gevale Indústria Mineira Lda, and Anglo-American have been carrying out exploration projects in the area since the 1990's. The accomplished work programs included soil sampling, geophysical surveys, and drilling, followed by geochemical analyses of the drilled core. ANL obtained a comprehensive bulk rock geochemical database, consisting of about 3 500 analyses, comprising of major, trace, and PGE from various borehole samples at the periphery of the KC. **Fig. 2** shows the geology of the area in which ANL focused their exploration and the locations of the MUM intrusions discussed in this report.

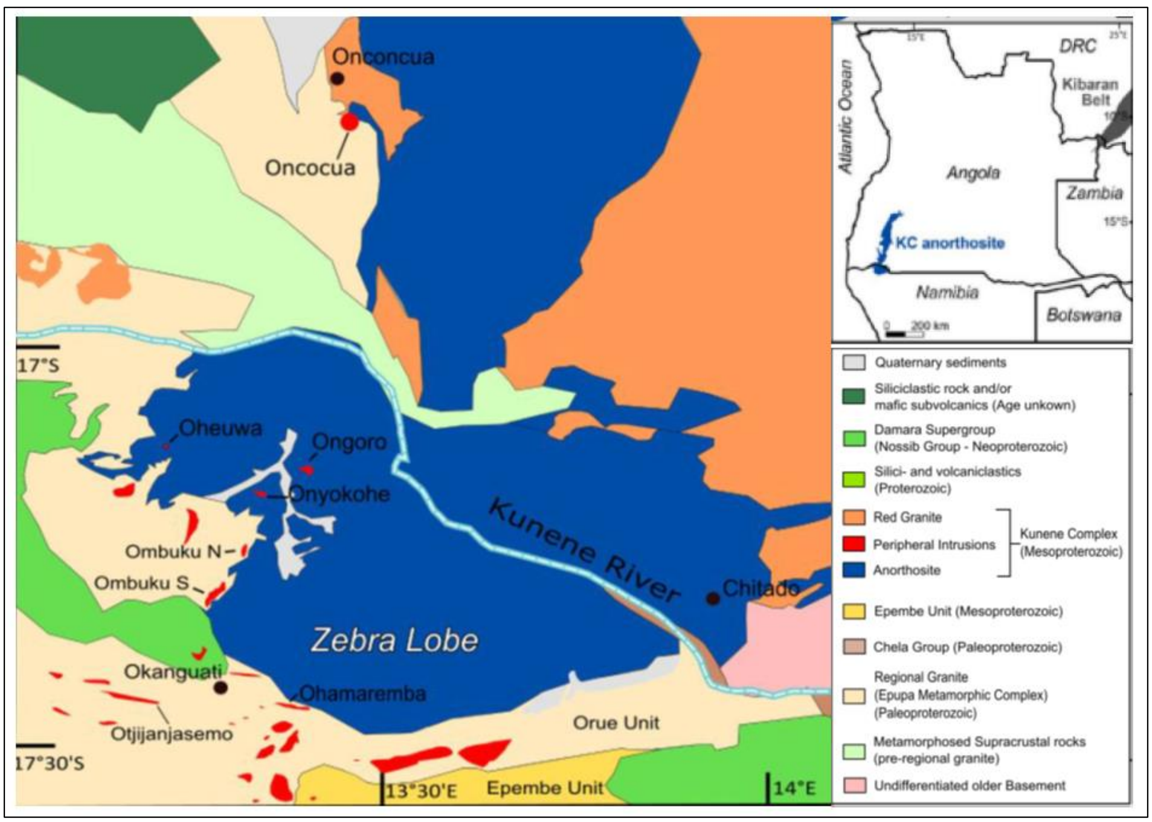

Fig. 2: Location and geology of the mafic-ultramafic intrusions peripheral to the Kunene Complex (van Zyl, 2022).

The MUM intrusions that are part of this study were analysed for PGE concentrations by fire assay, however, the Pd and Pt data are limited because of the very low concentrations of these elements in six of the MUM intrusions, with some concentrations being below the detection limit (**Table 1**).

Table 1: Summary of the total number of platinum and palladium analyses in six of the mafic-ultramafic intrusions at the margins of the Kunene Complex.

Intrusion	Total number of platinum analyses	Total number of palladium analyses
Ohamaremba	101	101
Oheuwa	244	244
Ombuku South	238	238
Ongoro	49	49
Onyokohe	139	94
Oncocua	0	6

The PGE assay data from the Ombuku North intrusion show the highest concentrations of platinum and palladium (e.g., > 500 ppb). A previous study by Ntuli (2022) was carried on these MUM intrusions, using a scanning electron microscope equipped with an energy dispersive x-ray system (SEM-EDS). The study focused on samples from the Ombuku North intrusion with PGE values >80 ppb, characterised the textural setting of the PGMs, and suggested the processes responsible for the mineralisation.

CHAPTER 2: REGIONAL GEOLOGY AND OVERVIEW OF THE MAFIC-ULTRAMAFIC INTRUSIONS AT THE MARGIN OF THE KUNENE AMCG COMPLEX

2.1. Regional Geology

The KC extends from northwestern Namibia into southwestern Angola (**Fig. 3**). It intruded early Proterozoic to late Archean rocks (granite basement rocks) and supracrustal rocks of Paleoproterozoic to Mesoproterozoic in the Epupa Complex (Lehmann et al., 2020). The complex is also largely overlain by Kalahari sediments (Rey-Moral et al., 2022). It consists predominantly of anorthosite and is primarily located near the southern boundary of the Congo Craton and was emplaced during the Mesoproterozoic era. (~ 1.4 Ga), and the timing of the KC emplacement was generally concurrent with the event of Kibaran Orogeny (Mayer et al., 2004; Gleißner et al., 2010; Bybee et al., 2019; Lehmann et al., 2020; Rey-Moral et al., 2022). In Angola, the KC intruded the southern boundary of the Congo Craton (Menge et al., 1998). The anorthosite intruded the 1915 to 2149 Ma metamorphosed rocks and supracrustal volcanic sedimentary sequences of the Chivanda Group, and granitoids of Paleoproterozoic, associated with the Eburnean Orogeny (Jelsma et al., 2018)**.** The tectonic setting of the Kunene Complex AMCG Complex is controversial.

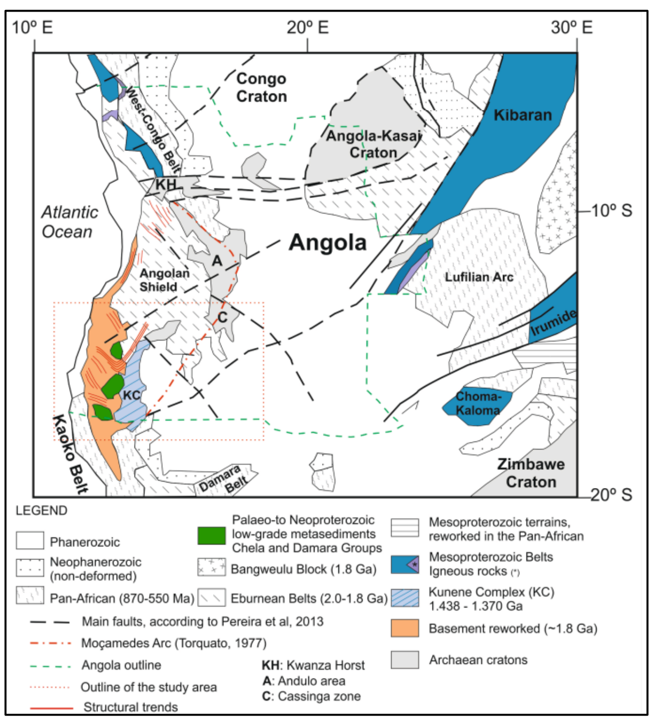

Fig. 3: A geological map illustrating geological units surrounding the Kunene Complex and associated orogenic belts as well as adjacent cratons (from Rey-Moral et al., 2022).

The Namibian section of the KC covers an area of about 4000 km^2 and is characterised by the occurrence of interlayered rocks forming the Zebra Lobe (Maier et al., 2013). The Zebra Lobe is comprised of alternating layers trending in an east-west direction (**Fig. 4**). These layers consist of highly altered leuconorite and of pale-coloured white anorthosite intruded by slightly altered anorthosite known as "dark and old anorthosite," which includes leucogabbronorite and leucotroctolite (Lehmann et al., 2020).

There are two distinct anorthosite suites in the Zebra Lobe (Gleißner et al., 2010; Gleißner et al., 2011). The older suite is characterised by a whitish appearance and is predominantly composed of leuconorite, with leucogabbronorite also present. In contrast, the younger suite appears darker and mainly consists of leucotroctolite (Gleißner et al., 2011). The Namibian part of the KC intruded the Paleo-Mesoproterozoic supracrustal rocks of the Epupa Complex (Maier et al., 2013). The Epupa Complex broadly includes para- and orthogneiss rocks, metasedimentary rock, and volcanic rocks belonging to the Orue Group (1334 Ma). Within the Orue Group, there is a predominance of migmatitic megagranitoids that intruded into a volcano-sedimentary succession (Gleißner et al., 2011). Following this intrusion, mafic dykes penetrated both units and underwent subsequent metamorphism to form amphibolites and granulites (Brandt, 2003). The volcano-sedimentary unit primarily comprises of migmatitic metagreywackes intercalated with mafic metavolcanic rocks along with detrital sedimentary rocks such as metaquartzites and meta-arkoses (Gleißner et al., 2010). Meanwhile, the Epempe unit is predominantly composed of alternating felsic and mafic rocks (Gleißner et al., 2011).

The horizontal and undeformed Chela sedimentary sequence, dated at approximately 1800 Ma (McCourt et al., 2013) is underlain by the granitoids, comprising of granites, syenites, and syenodiorites (commonly known as "Red granite"). This sedimentary sequence forms the Humpata Plateau located in the western part of the KC (Gleißner et al., 2010; Lehmann et al., 2020). Additionally, the KC contains MUM intrusions primarily situated along its western and southwestern boundaries (Ashwal and Twist, 1994; Drüppel et al., 2007; Rey-Moral et al., 2022). In Angola, the KC is characterised by north-south elongated bodies of anorthosite, separated by areas of coeval granitoids known as the "Red Granite Suite" (Lehmann et al., 2020). Additionally, there are MUM intrusions and small oxide-rich diorite mafic intrusions near the southern boundary of the KC (Gleißner et al., 2010; Gleißner et al., 2011).

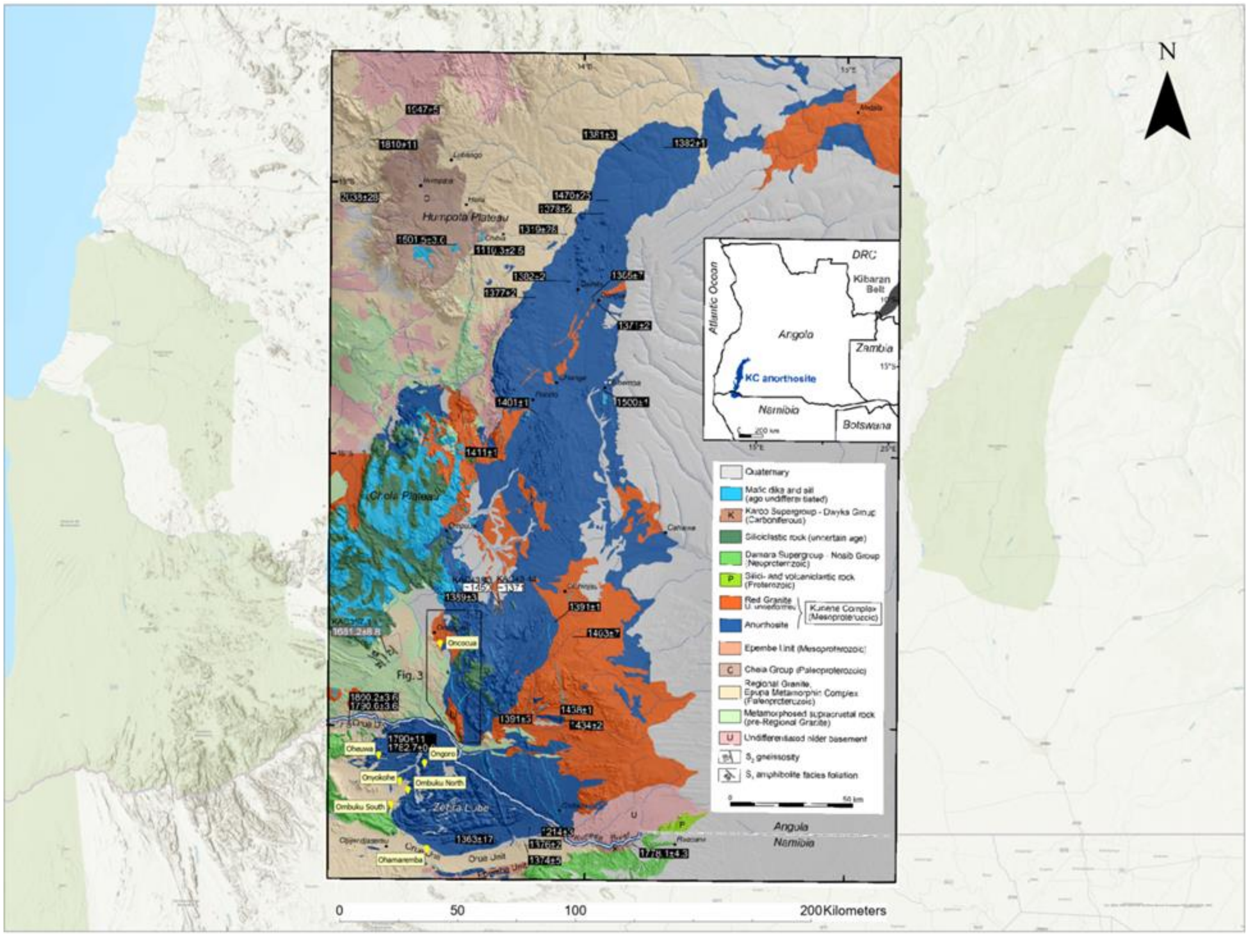

Fig. 4: The geological map illustrates the Mesoproterozoic Kunene Complex along with adjacent geological units in southwestern Angola and northwestern Namibia. It also highlights related geological structures, volcanic rocks and the location of the intrusions discussed in this report. Geochronological data are provided, with argon dating ages displayed in grey boxes and U–Pb ages in white boxes and the black boxes show published crystallisation ages. Additionally, there is an inset map illustrating the location and size of the KC in the south Angola and north of Namibia (adapted from Lehmann et al., 2020).

2.2. Kunene Complex mafic-ultramafic intrusions

The study focuses on Ombuku North, and several other mafic-ultramafic intrusions peripheral to the KC are also discussed (e.g., Oncocua, Ombuku South, Ohamaremba, Oheuwa, Onyokohe and Ongoro). A large geochemical dataset was generated by African Nickel Limited and Anglo American. Significant datasets generated include regional stream geochemistry data, soil sampling, gossan mapping, geophysical surveys, drilling, and borehole geochemical data (Van der Mescht, 2023).

2.2.1. Oncocua

Oncocua is located on the western boundary of the KC in the southern part of Angola (Smuts, 1998). It is located approximately 30 km SW of Oncocua and approximately 55 km north of the Zebra Lobe (**Fig. 5**).

Fig. 5: The geographical location of the Oncocua intrusion.

The intrusion appears as a NW-SE elongated body as shown on the geological map in **Fig. 6**. The intrusion is primarily hosted by massive anorthosite. The red line trending northwest-southeast indicates an electromagnetic anomaly detected by the Dighem conductivity survey conducted in 1998 over the Oncocua gossans (Selfe, 2003).

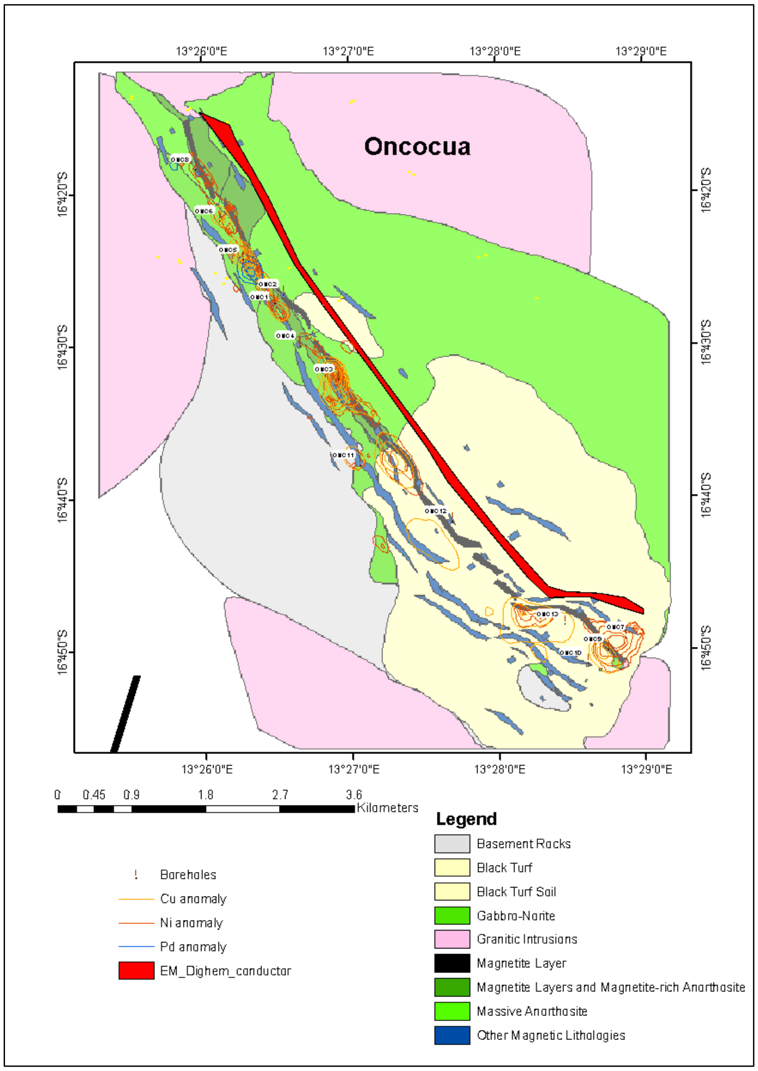

Fig. 6: A geological map of the Oncocua intrusion with the location of the boreholes and geochemical anomalies (contour-like lines) with Dighem conductor lying 450 m to the east of the intrusion. The Dighem represents a shallow (40-50 m deep) conductive body, perhaps sulphides rich (Selfe,2003).

Exploration by Anglo American Group Discovery and Geosciences (previously called Anglo American Prospecting Services Pty Ltd) included follow up work over the Oncocua intrusion, obtaining grid soil sampling, rock sampling, and geophysics surveys, i.e., ground magnetic and electromagnetic over the gossans (Identified during 1990's reconnaissance exploration work) to determine target areas for drilling (Smuts 1998). Additional samples were collected from the gossan during this exploration program and analysed for copper, nickel, cobalt, gold, and palladium. Areas of mineralisation were identified from the geophysical and geochemical work. Subsequently, a total of thirteen boreholes were drilled, and geochemical analyses were completed for borehole ONC01. Based on the geophysical, sampling and geochemical results, the Oncocua intrusion was identified as a target of potential for discovery of a Ni-Cu-PGE deposit (Smuts, 1998).

2.2.2. Ombuku North and South

Ombuku North and Ombuku South intrusions are situated at the western margin of the Zebra Lobe in Namibia and are approximately 10 km apart. The location of the intrusions and boreholes drilled are shown in **Fig. 7a-b.**

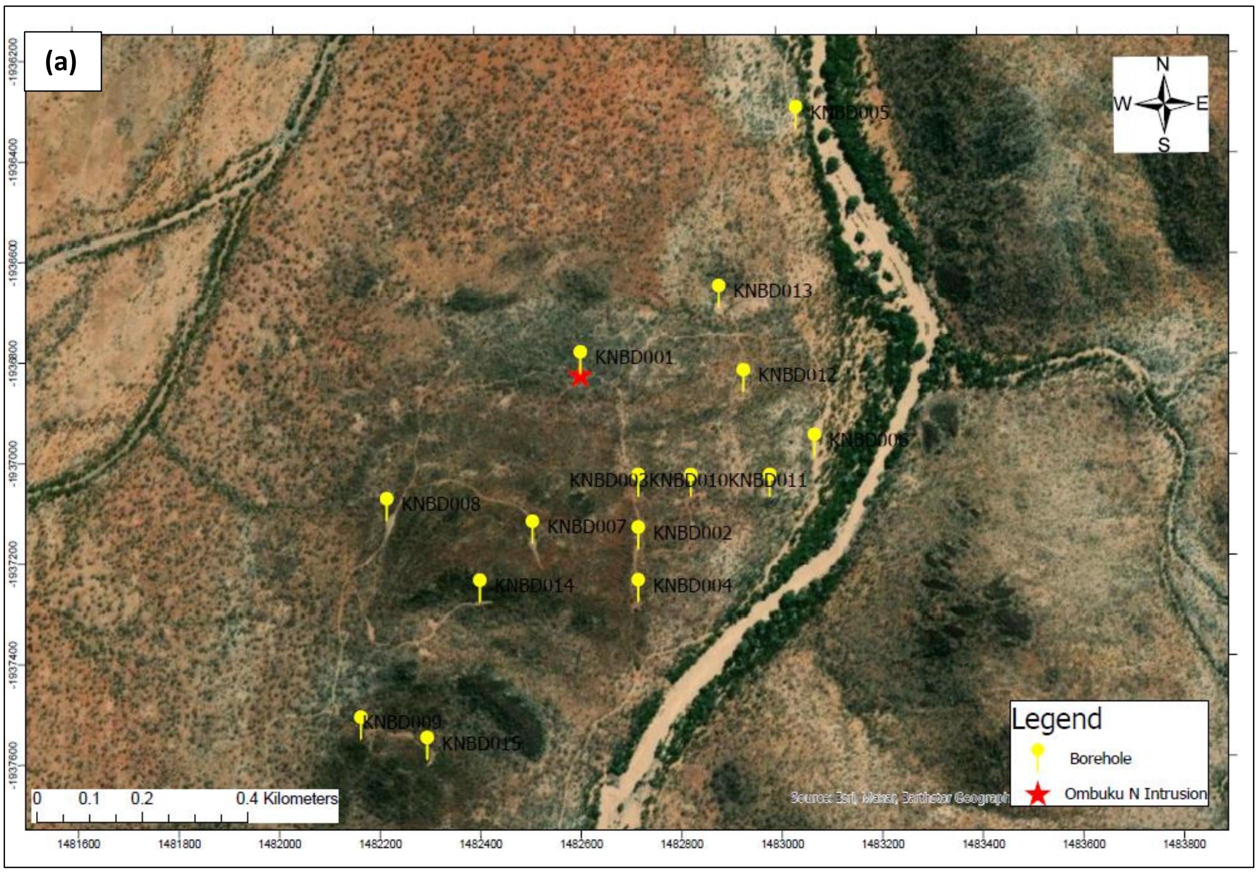

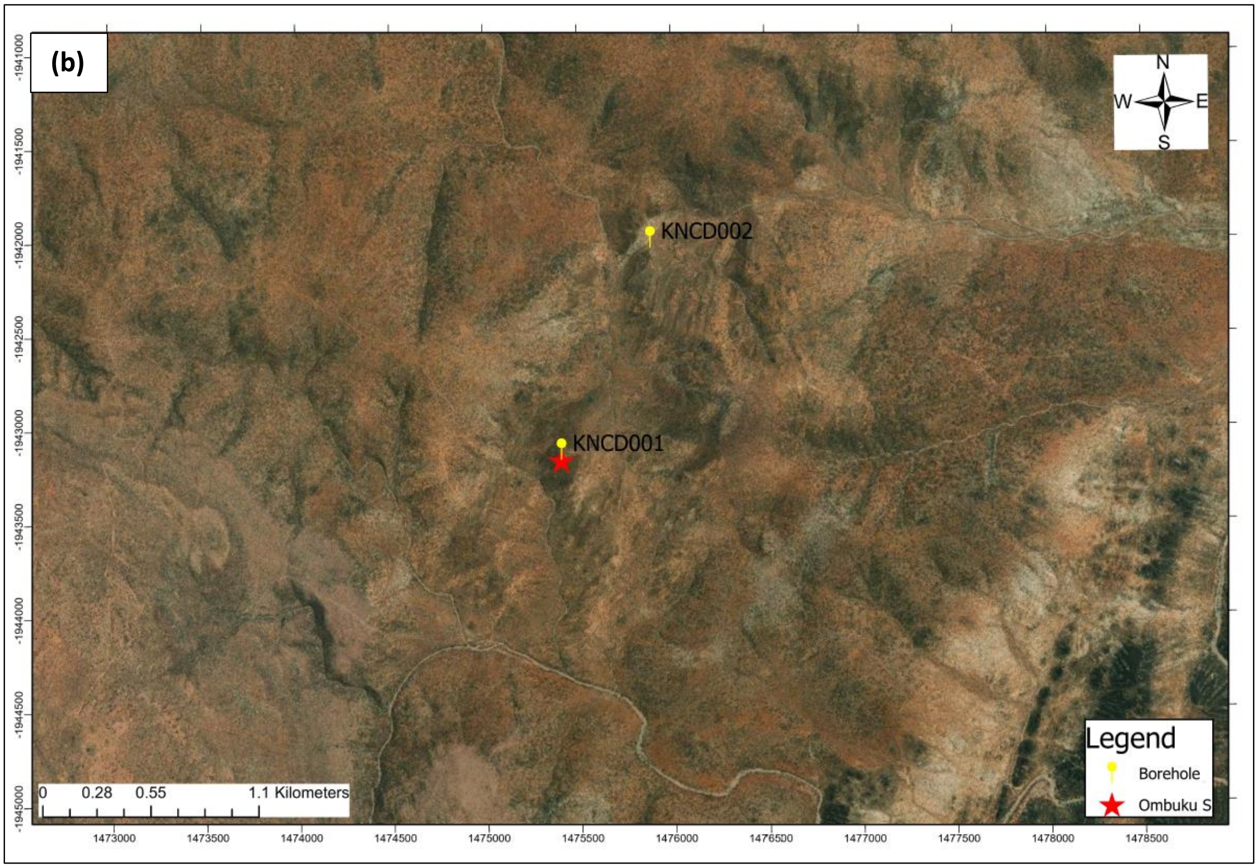

Fig. 7: The geographical location of the Ombuku North (**a**) and Ombuku South (**b**) intrusions and boreholes.

The Ombuku intrusions are mainly composed of mafic-ultramafic rocks. They are relatively small bodies with Ombuku North and Ombuku South covering an area of approximately 0.88 km^2 and 28 km^2 respectively (Maier et al., 2013). Ombuku North consists predominantly of altered ultramafic rocks and these are mainly serpentinite (altered dunite), harzburgite orthopyroxenite, and minor mafic rocks such as norite websterite, gabbronorite, and olivine-norite (Maier et al., 2013). Some mafic-ultramafic rocks occur as interlayers within the gneissic host rocks. (Maier et al., 2013). The eastern portion of the intrusion is in contact with anorthosite and leucotroctolite, while the western portion is in contact with country rocks of felsic and mafic orthogneiss of the Epupa Complex (Maier et al., 2013). Ombuku South ultramafic rocks are found mainly in the western portion of the intrusion, and these are predominantly dunite, harzburgite, and orthopyroxenite with chromitite layers (Maier et al., 2013). The intrusion is hosted by amphibolites and granites of the Epupa Complex (Maier et al., 2013).

Numerous boreholes were drilled into the Ombuku intrusions by ANL in 2008 and some boreholes were drilled by Anglo American, between 2012 and 2013. A total of fifteen boreholes (KNBD001, KNBD002, KNBD003, KNBD004, KNBD005, KNBD006, KNBD007, KNBD008, KNBD009, KNBD010, KNBD011, KNBD012, KNBD013, KNBD014 and KNBD015) were drilled into Ombuku North and two boreholes (KNCD001 and KNCD002) were drilled into Ombuku South. The drillcore samples underwent whole-rock geochemical analyses (major and trace elements, including PGE).

2.2.3. Ohamaremba

Ohamaremba intrusion is located approximately 1 to 2 km to the south of the Zebra Lobe, (Maier et al., 2013) and was drilled by ANL (**Fig. 8**).

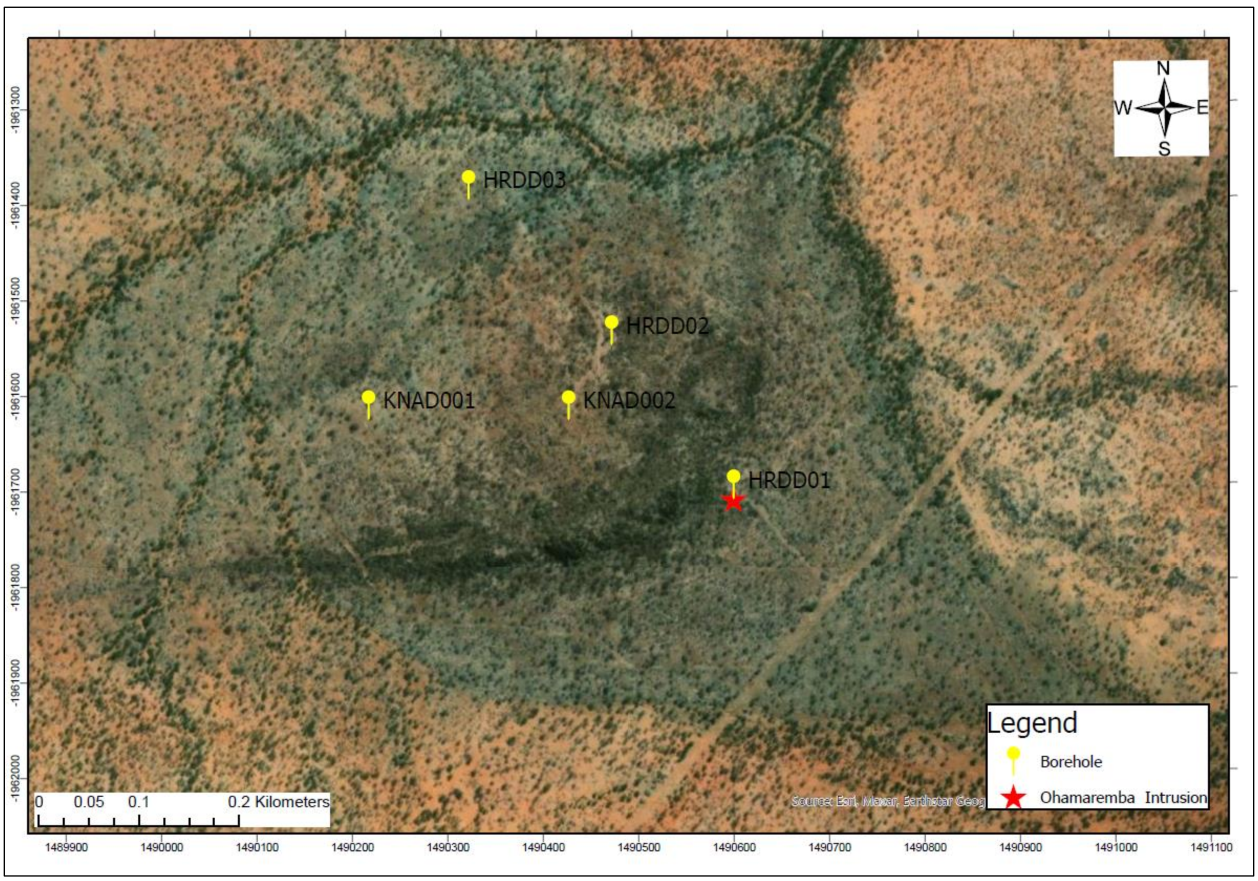

Fig. 8: The geographical location of the Ohamaremba intrusion and boreholes.

The surface geology of Ohamaremba predominantly comprises foliated leucotroctolite, with minor anorthosite and olivine gabbronorite (**Fig. 9**), (Maier et al., 2013).

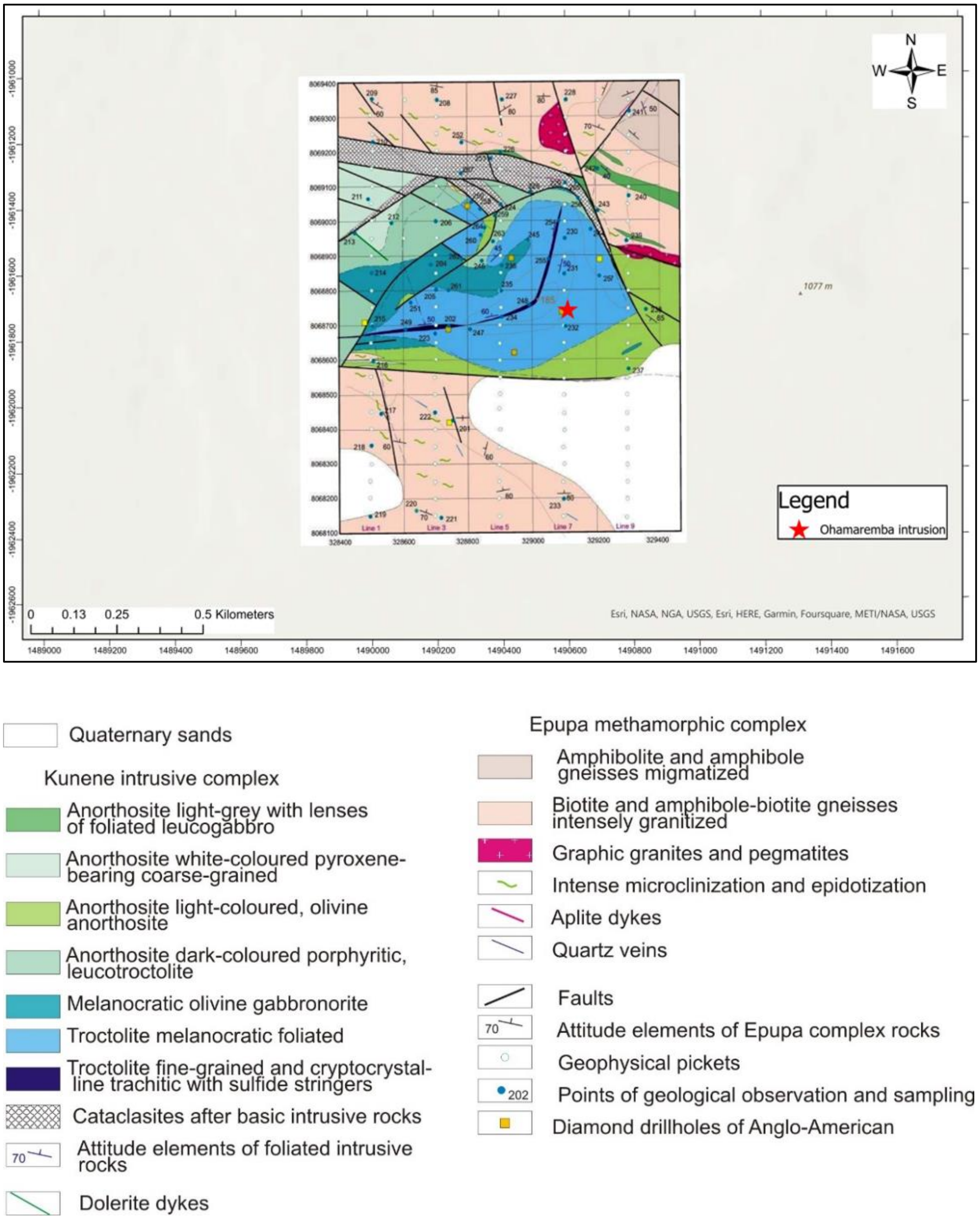

Fig. 9: A geological map of the Ohamaremba intrusion (Naumov, 2010).

A total of five boreholes were drilled into Ohamaremba, three boreholes (HRDD1, HRDD2, and HRDD3) drilled by ANL in 2000 intersected disseminated nickel sulphides (Maier et al., 2013). Further drilling in 2008 (boreholes KNAD001 and KNAD002) intersected a > 100 m thick zone of low-grade mineralisation containing < 0.2% of nickel (Maier et al., 2013), (**Fig. 10**).

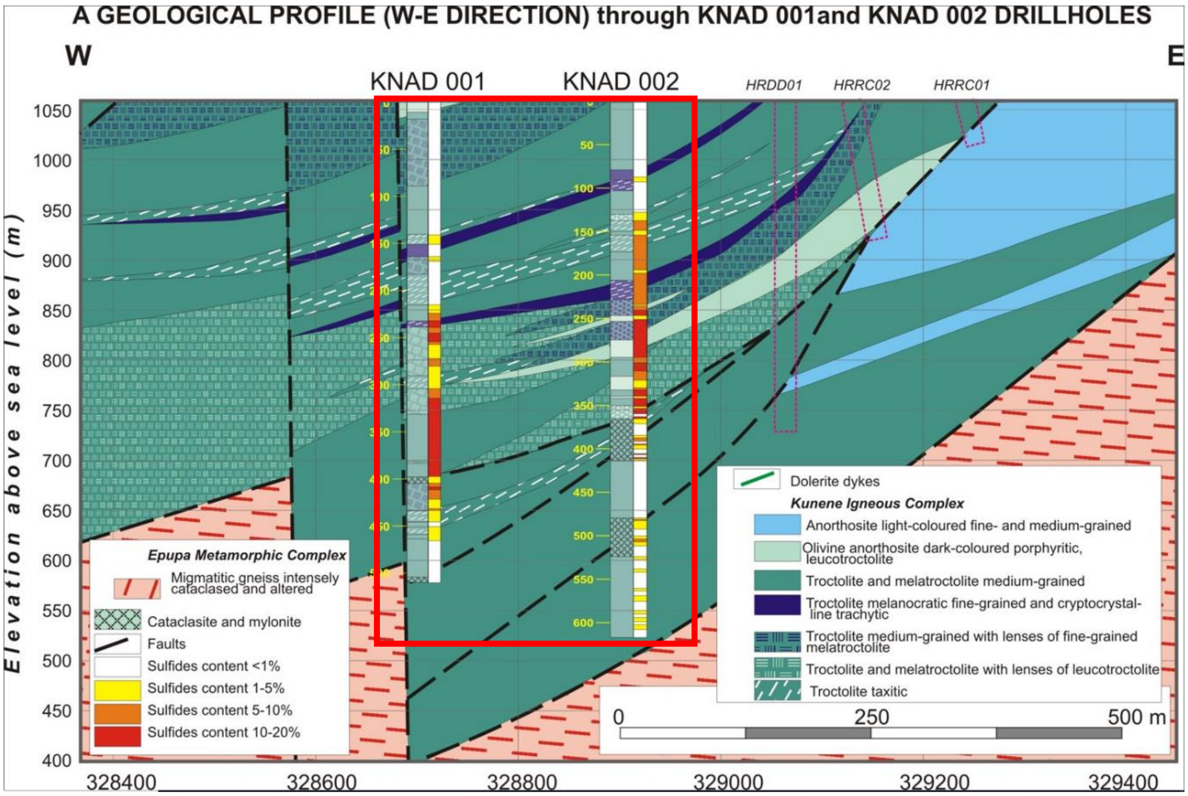

Fig. 10: A geological cross section of Ohamaremba and boreholes KNAD001 and KNAD002 showing zones of sulphide mineralisation (Naumov, 2010). The geochemical analyses from the drillcores also included PGE (platinum and palladium), however the concentrations are very low (Pd ≤10 ppb and Pt ≤ 5ppb).

2.2.4. Oheuwa

Oheuwa intrusion is located on the northwestern side of the Zebra Lobe and is comprised of dark leuco-troctolite (Maier et al., 2013). A total of four boreholes (KNV002, KNV003, KNV004 and KNV005) were drilled into this intrusion in 2013 (**Fig. 11**). The drill cores were analysed for PGEs and the concentrations are very low (Pd ≤ 8 ppb and Pt ≤ 29 ppb).

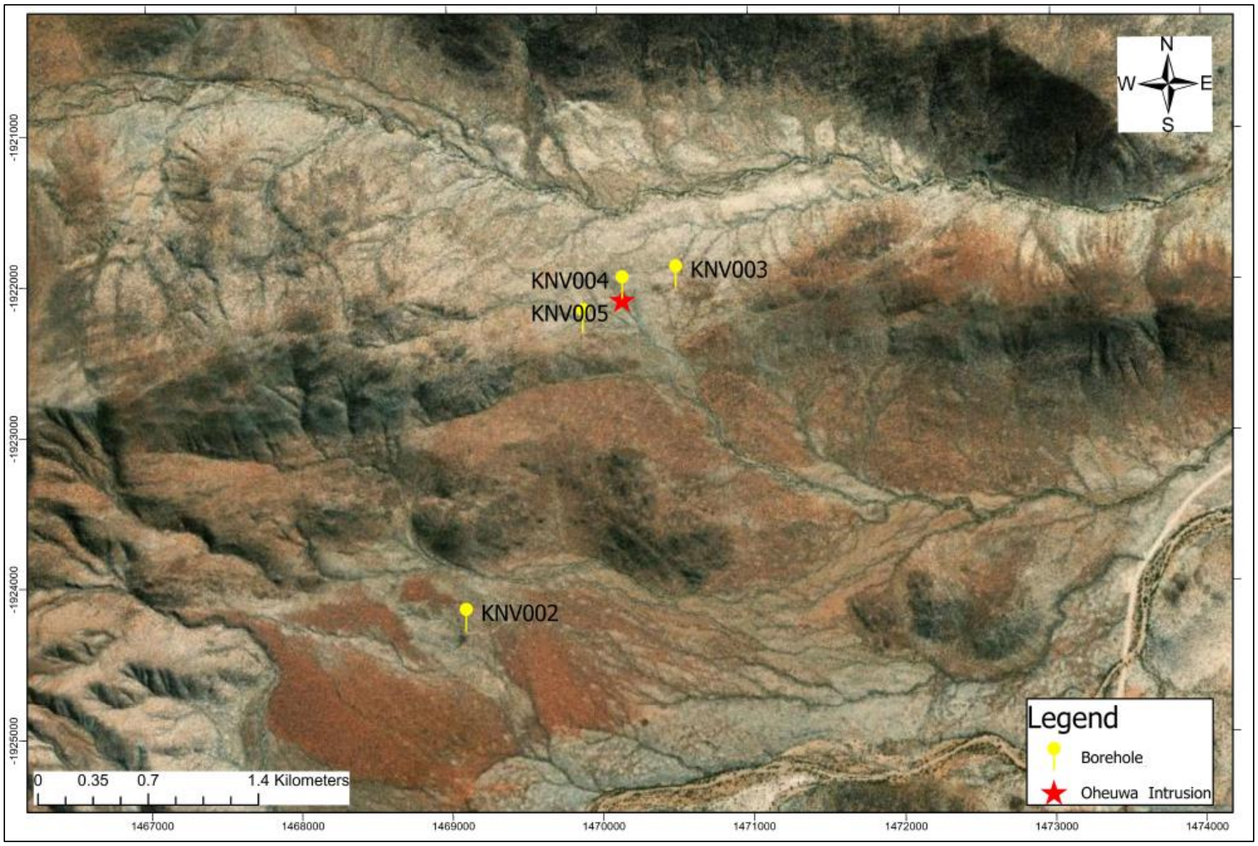

Fig. 11: The geographical location of the Oheuwa intrusion and boreholes.

2.2.5. Onyokohe

Onyokohe intrusion is located approximately 6.2 km away from the northwestern side of the Zebra Lobe (**Fig. 12**). The intrusion comprises white anorthosite and dark-leucotroctolite and anorthosite (Maier et al., 2013). A total of four boreholes were drilled into the intrusion (boreholes KNDD001, KNV001, KNV006, KNV007). The PGE values are very low, but a few analyses revealed the presence of anomalies with Pt concentrations of 104 ppb in borehole KNV007 and Pd concentrations of 710 ppb in borehole KNDD001.

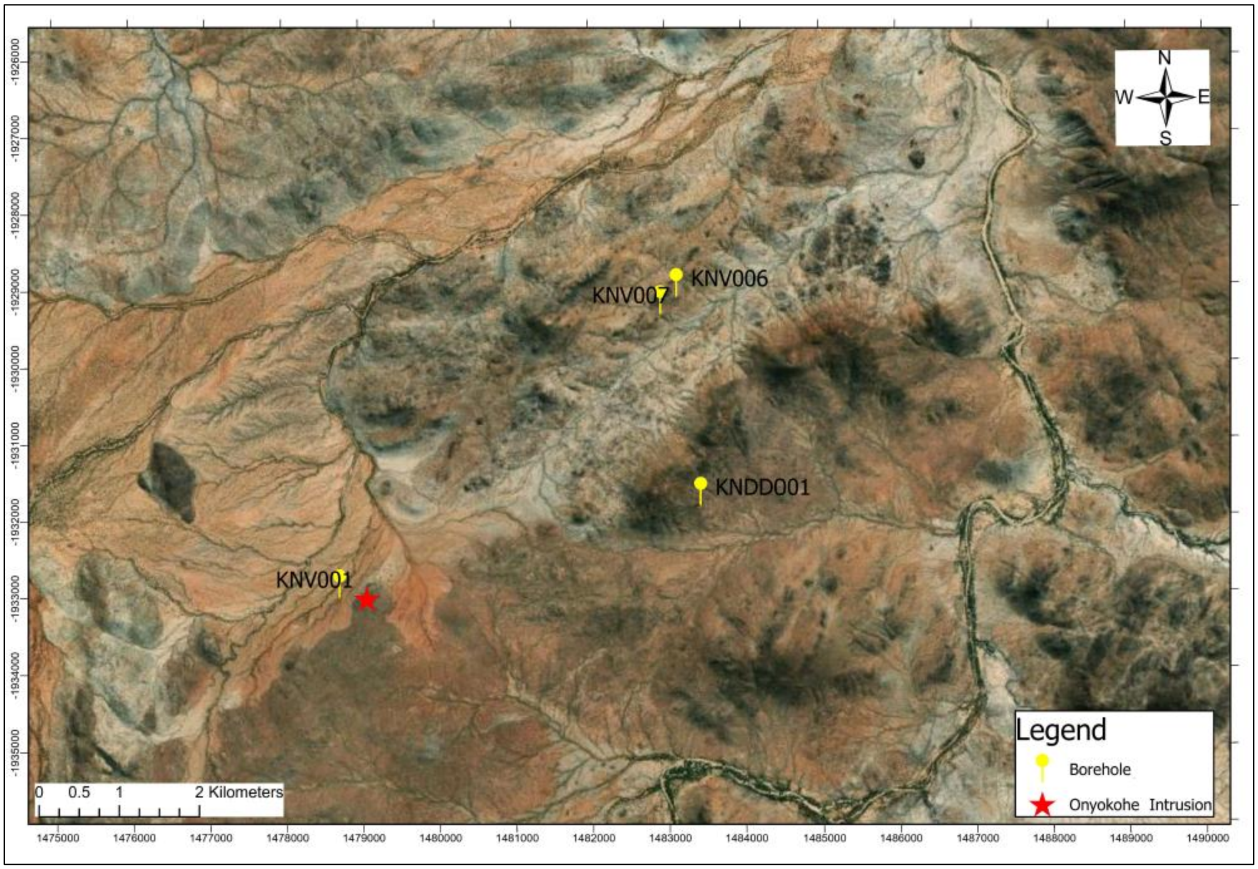

Fig. 12: The geographical location of the Onyokohe intrusion and boreholes.

2.2.6. Ongoro

Ongoro intrusion is located ~ 9.5 km north of the Zebra Lobe (**Fig. 13**). Two boreholes were drilled into the intrusion (boreholes KNV008 and KNV009), and it largely consists of anorthositic lithologies and dark leucotroctolite (Maier et al., 2013).

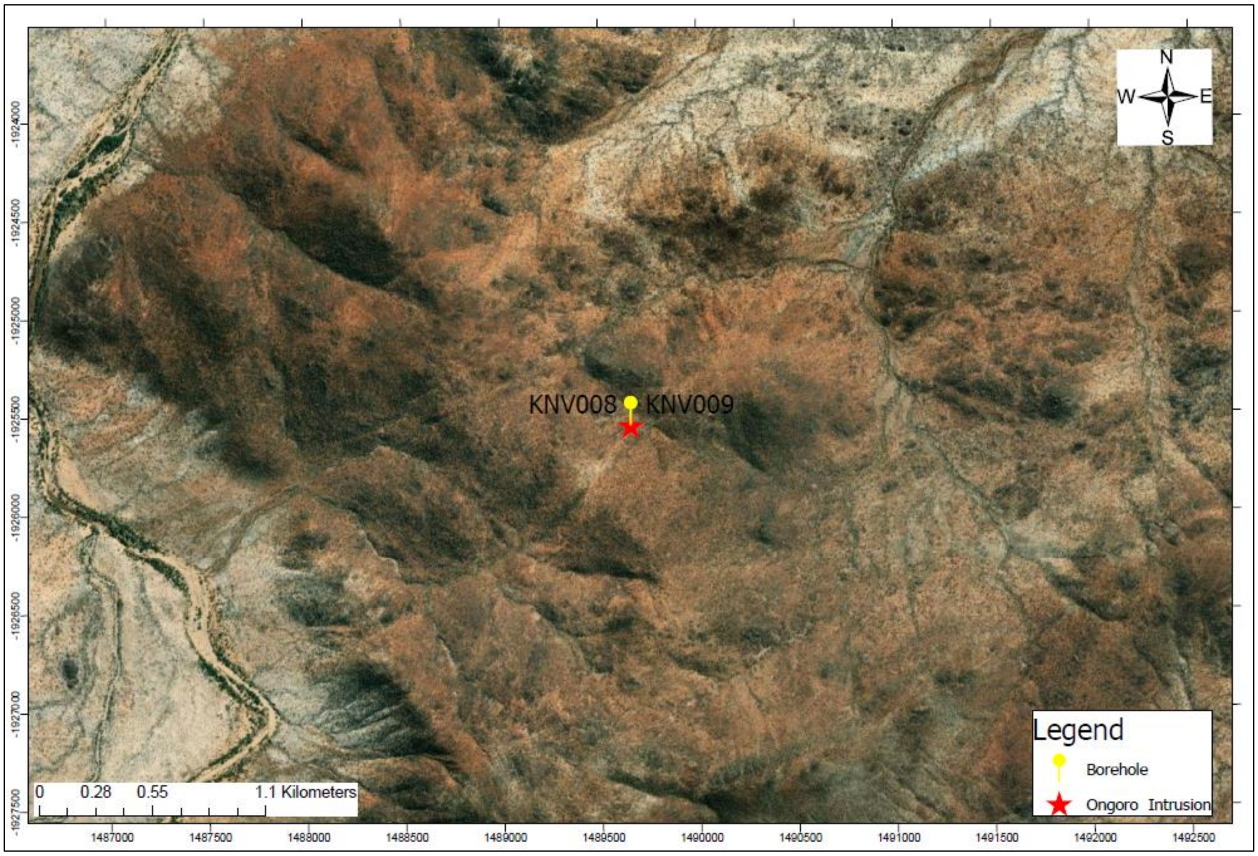

Fig. 13: The geographical location of the Onyokohe intrusion and boreholes.

2.3 The genesis of Ni-Cu-PGE magmatic sulphide deposits

Magmatic Ni-Cu-PGE sulphide deposits are formed when the magma intrudes the crust, fractionates, and subsequently becomes saturated in sulphur. This process, result in the segregation of immiscible sulphide liquids from the silicate magma (Holwell and Macdonald, 2010). Magmatic sulphide deposits can be categorised into two widely recognised types, one containing high levels of Ni and Cu along with PGE-Au as by-products, and those deposits enriched in PGE (± Au) with Ni and Cu as by-products (Maier et al., 2005). PGE-enriched reefs are characterised by stratiform horizons with 1–2 % of sulphide minerals in silicate cumulates (for example, the Bushveld Complex and Stillwater Complex) whereas small mafic-ultramafic intrusions that occur as magma conduits (for example, Voisey's Bay and Noril'sk-Talnakh) are characterised by rocks containing 20 % or more sulphides enriched in Ni-Cu (Barnes et al., 2018).

Ni-Cu-PGE have high partition coefficients for iron or sulphur-rich minerals, and they behave either as chalcophile or siderophile (Barnes and Ripley, 2016). The accumulated immiscible sulphide liquid removes the chalcophile elements present in the silicate magma (Barnes et al., 2018). These elements (Ni-Cu-PGE, Au and Ag) in the sulphide liquid co-exist with tellurium, arsenic, bismuth, antimony, and tin (Holwell and Macdonald, 2010).

The model for the processes that control the distribution of PGEs is illustrated in **Fig. 14**. Following the segregation of the sulphide liquid from the silicate magma, the immiscible sulphides will initially crystallise forming a monosulphide solid solution (MSS) at about 1000 °C, which is depleted in Iridium Platinum Group Minerals (IPGEs). The residual Cu-rich liquid crystallises to form an intermediate solid solution (ISS) at about 900 °C (Barnes and Maier, 1999; Holwell and Macdonald, 2010). As the temperature continues to decrease, at <600 °C, the MSS crystallises forming sulphides, including pyrrhotite (FeS) and pentlandite $(Fe, Ni)_9S_8$), while chalcopyrite ($CuFeS_2$) fractionates from the ISS. The IPGEs iridium (Ir), osmium (Os), and ruthenium (Ru) form at high temperatures (Barnes and Maier, 2002). The Pt and Pd with electrum (Au and Ag) are incompatible in ISS and may form their own semi-metal alloys (Peregoedova, 1998), with other trace elements such as antinomy, bismuth, tellurium, arsenic as a separate melt phase (Holwell and McDonald, 2010). PGMs form discrete minerals around the margins of sulphides or possibly away from the sulphides, and factors such as sulphide-PGE ratio and the distribution of the trace element or semi metals (Sb, Bi, Te, As) in the magma influence where the PGMs are going to occur in the final crystallised rock (Helmy et al., 2007).

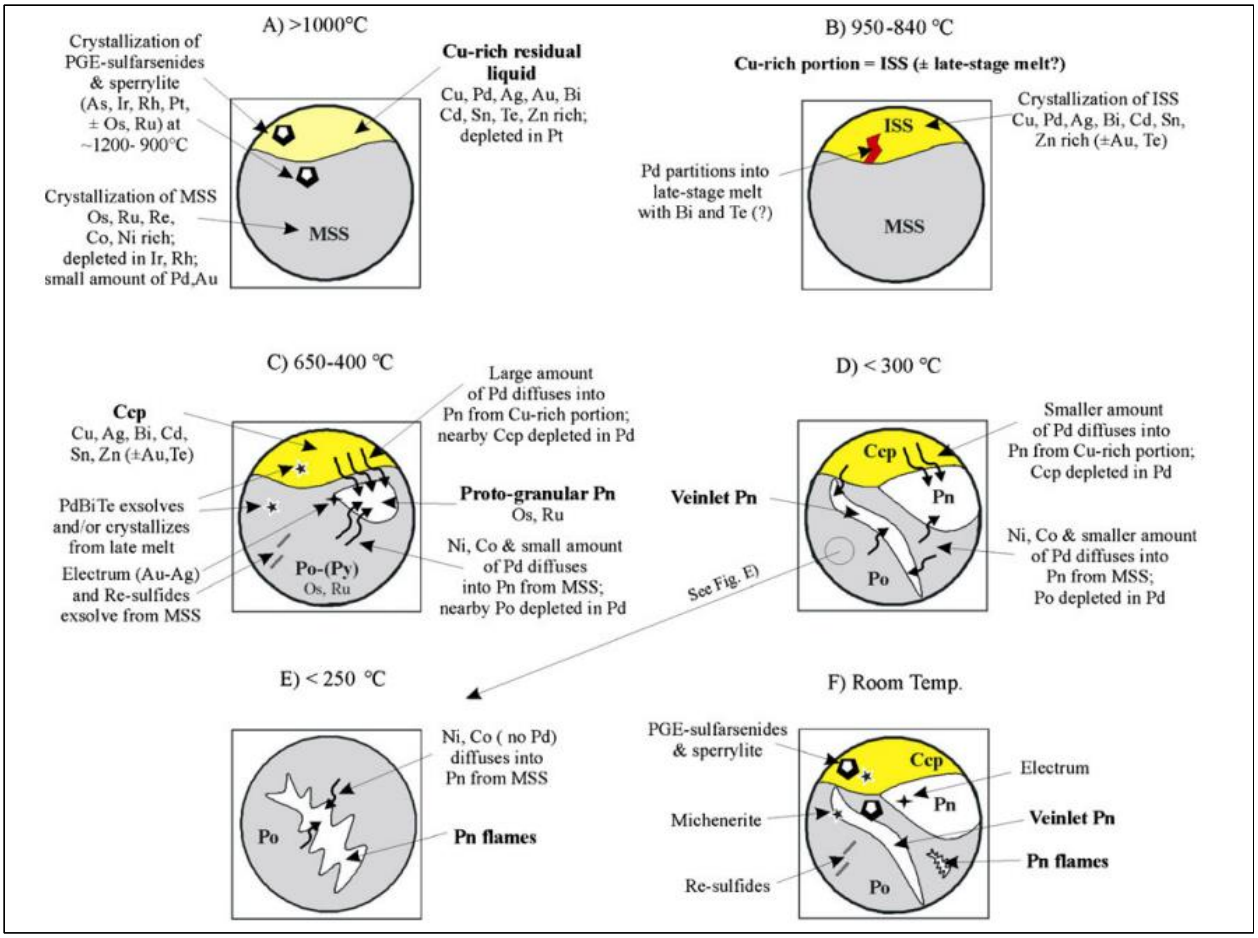

Fig. 14: A summary of the high to low temperature evolution of an immiscible sulphide liquid that segregates from a silicate magma (Dare et al., 2010). This evolution controls the distribution of Ni, Fe, Cu and PGE (**a**, **b**). Partitioning of PGE and chalcophile elements between MSS and residual liquid at temperatures < 1000 °C (**c**-**e**). Exsolution of base metal sulphides from MSS and ISS and the complete BMS and PGM assemblage at room temperature with PGEs mostly concentrated in discrete late-stage minerals such as sulfararsenides (**f**).

2.4 Distribution and composition of platinum group minerals in magmatic sulphide deposits

PGEs are found in various geological settings, including alluvial deposits, magmatic layered intrusions, and magmatic nickel sulphide deposits (O'Driscoll and González-Jiménez, 2016). Globally, around 99 % of PGE resources are hosted in magmatic sulphides (Bai et al., 2023), because of the extremely high partition coefficients of PGE for sulphide liquids present in silicate magmas (Mungall, 2005). Economically, these magmatic ore deposits are classified into high sulphur magmatic deposits, such as Noril'sk-Talnakh, and low sulphur magmatic deposits, like the Bushveld Complex (Cabri, 1994; Green and Peck, 2005). Low sulphur magmatic deposits are associated with intrusions from the Archean or Paleoproterozoic ages, while high sulphur magmatic deposits are typically linked to continental flood basalt volcanism (Green and Peck, 2005).

The mineralisation of PGEs is primarily associated with mafic-ultramafic intrusions, where PGEs occur as discrete PGMs often associated with sulphides (Junge et al., 2015; Barnes and Ripley, 2016). In magmatic sulphide deposits, PGEs are found within the structure of base metal sulphide minerals (Mansur et al., 2020). These base metal sulphide minerals, including pyrrhotite, pentlandite, chalcopyrite, and cubanite, are the most common hosts of PGEs as platinum group minerals (O'Driscoll and González-Jiménez, 2016). The PGEs are group VII transition metals on the periodic table. These metals can exist in solid solution and can also combine with other siderophiles (e.g., iron) and TABS (tellurium, arsenic, bismuth, antimony, and tin) as essential elements (Cabri, 1981). The role of TABS in forming PGE-dominated complexes, has not been fully investigated (Mansur et al., 2020). However, palladium, platinum, and the TABS are incompatible in MSS and ISS and are concentrated in fractionated sulphide liquid during crystal fractionation and they are often found in sulphides (Rao and Reddi, 2000).

Within the Earth's crust, PGEs occur in a variety of compositions as discrete PGMs and they can appear in their native form or be associated with one or more other PGMs, as well as alloys with elements like gold, iron, or copper (Cabri, 1994). The most common platinum and palladium minerals and their compositions are listed in the **Table 2** below:

Table 2: Most common platinum and palladium minerals (Cabri, 1994).

Platinum Minerals	**Formula**	**Palladium Minerals**	**Formula**
Braggite	(Pt, Pd) S	Braggite	(Pt, Pd) S
Cooperite	PtS	Cabriite	Pd_2SnCu
Isoferrplatinum	Pt_3Fe	Isomertieite	$Pd11As_2Sb_2$
Moncheite	$PtTe_2$	Kotulskite	PdTe
Sperrylite	$PtAs_2$	Merenskyite	$PdTe_2$
		Michenerite	PdBiTe
		Plumbopalladinite	Pd_3Pb_2
		Polarite	Pd (Bi, Pb)
		Stannopalladinite	Pd_5Sn_2Cu
		Sudburyite	PdSb
		Taimyrite	$Pd_9Sn_4Cu_3$
		Taimyrite	PdS

CHAPTER 3: METHODS AND MATERIALS

3.1. Geochemical datasets

A large dataset for this study was compiled from results of exploration projects conducted by African Nickel Limited (ANL). ANL conducted exploration on the mafic-ultramafic around the margins of the Zebra Lobe from 2007 to 2011 (Hornsey, 2020). The geochemical analyses of the drill core were conducted by Genalysis Laboratories from 2007 to 2011 using two methods. The Aqua Regia Optical Emission Spectroscopy (AR01/OES) method was used to analyse for Co, Cu, Ni, S whereas Pd, Pt and Au analyses were performed using the Fire Assay Mass Spectrometry (FA25/MS) method. Major and trace element analyses were conducted by ALS Chemex Laboratories from 2012 to 2013. The Multi Element-Inductively Coupled Plasma (ME-ICP41) method was used to analyse broad spectrum of elements (Na Ba, Be, B, Ca, Mg, Al, P, S, K, Sc, Ti, V, Cr, Fe, Co, Ni, Cu, Zn, Ga, As, Sr, Mo, Ag, Cd, Sb, W, Hg, Pb Bi, La, Th, U). Au, Pd and Pt were analysed using the Platinum Group Mineral Inductively Coupled Plasma (PGM-ICP23) method (Hornsey, 2020). The summary of the assay data is in the table below (**Table 3**).

Table 3: Analysed major and trace elements, including PGE analysed for each of the intrusions, associated boreholes, and lithologies.

Intrusion	Boreholes	Intersected Lithologies	Major elements analyses (ppm)	Trace element analyses (ppm)	Platinum group elements analyses (ppb)
Ombuku South	KNCD001	Dunite	Fe,Ca,Na, Mg, Al, P, K, Mn.	Li, B,Bi, S, Sc,Sr Cr, Co, Ni, Co, Ga, Ge, As, Se, Rb,Nb, Mo, Ag, Cd, In, Sn, Sb, Ba, La, Hf, Au, Pb, .	Pd, Pt
	KNCD002	Harzburgite			
		Norite			
		Serpentinite			
		Troctolite			
Oncocua	Onc-1	Anorthosite	Fe,Ca,Na, Mg, Al, P, K, Mn.	Li, B, S, V, Sc, Cr, Co, Ni, Cu, Zn, Ga, Ge, As, Se, Rb, Sr, Y, Zr, Nb, Mo, Ag, Cd, In, Sn, Sb, Te, Hf, Ta, W, Ba, La, Th, U, Pb, Bi.	Pd
		Pyroxenite			
Ongoro	KNV008	Anorthosite	Fe,Ca,Na, Mg, Al, P, K, Mn.	Li, B, S, Sc, Cr, Co, Ni, Co, Ga, Ge, As, Se, Rb, Sr, Nb, Mo, Ag, Cd, In, Sn, Sb, Ba, La, Hf, Au, Pb, Bi.	Pd, Pt
	KNV009	Norite			
		Pyroxenite			
		Troctolite			

Intrusion	Boreholes	Intersected Lithologies	Major elements analyses (ppm)	Trace element analyses (ppm)	Platinum group elements analyses (ppb)
Ohamaremba	HRDD1	Anorthosite	Na, Mg, Al, P, K, Ca, Ti, Mn, Fe.	B,Bi S,Sn,Sr,Cd, V,Ag, Cr, Co, Ni, Cu,Te, Ba, La, Ta, W, Au, Pb,Y,Zn Zr.	Pd, Pt
	HRDD2	Pyroxenite			
	HRDD3	Serpentinite			
	KNAD001	Troctolite			
	KNAD002				
Oheuwa	KNV002	Anorthosite	Na, Mg, Al, P, K, Ca, Mn, Fe.	Li, La, B, Sb, Sc, Se, Cr, Hf,Co, Ni, Cu, Ga, Ge, As, , Rb, Sr, Nb, Mo, Ag, Cd, In, Sn, Ba,S, Au, Pb, Bi.	Pd, Pt
	KNV003	Dunite			
	KNV004	Gabbronorite			
	KNV005	Harzburgite			
		Norite			
		Pyroxenite			
		Serpentinite			
		Troctolite			
		Websterite			
Ombuku North	KNBD001-KNBD015	Anorthosite	Na, Mg, Al, P, K, Ca, Mn, Fe.	Li, La, B, Sb, Sc, Se, Cr, Hf,Co, Ni, Cu, Ga, Ge, As, , Rb, Sr, Nb, Mo, Ag, Cd, In, Sn, Ba,S, Au, Pb, Bi.	Pd, Pt
		Dunite			
		Gabbronorite			
		Harzburgite			
		Norite			
		Peridotite			
		Pyroxenite			
		Serpentinite			
		Troctolite			
Onyokohe	KNDD001	Harzburgite	Na, Mg, Al, P, K, Ca, Mn, Fe.	Li, La, B, Sb, Sc, Se, Cr, Hf,Co, Ni, Cu, Ga, Ge, As, , Rb, Sr, Nb, Mo, Ag, Cd, In, Sn, Ba,S, Au, Pb, Bi.	Pd, Pt
	KNV001	Norite			
	KNV006	Pyroxenite			
	KNV007	Troctolite			

3.2. Petrographic analysis

Thin sections were selected from the sample collection. Twelve samples were selected based on their relatively high Pt and Pd concentrations from the historical PGE analyses. Thin section samples corresponding to >80 ppb of Pt and Pd in whole rock were selected for petrographic analysis. The petrographic examination was done at Wits Petrology facility using an Olympus BX63 microscope and photomicrographs were taken with a magnification of 10x and 4x. Scale bars in each photomicrograph are either 200 µm or 500 µm.

3.3. IoGAS data analysis and visualisation

IoGAS IMDEX software was used for data visualisation and interpretation of the geochemical data. An excel sheet file containing the available geochemical data was imported into the software and saved as an IoGAS file which allows manipulation of the data without changing the imported data file. The imported datasets underwent a series of clean ups and data validation by the software. All empty columns on the datasets were automatically flagged by the software and were excluded from the datasets. The software also filters out the non-numeric values (for example below detection limits were discarded) and zero values in the dataset. The missing data tab was used to remove columns with missing data, for example empty columns where analyses for the elements were not conducted. Data doctor was used to filter out data with issues such as null values. These values were replaced with the number which is an estimate of the half value of the lowest estimated detection limit, which is calculated by IoGAS. Different graphs of various elements were plotted using XY scatter plots and the downhole plots were created for Ombuku North, as the focus of this study because of its greater Pt and Pd concentrations.

3.4. Tescan Integrated Mineral Analyser (TIMA)

The Tescan Integrated Mineral Analyser (TIMA) at the University of the Witwatersrand was used to determine the presence of PGMs in the samples by scanning the thin sections. TIMA Vega3 unit combines backscattered electron (BSE) images and energy dispersive spectroscopy (EDS) analyses to identify minerals and create images. The BSE images were processed to identify and characterise the PGMs. The identified potential PGMs were characterised by matching the mineral spectra with an online database, followed by quantifying the elements of the identified mineral to produce quantitative weight percentage compositions.

The advantage of TIMA is that it is a fully automated high-resolution mapping technique where BSE and EDS data are collected simultaneously during mapping, and this thus reduces the amount of X-ray acquisition time which is dependent on the pixel size of the area of interest. The technique is equipped with a comprehensive library of mineral spectra and allows quantifying mineral composition to get the best match of the mineral species from webmineral mineralogy database. Like other techniques, the TIMA technique depends on a set of predetermined parameters. The disadvantage is that the sample holder needs a standard thin section size for TIMA and the majority of the samples used for this study were too small to fit in the sample holder, resulting in some selected samples being excluded for analysis.

3.4.1. Sample preparation and instrument set up

The high-pressure nitrogen gas was used to clean the samples and to remove any dust particles and debris on the sample prior to analyses. Thereafter, the samples were placed in a sample holder ensuring the top of the thin section is facing up for carbon coating. The purpose of carbon coating is to ensure the samples do not contain charged surfaces and to boost the electrical conductivity of the sample surface. Two thin sections were loaded in the TIMA sample holder at a time, however, due to the size of the thin sections, foil paper was used to fit the sample in the holder which resulted in missing some part of the sample edges (e.g., sample 4/4135). The machine calibrations were done before the measurements. These calibrations are performed on a Faraday cup and a platinum standard in the system, and these are automated checks that are performed before each analysis (Hrstka et al., 2018). Thereafter, the samples were focused on the beams. The electron beams operated at a voltage of 25.00 kilovolts.

3.4.2. Bright phase search

The first step of data acquisition was to search for bright phases (i.e., high density minerals) which would be areas of interest to map in detail for platinum group elements. The bright phase search was acquired with a pixel spacing of 1 micron, minimum brightness of 48, and maximum brightness of 100 under high resolution mapping. This mode is optimised to search for phases with a specfic BSE signal and chemical composition. The bright phase search was completed across the whole thin section.

3.4.3. Mapping of Platinum Group Minerals

After the bright spots/phases were identified on the BSE image, the spots were then analysed with liberation analysis under high-resolution mapping. The identified bright phases or points of measurement were then delineated as regions of interest for each grain. The liberation analyses were conducted under set parameters of 1-micron pixel spacing, minimum brightness of 10, and a maximum brightness of 100 under high-resolution mapping. The PGMs were mapped using elemental map association for the PGMs family.

3.4.4. BSE data processing

The BSE images produced by TIMA were used for data processing to determine the composition of magmatic sulphides/oxides/silicates associated with the PGMs using phase maps and elemental maps to identify the platinum group elements association. The identification of all unclassified minerals was accomplished through spectral analysis, which involved the spectral data and quantification to determine the elemental composition of each unclassified mineral. This elemental composition facilitated the identification of the most closely matching mineral, and the corresponding mineral spectra were subsequently incorporated into the mineral library. Some of the minerals available in the mineral library were not recognised by TIMA because of different chemistry. In this case, any unknown spectra collected was used to find the best or closest match to the records in the database providing mineral phase identification. The match is a combination of mineral name, TIMA mineral classification rules and this is determined automatically from a standard spectra.

CHAPTER 4: RESULTS

4.1. Petrography

A total of 12 thin sections from Ombuku North intrusion were used for petrographic analysis. The samples used are summarised in **Table 4** below.

Table 4: Summary of the thin sections that were studied using petrographic microscope.

Sample ID	Borehole ID	Corresponding sample depth and whole rock sample interval (m)	Rock type	Palladium (ppb)	Platinum (ppb)
4/2802	KNBD002	279.52 m to 282.98 m	Serpentinite	201	160
4/2833	KNBD002	279.52 m to 282.98 m	Serpentinite	201	160
4/2827	KNBD002	279.52 m to 282.98 m	Serpentinite	201	160
4/3426	KNBD002	341.93 m to 342.86 m	Harzburgite	239	166
4/4489	KNBD002	445.42 m to 449.33 m	Serpentinite	653	409
4/4135	KNDB002	413.29 m to 413.67 m	Serpentinite	362	250
4/4400	KNBD002	441.85 m to 440.26 m	Serpentinite	460	337
5/595	KNBD004	594.50 m to 595.00 m	Serpentinite	625	444
4/2360	KNBD002	234.99 m to 239.00 m	Serpentinite	306	253
KSAT280/159	KNBD003	234.51 m to 236. 00 m	Serpentinite	301	273
KSAT280/160	KNBD003	236.00 m to 238.30 m	Serpentinite	399	340
KSAT/166	KNDB001	455.25 m to 458.49 m	Harzburgite	11	7

The number after the forward slash for samples 4/2802 to 4/2360 represent the sample depth in decimetres (e.g., 2802mm = 280.20 m).

The Ombuku North intrusion is primarily composed of serpentinite (altered dunite) and harzburgite, with smaller amounts of norite and orthopyroxenite. In the selected thin sections, the serpentinite contains coarse-grained altered olivine crystals that are anhedral and subhedral. Secondary oxides are also present within olivine. The process of serpentinisation creates a series of irregular veinlets that cut through the sulphide mineral assemblage (**Fig. 24**). In the serpentinite, most of the grains are fully altered, exhibiting a relict mesh texture with irregular veins containing interstitial oxides (**Fig. 19**). Few larger zircons xenocrysts have been found in one sample and appear as large anhedral grains associated with altered olivine (**Fig. 25**).

The harzburgite displays an equigranular texture, consisting of 45 vol % olivines, 40–45 vol % orthopyroxenes, and a minor clinopyroxenes (15 vol %). The olivines are coarse-grained with alteration phases and contains lesser magnetite (**Fig. 18**).

The Ombuku North intrusion is characterised by altered rocks that generally retain their primary sulphide mineralogy. These rocks are predominantly serpentinite, consisting of disseminated, fine-grained blebby inclusions of pyrrhotite (Po) and pentlandite (Pn). Both fine and coarse-grained Pn and Po are commonly found at the grain boundaries of silicates. Additionally, anhedral grains of bornite (Bn) are present in serpentinite (**Fig. 20**), occurring alongside irregularly shaped oxides. Magnetite (Mgt) appears as discrete, irregularly shaped crystals and fine-grained veinlets within the silicates. Pentlandite and chalcopyrite (Ccp) are characterised by anhedral and subhedral crystal faces. Olivine exhibits anhedral shapes with alteration to serpentine along fractures. Aggregates of Po, Pn and Ccp are anhedral to subhedral, with Mgt primarily observed as discrete grains within the olivine (**Fig. 15** and **Fig. 16**). The sulphide assemblage (Ccp, Po) abundance is ≥ 10 vol %, while the oxide (Mgt) abundance is low, around 3 vol % in the samples.

Sample 4/2802, Ombuku North Intrusion (borehole KNBD002 core sample depth 279.52 m to 282.98 m), serpentinite (altered dunite). Pd and Pt concentrations of 201 ppb and 160 ppb, respectively.

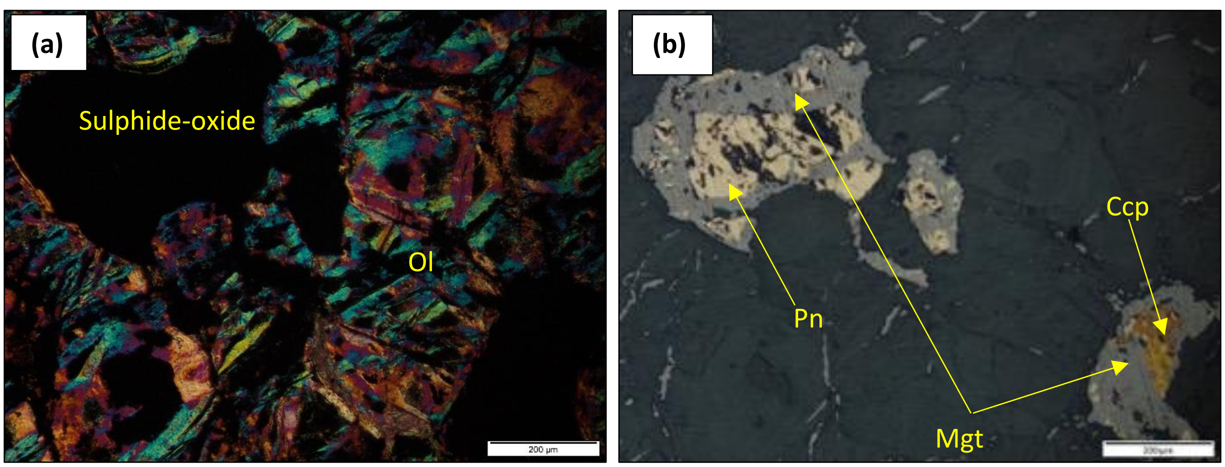

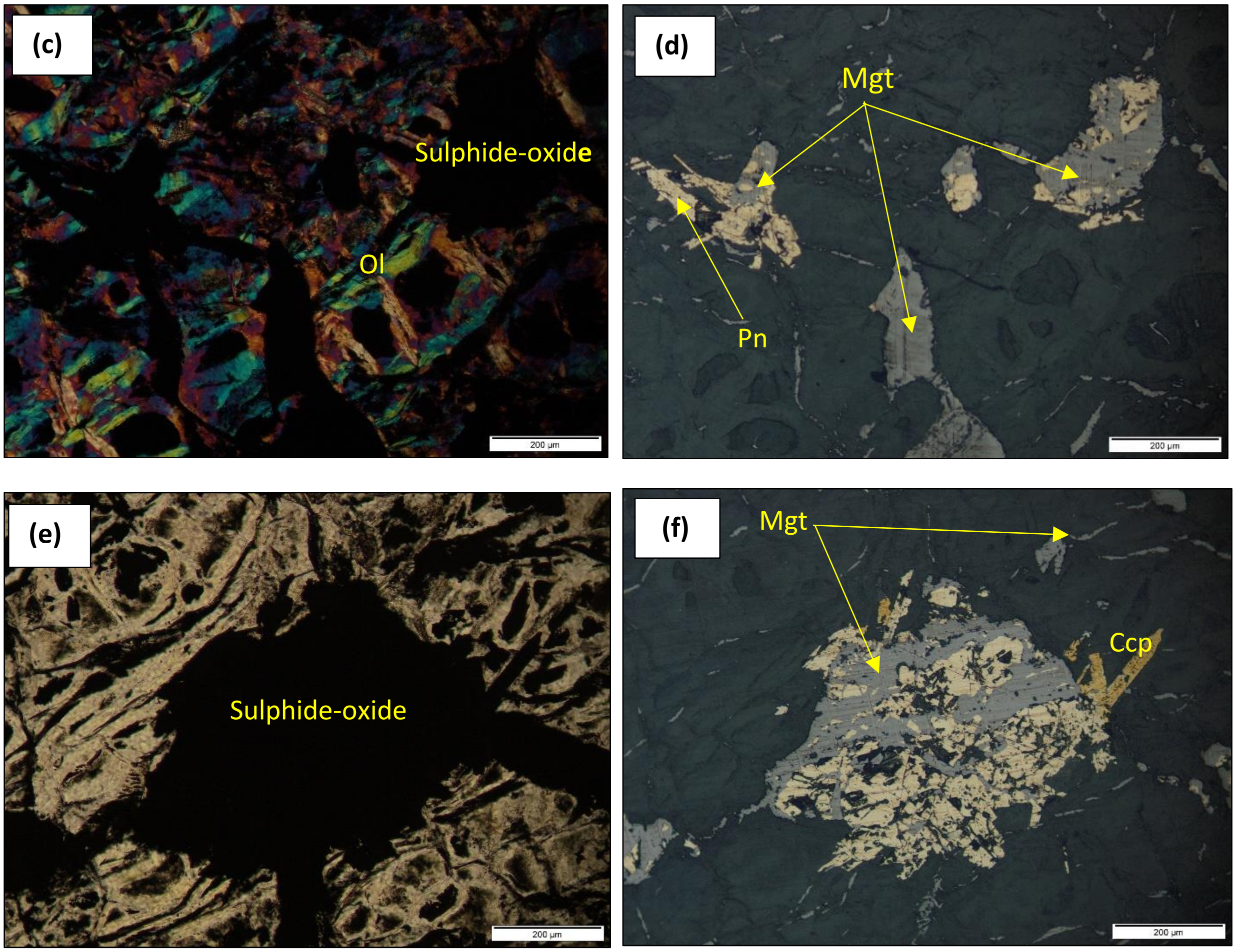

Fig. 15: Photomicrographs of sample 4/2802 **(a)** and **(c)** sulphide assemblage in a highly altered olivine megacryst (10X magnification, cross polarised light), **(b)** and **(d)** Mgt replacing Pn and Po, with some secondary mineralisation of Ccp overprinting Pn (10X magnification, reflected light), **(e)** and **(f)** discrete grains of sulphide and sulphide-oxide intergrowths, Mgt replacing sulphide, and occurring as veinlets. (10X magnification, **e** is plane polarised light, and **f** is reflected light).

Sample 4/2833, Ombuku North Intrusion (borehole KNBD002 core sample depth 279.52 m to 282.98 m), serpentinite (altered dunite). Pd and Pt concentrations of 201 ppb and 160 ppb respectively.

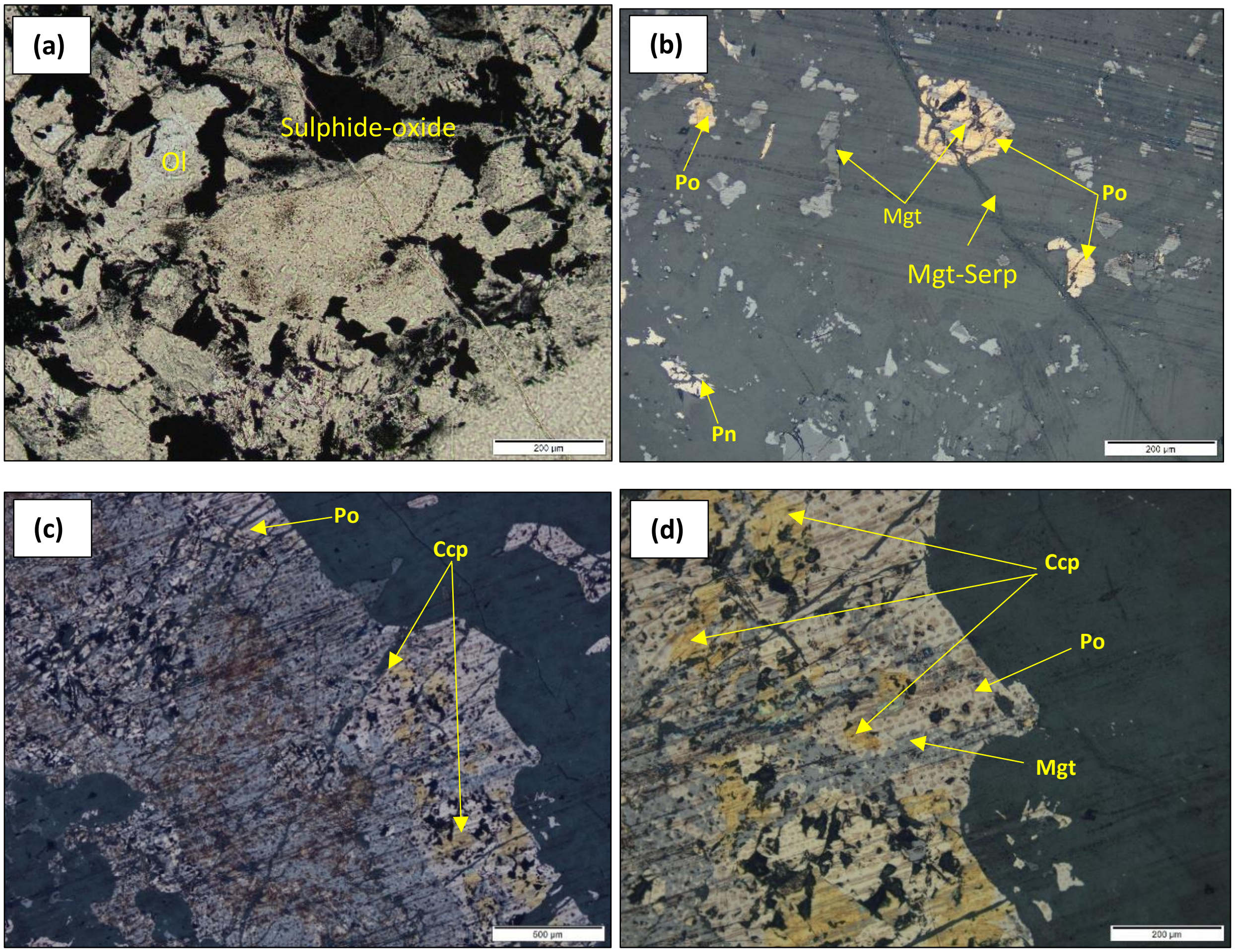

Fig. 16: Photomicrographs of sample 4/2833 **(a)** discrete grains of sulphide-oxide hosted by altered olivine grain (10x magnification, plane polarised light), **(b)** rounded sulphide-oxide assemblage, Pn and Po. Mgt occurs as discrete grains, veinlets and locally replaces Pn. Some sulphides, predominantly Pn are disseminated. Mgt-vein cutting through sulphides-oxides mineralisation, (10x magnification, reflected light), **(c)** predominant Mgt also filling interstitial spaces (10x magnification, reflected light), and **(d)** secondary mineralisation of Ccp overprinting Po (4x magnification, reflected light).

Sample 4/2827, Ombuku North Intrusion (borehole KNBD002 core sample depth 279.52 m to 282.98 m), serpentinite (altered dunite). Pd and Pt concentrations of 201 ppb 160 ppb respectively.

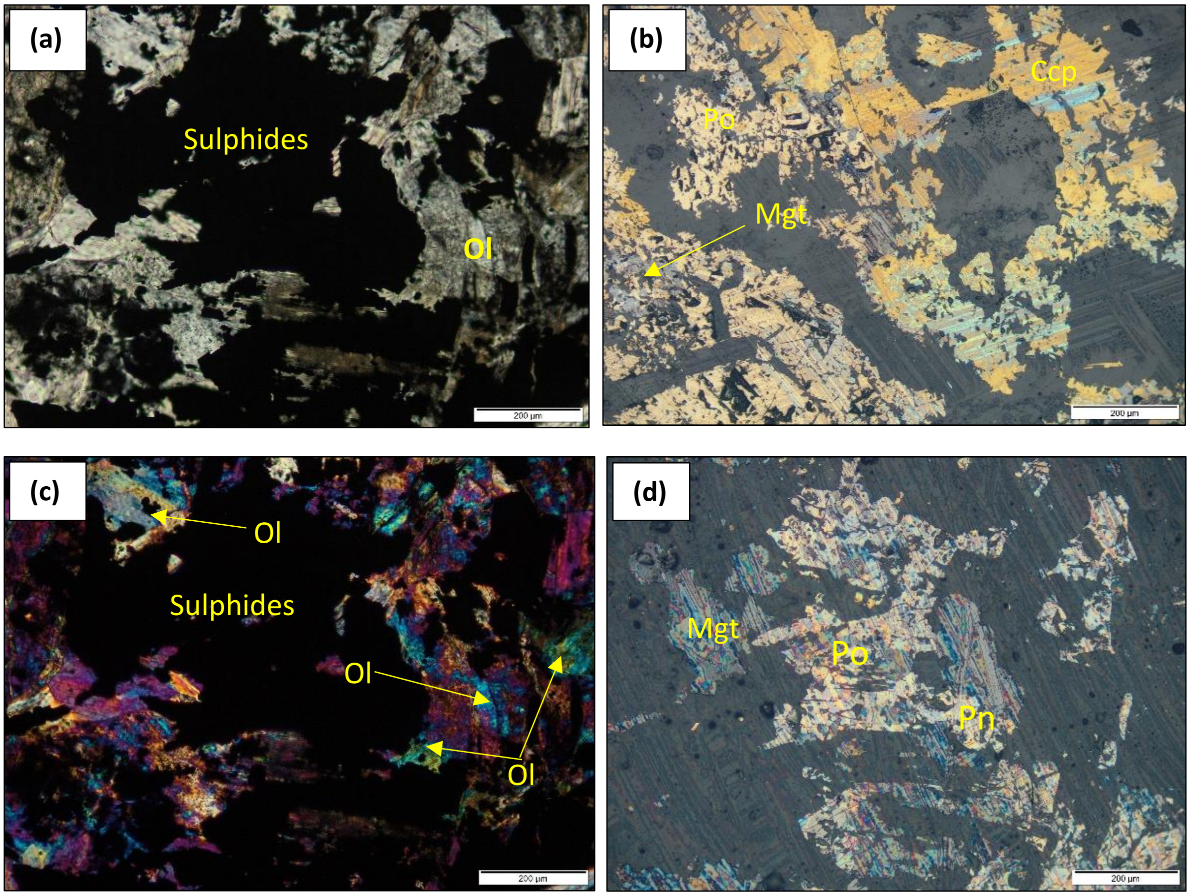

Fig. 17: Photomicrographs of sample 4/2827 **(a)** silicate (altered olivine) and sulphides assemblage (10x magnification, plane polarised light), (**b**) Ccp, Po aggregates. Late Ccp has developed inside Po together with Mgt (10x magnification reflected light), **(c)** sulphide assemblage in silicates (anhedral grains of olivine) (10x magnification, cross polarised light), and (**d**) Mgt replacing Pn and Po (10x magnification, reflected light).

Sample 4/3426, Ombuku North intrusion (borehole KNBD002 core sample depth 341.93 m to 342.86 m), altered harzburgite with discrete grains of sulphides and highly altered olivines and orthopyroxenes. Pd and Pt concentrations of 239 ppb and 166 ppb respectively.

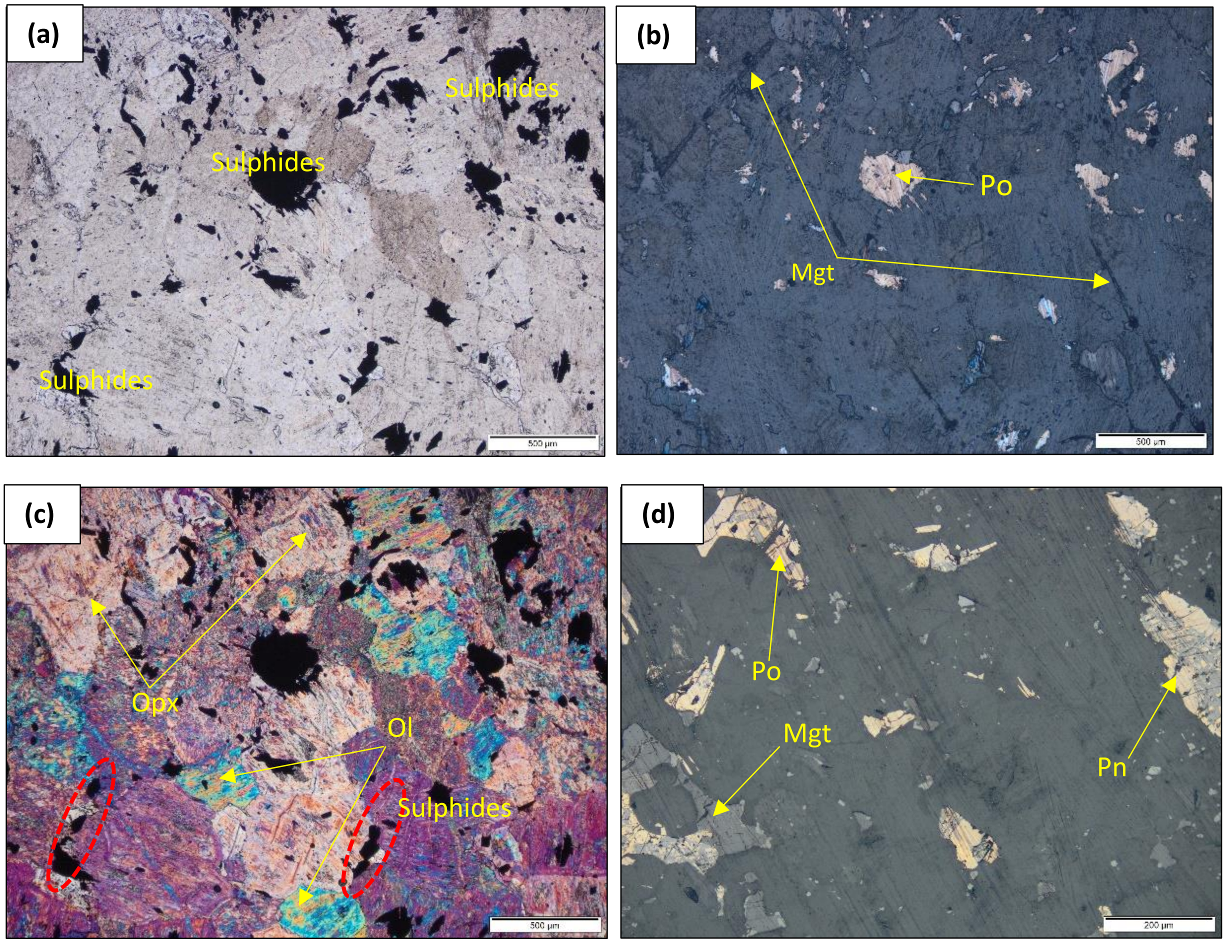

Fig. 18: Photomicrographs of sample 4/3426 **(a)** predominantly disseminated sulphides (4X magnification, plane polarised light, **(b)** interstitial Mgt in planar veins (4X magnification, reflected light), **(c)** sulphide mineralisation at the grain boundaries of altered orthopyroxene (Opx). Sulphides also occur as discrete grains (4X magnification, cross polarised light), and **(d)** secondary mineralisation, Mgt replacing Pn and Po, also as discrete grains (10X magnification, reflected light).

Sample 4/4489, Ombuku North intrusion (borehole KNBD002 core sample depth 445.42 m to 449.33m), serpentinite (altered dunite). Pd and Pt concentrations of 653 ppb and 409 ppb respectively.

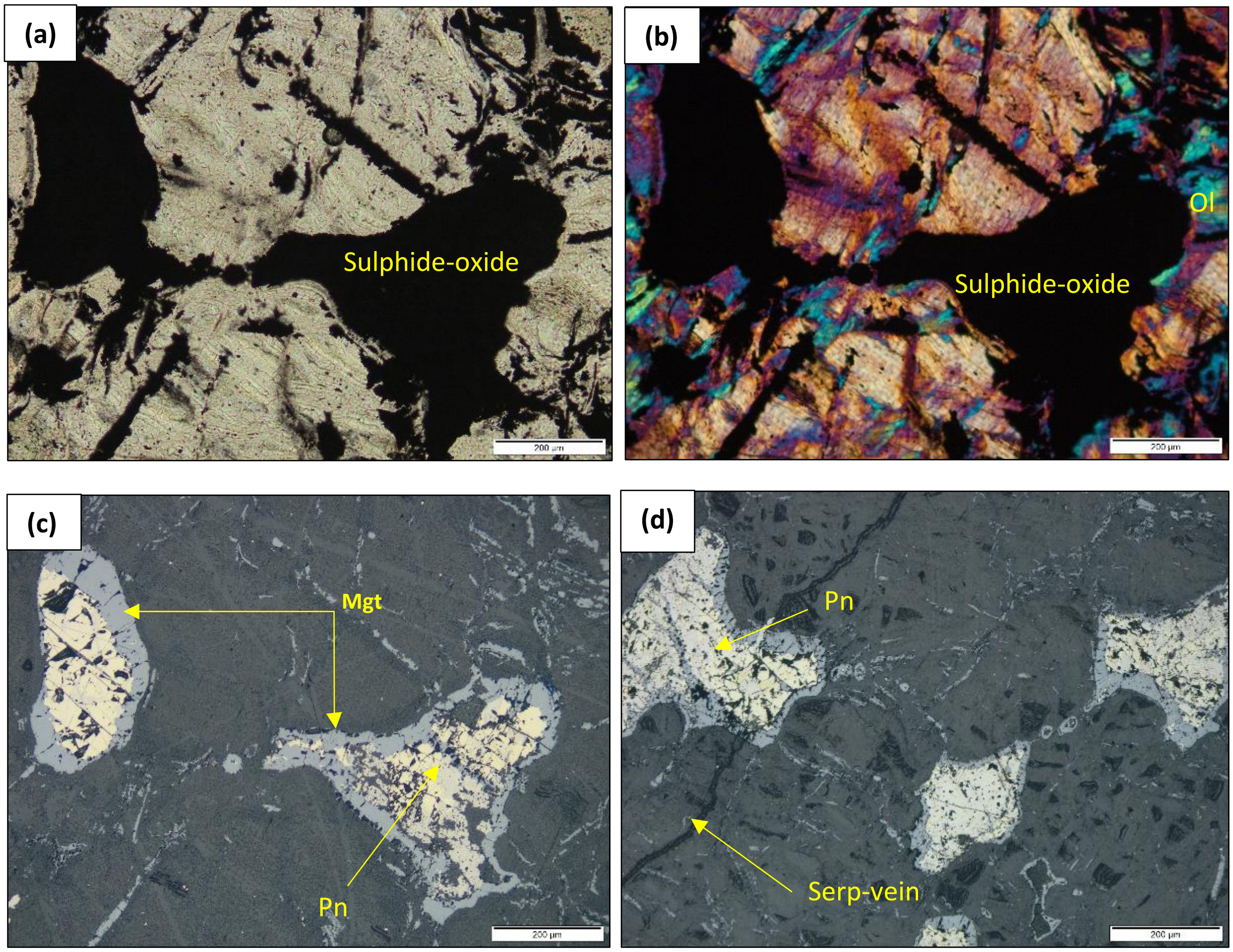

Fig. 19: Photomicrographs of sample 4/4489 **(a)** and **(b)**, blebs of sulphides (10X magnification, **a** is plane polarised light and **b** is cross polarised light), **(c)** and **(d)** Mgt replaces sulphide (Pn) irregular and tiny Mgt veinlets and serpentine veins crosscutting the sulphide assemblage (10x magnification, reflected light).

Sample 4/4135, Ombuku North intrusion (borehole KNBD002 core sample depth 413.29 m to 413.67 m), serpentinite (altered dunite), Pd and Pt concentrations of 362 ppb and 250 ppb respectively.

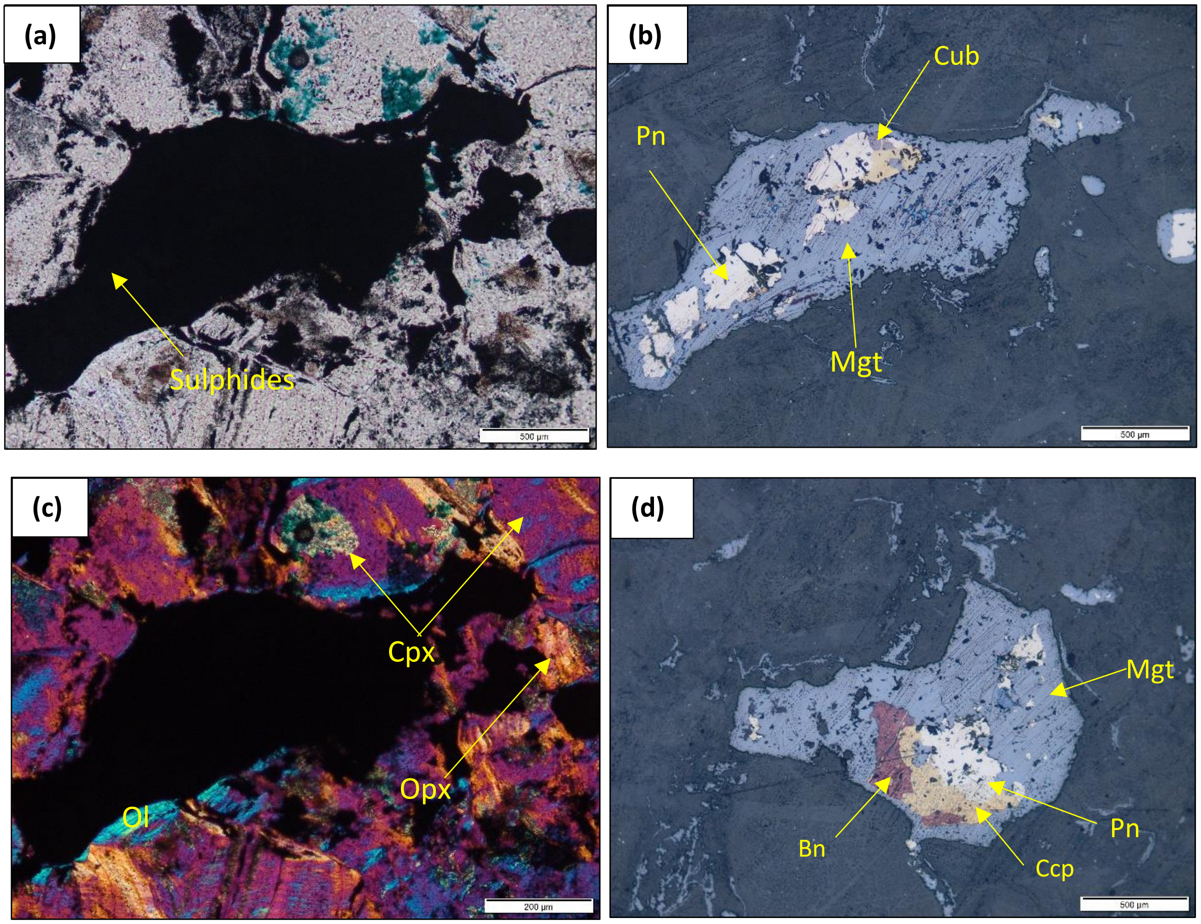

Fig. 20: Photomicrographs of sample 4/4135 **(a)** opaque minerals (appearing as black), predominantly Mgt replacing Pn, (4x magnification, plane polarised light), **(b)** and **(d)** zoned sulphide aggregate with (Ccp), (Pn), and Bn located close to the contact with Mgt. Secondary mineralisation of cubanite (Cub) overprinting Pn (4x magnification, reflected light), and **(c)** sulphide assemblage in silicates (predominantly clinopyroxene (Cpx) with serpentine alteration) (10x magnification, cross polarised light).

Sample 4/4400, Ombuku North intrusion (borehole KNBD002 core sample depth 440.26 m to 441.85 m), serpentinite (altered dunite). Pd and Pt concentrations of 460 ppb of 337 ppb respectively.

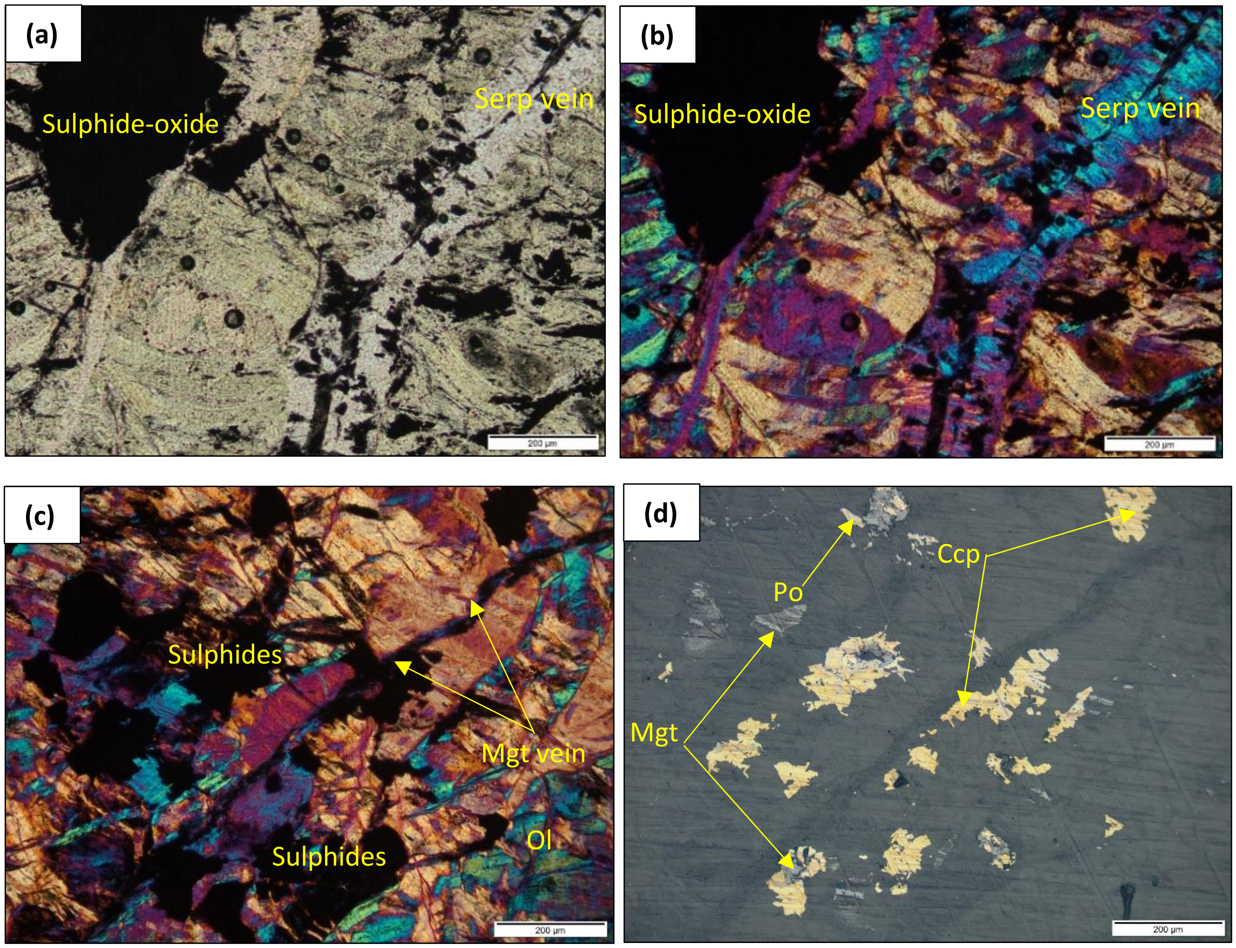

Fig. 21: Photomicrographs of sample 4/4400 **(a)** and **(b)** sulphide-oxide with serpentine vein (10x magnification **a** is plane polarised **b** is cross polarised light), **(c)** and **(d)** disseminated large anhedral grains of sulphide. Sulphide-oxide mineralisation occurs together, with Mgt replacing the sulphide assemblage. Some Pn replacing Po (10x magnification **c** is cross polarised light **d** is reflected light).

Sample 4/595 Ombuku North intrusion (borehole KNBD004 core sample depth 594.50 m to 595.00 m), serpentinite (altered dunite). Pd and Pt concentrations of 625 ppb and 444 ppb respectively.

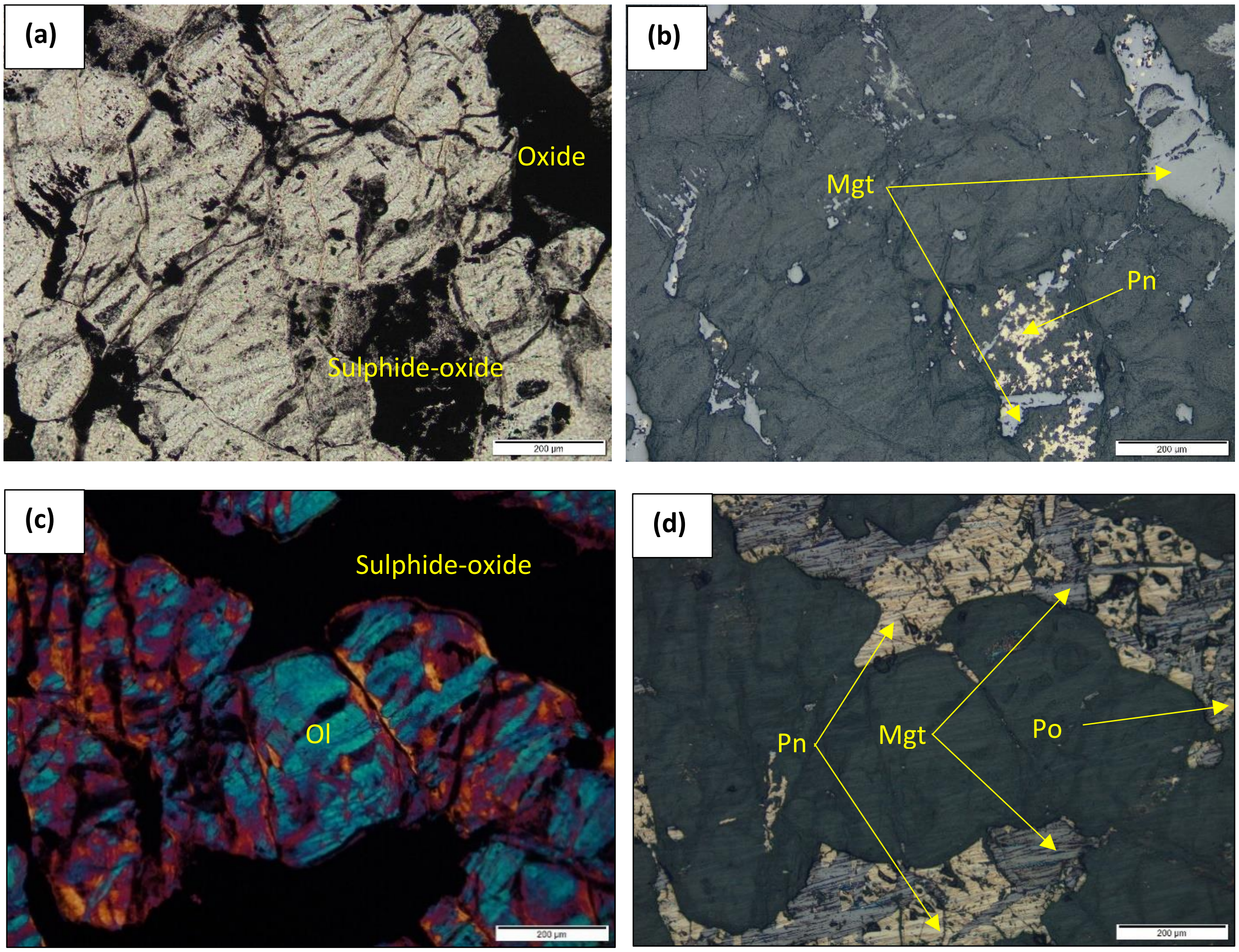

Fig. 22: Photomicrographs of sample 5/595**: (a)** sulphide-oxide assemblage (10x magnification, plane polarised light), **(b)** sulphide-oxide mineralisation, Pn replaced by secondary mineralisation of Mgt, almost completely replacing the sulphide. Interstitial Mgt filling in tiny veinlets (10x magnification, reflected light), **(c)** sulphide-oxide mineralisation hosted in highly altered olivine megacryst (10x magnification cross polarised light) and **(d)** Mgt secondary mineralisation overprinting Po, Pn (10x magnification reflected light)

Sample 4/2360 Ombuku North intrusion (borehole KNBD002 core sample depth 234.99 m to 239.00 m), serpentinite (altered dunite). Pd and Pt concentrations of 306 ppb and 253 ppb respectively.

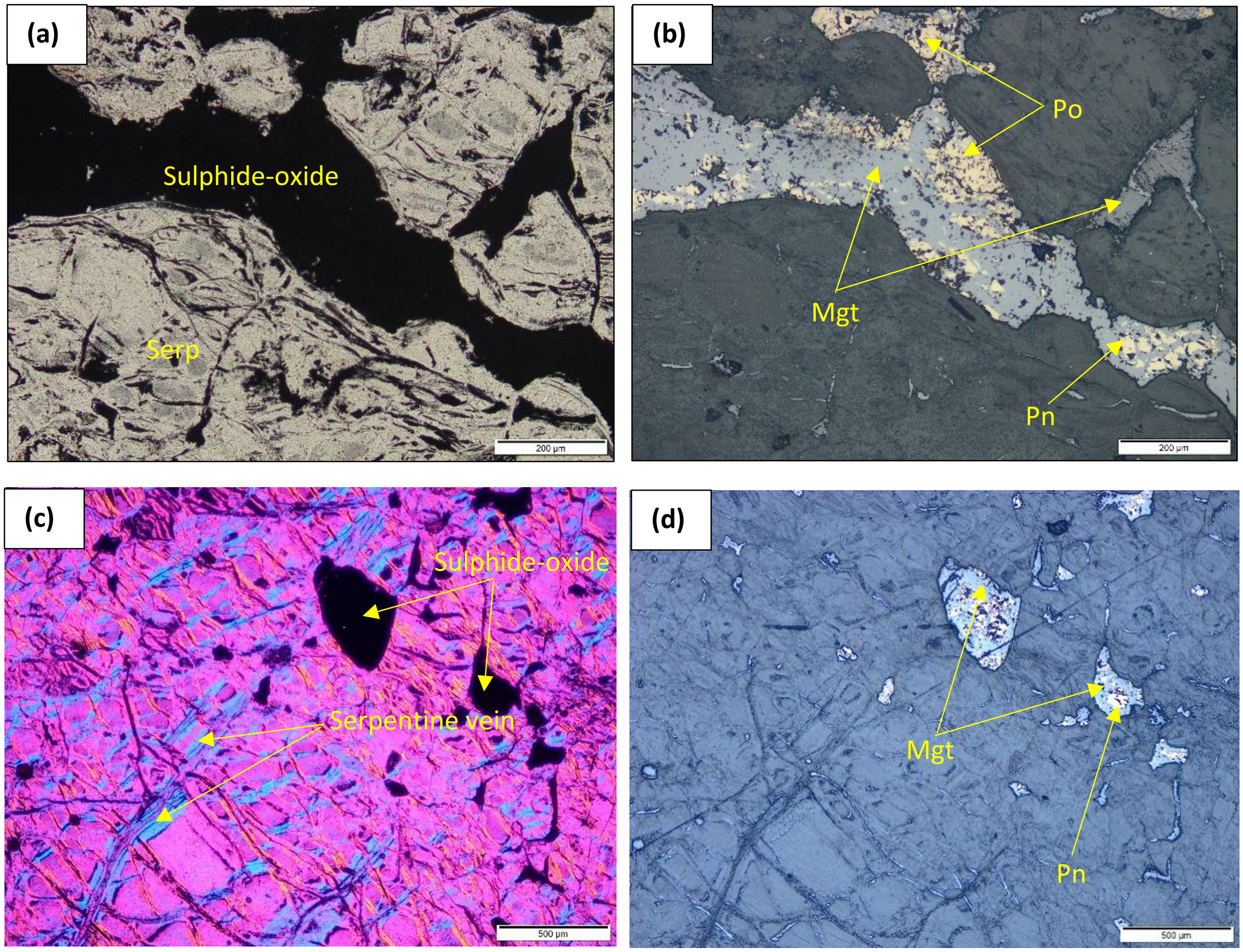

Fig. 23: Photomicrographs of sample 4/2360 **(a)** sulphide-oxide assemblage and serpentine (10x magnification, plane polarised light), **(b)** predominantly oxide, Mgt replacing Pn and Po, Mgt occurs as discrete grains and irregular veinlets (10x magnification reflected light), **(c)** and **(d)** sulphide-oxide mineralisation set in highly altered olivine, serpentine filling interstitial spaces (4x magnification **c** is cross polarised light **d** is reflected light).

Sample KSAT280/159 Ombuku North intrusion (borehole KNBD003 core sample depth 234.51 m to 236.00 m), serpentinite (altered dunite). Pd and Pt concentrations of 301 ppb 273 ppb respectively.

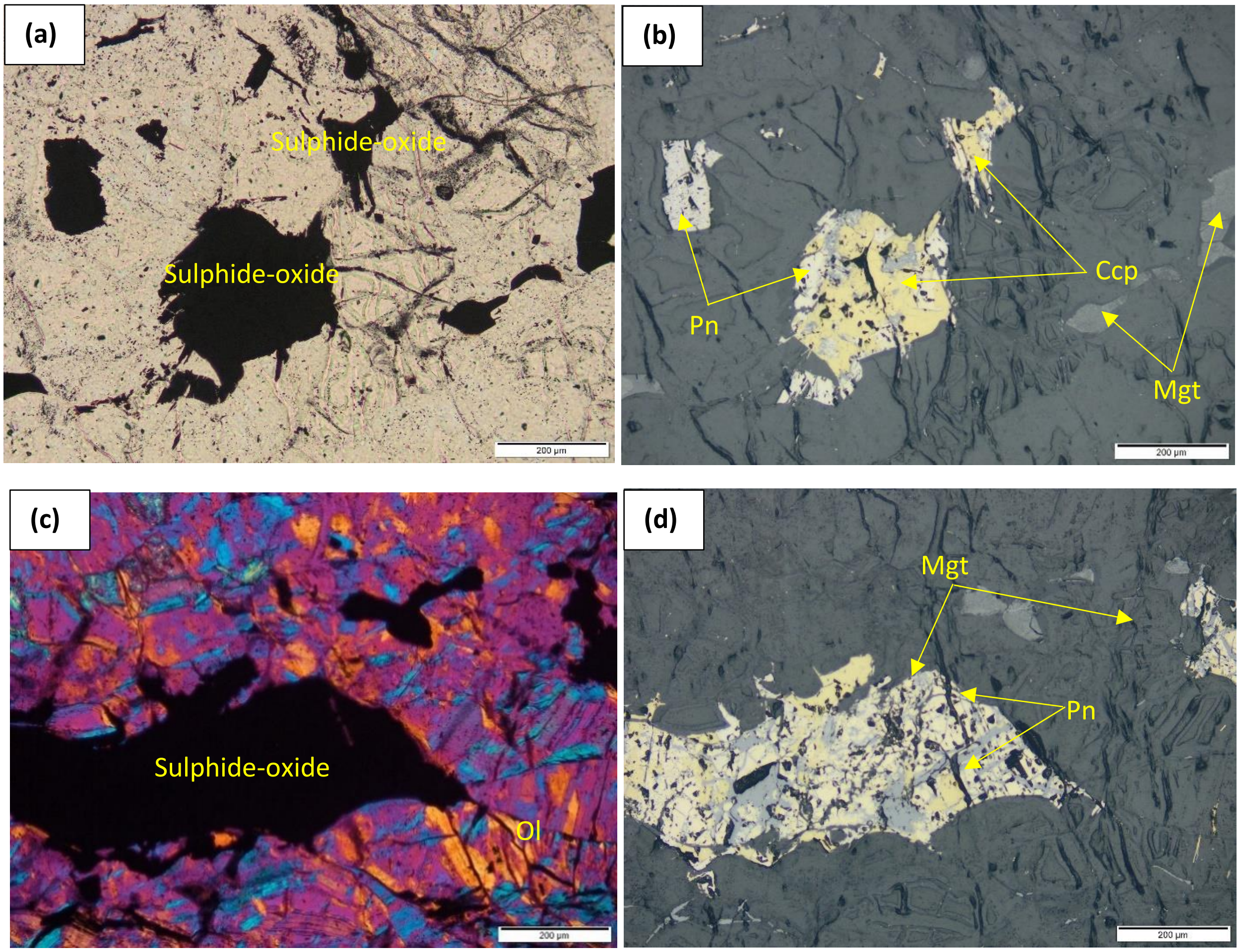

Fig. 24: Photomicrographs of sample KSAT280/159 **(a)** opaque minerals appearing as black spots (10x magnification, plane polarised light), **(b)** Ccp-Pn assemblage and discrete Mgt (10x magnification reflected light), **(c)** and **(d)** subhedral Mgt replaces Pn crystal (10x magnification **c** is cross polarised light and **d** is reflected light).

Sample KSAT 280/160 Ombuku North intrusion (borehole KNBD003 core sample depth 236.00 m to 238.30 m), serpentinite (altered dunite). Pd and Pt concentrations of 399 ppb and 340 ppb respectively.

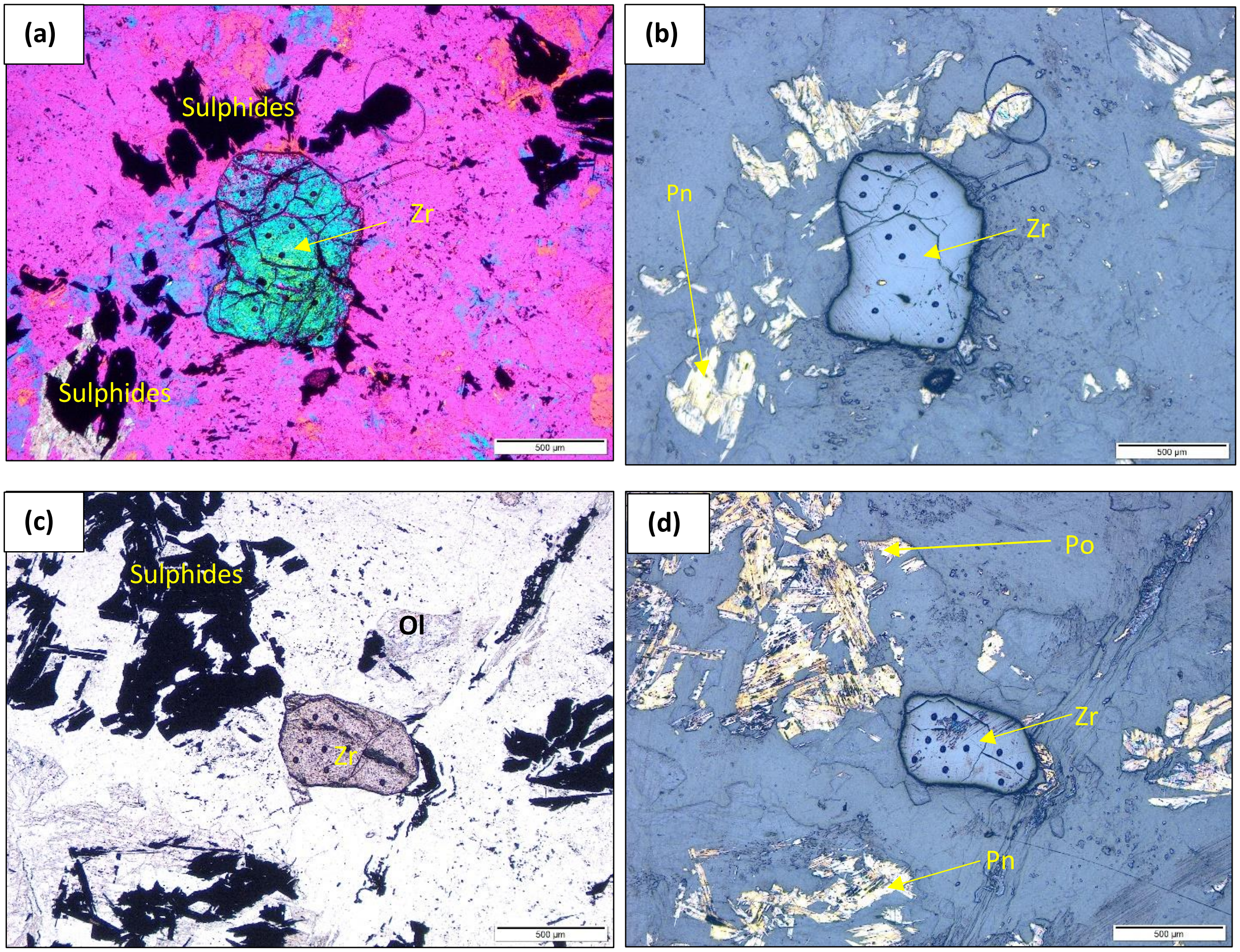

Fig. 25: Photomicrographs of sample KSAT 280/160 **(a)** disseminated sulphide mineralisation, Mgt is minor, and it commonly occurs as interstitial material in veinlets (.4x magnification cross polarised light), (**b**) anhedral zircon (Zr) grain, discrete grains of Pn hosted in olivine, disseminated in some places (4x magnification reflected light), **(c) and (d)**, Po replaced by Ccp hosted by olivine, ~ 500 µm zircon (Zr) grain (4x magnification **c** is plane polarised light and **d** is reflected light).

Sample KSAT/166 Ombuku North intrusion (borehole KNBD001 core sample depth 455.25 m to 458.49 m), harzburgite. Pd and Pt concentrations of 11 ppb and 7 ppb respectively.

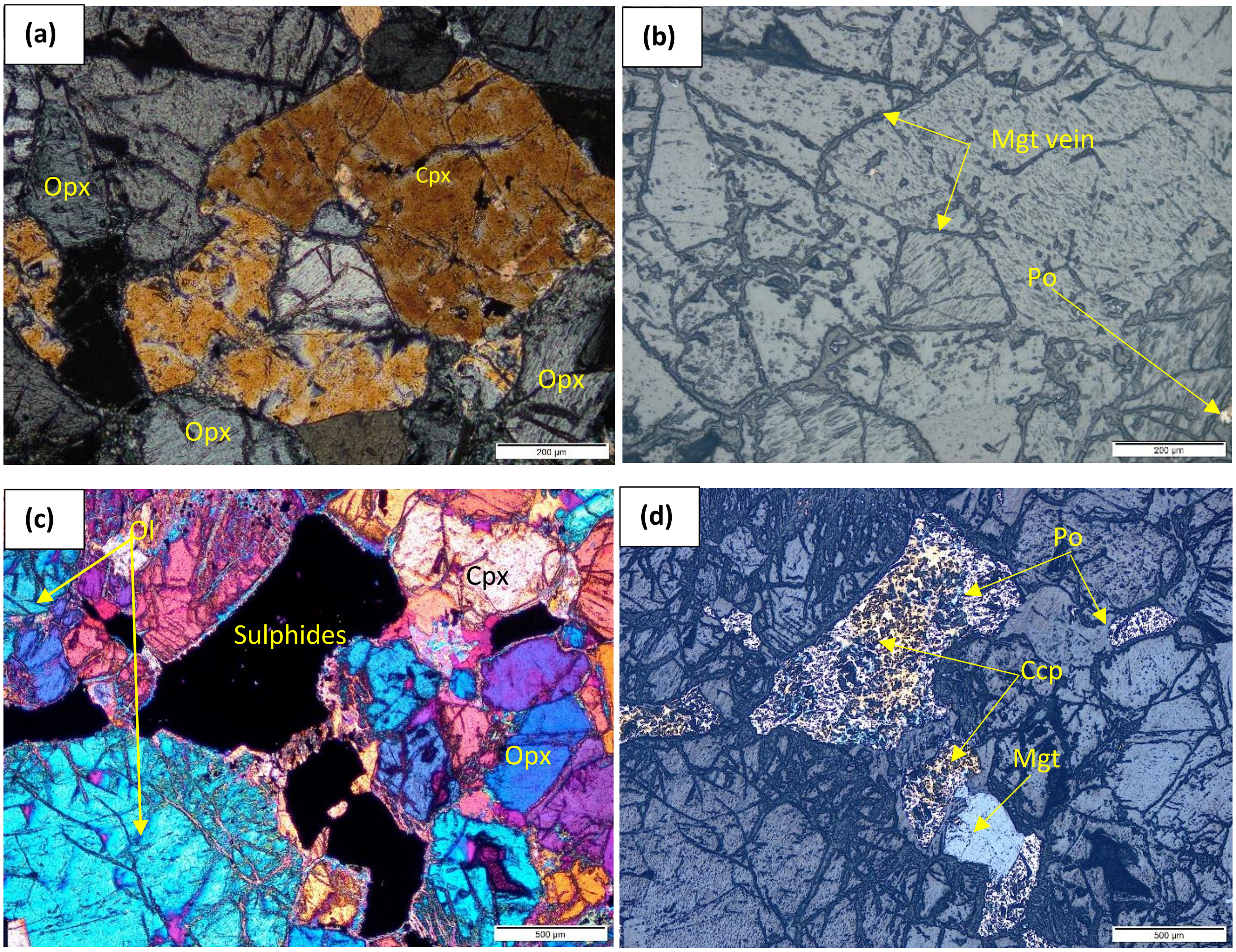

Fig. 26: Photomicrographs of sample KSAT 166 **(a)** harzburgite with minor disseminated sulphides in a silicate assemblage, Opx, Cpx), (10x magnification plane polarised light), (**b)** Irregular Mgt veinlets, (10x magnification reflected light), **(c)** sulphide mineralisation hosted by Opx, Cpx, Ol (4x magnification cross polarised light), and **(d)** minor oxide, anhedral discrete Mgt grain, subhedral-euhedral Po replaced by Ccp in some places (4x magnification reflected light).

4.2. Geochemistry

The main rock types intersected on the boreholes are anorthosite, dunite, gabbronorite, harzburgite, norite, orthopyroxenite, peridotite, pyroxenite, serpentinite, troctolite and websterite. The geochemistry dataset for Ombuku North was used to define the geochemical relationships. Ombuku North has PGE values >80 ppb. Ombuku North is characterised by higher PGE values (Pd from 0. 5 ppb to 653 ppb, Pt from 1 ppb to 444 ppb) compared with the other mafic-ultramafic intrusions that have been drilled in the Zebra Lobe region. The plots in **Fig. 27** show the correlation of PGE with base (nickel, copper, cobalt), and precious (gold) metals, and PGEs with non-metallic sulphur plotted on a logarithmic scale. Generally, there is good correlation between Pt and Pd.

The PGE concentrations are significantly influenced by nickel. The relationship between nickel and the PGE indicates a good positive correlation. This is predominantly observed in the serpentinite, harzburgite, and orthopyroxenite lithologies (**Fig. 27 a-b**). The PGE contents also correlate with copper contents, and there is also a significant overlap of low PGE values and low copper values (**Fig. 27 c-d**).

Cobalt concentration values range from 1 ppm to 364 ppm, with the higher concentrations (>1000 ppm) in serpentinite and harzburgite. The high concentration of PGE correlates with high cobalt concentrations <500 ppm (**Fig. 27 e-f**).

Gold concentration ranges from 0.5 ppb to 293 ppb and correlates with PGE (**Fig. 27 g-h**). The highest PGE values also correlate with the highest sulphur contents. Ombuku North lithologies (dunite, harzburgite, norite, serpentinite, pyroxenite, orthopyroxenite) containing PGE >80 ppb also show relatively high sulphur contents >500 ppm (**Fig. 27 i-j**).

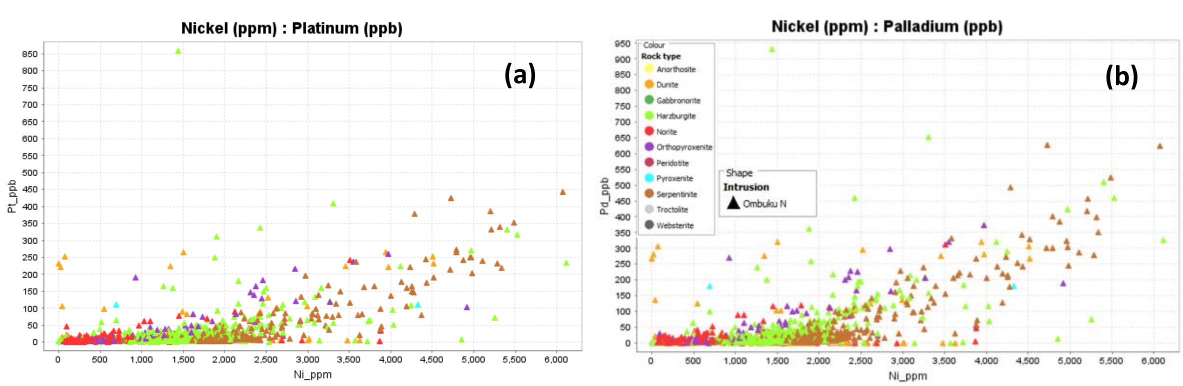

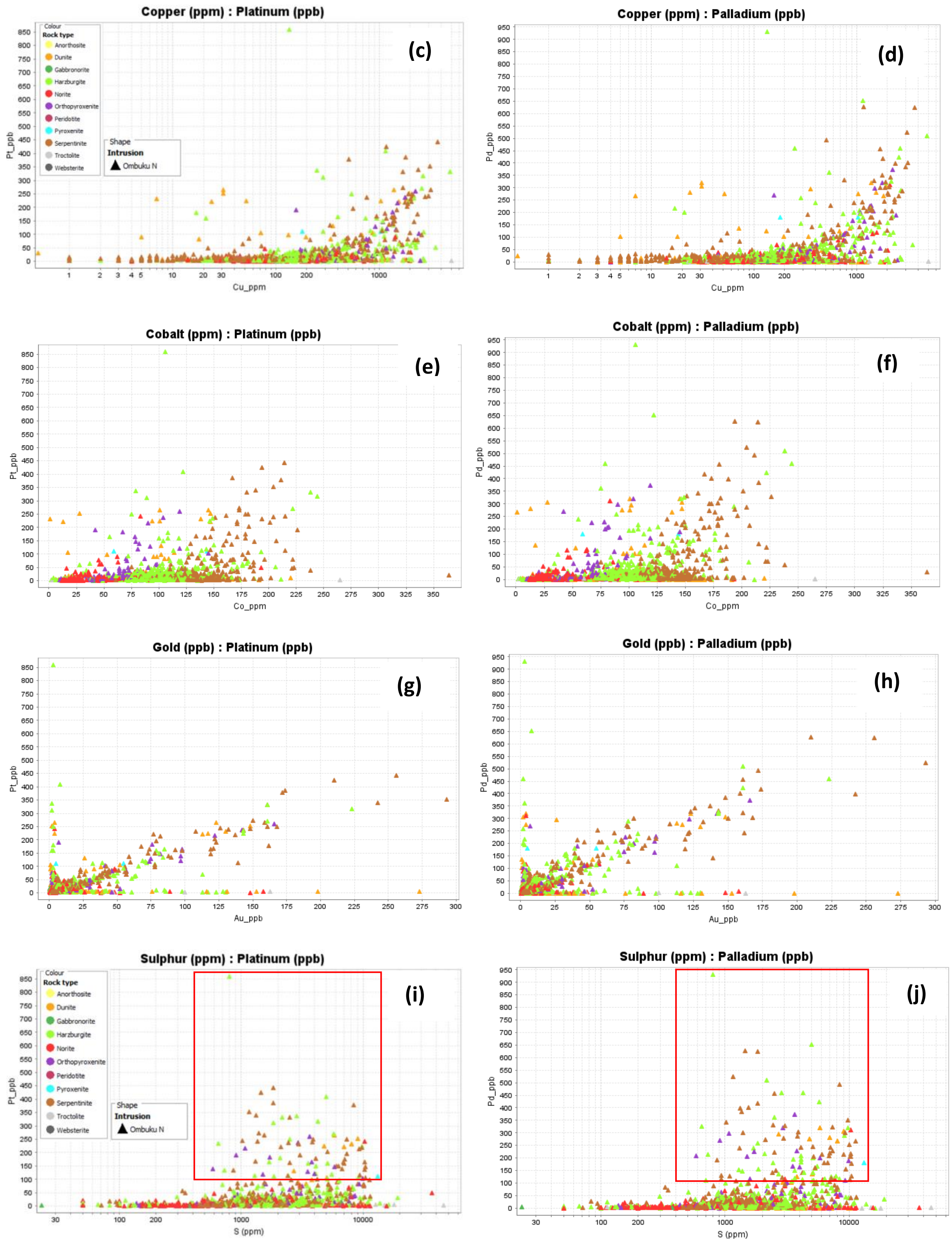

Fig. 27: XY plots of the Ombuku North intrusion, illustrating the correlation between the PGE and base metals as well as sulphur.**(a)** Pt versus Ni, **(b)** Pd versus Ni, **(c)** Pt versus Cu **(d)** Pd versus Cu, **(e)** Pt versus Co **(f)** Pt versus Co **(g)** Pt versus Au**,** **(h)** Pd versus Au **(i)** Pt versus S and **(j)** Pd versus S**.**

Downhole logs with analyses from Ombuku North boreholes (KNDB001 and KNBD002, KNBD003, and KNBD004) are illustrated in **Fig. 28** and **Fig. 29** below. Lithologies intersected in borehole KNBD001 are harzburgite, norite, gabbronorite and dunite, and the Pt and Pd values are relatively low (Pd 2 – 70 ppb, Pt 1 – 34 ppb). Borehole KNDB002 has slightly higher PGE values and these are obtained predominately from harzburgite, dunite and norite (**Fig. 28**).

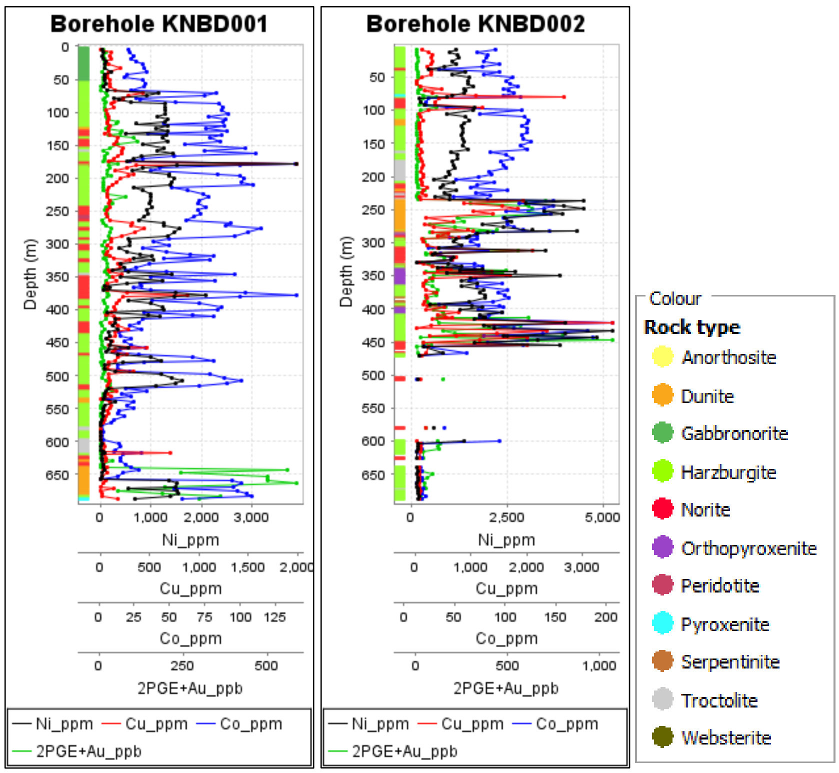

Fig. 28: Downhole lithologies and PGE, Ni, Cu, Co abundances for boreholes KNBD001 and KNBD002 from Ombuku North. The gaps on the downhole log represent intervals where samples were not collected for analyses.

KNBD003 and KNDB004 boreholes contain high metal concentrations (**Fig. 29**), with significantly higher nickel, cobalt and copper. KNBD003 show a good metal concentration overlap and high concentration of Ni-Cu-PGE are observed between ~180 m to 300 m. Borehole KNDB004 also have significant overlap of metal concentrations (Ni, Co, Cu, and PGE), between 230 m and 600 m.

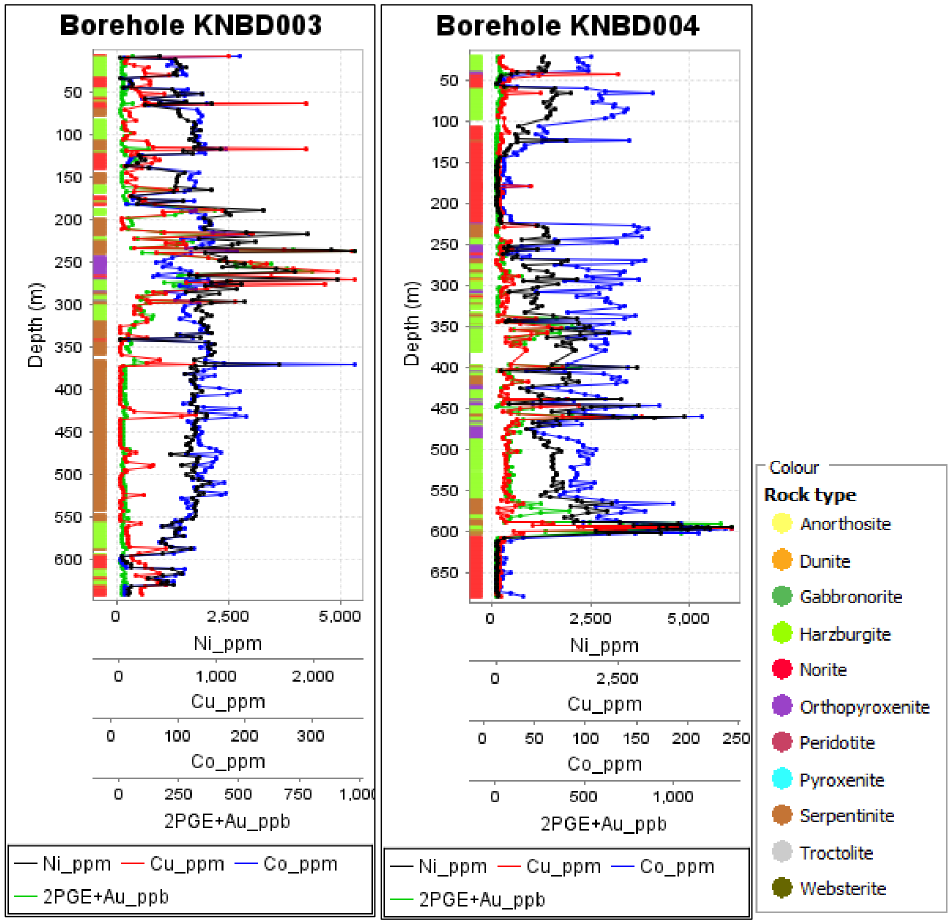

Fig. 29: Downhole lithologies and PGE, Ni, Cu, Co abundances for boreholes KNBD003 and KNBD004 from Ombuku North. The gaps on the downhole log represent intervals where samples were not collected for analyses.

4.3. TIMA

A total of 8 thin sections (4/2833, 4/4400, 4/595, 4/4135, 4/3426, 4/4489, 4/2827 and 4/2802) corresponding with PGE values >80 ppb were selected for TIMA analyses. The samples were analysed using a bright phase search in order to identify “bright spots”, which are potential PGM. Bright spots were identified in 7 of the 8 selected samples (4/2833, 4/4400, 5/595, 4/4135, 4/3426, 4/2827, and 4/2802) with no bright spots identified in sample 4/4489. This was followed by high resolution mapping on all the bright spots identified in an attempt to classify their mineral species. Samples 4/2827 and 4/2802 were excluded for high resolution PGM mapping because the bright spots were not associated with PGE on elemental map analysis, indicating they were not associated with PGM. A summary of the PGMs identified in the samples is shown below (**Table 5**).

Table 5: Summary of assay data for samples used for identification of PGMs.

Sample 4/2833		Sample 4/4400		Sample 4/595		Sample 4/4135		Sample 4/3426	
Intrusion	Ombuku N	Intrusion	Ombuku N	Intrusion	Ombuku N	Intrusion	Ombuku N	intrusion	Ombuku N
Sampe ID	KNBD002	Sampe ID	KNBD002	Sampe ID	KNBD004	Sampe ID	KNBD002	Sampe ID	KNBD002
East	321337	East	321337	East	321337	East	321337	East	321337
South	8092107	South	8092107	South	8092007	South	8092107	South	8092107
Depth from	279.52	Depth from	440.26	Depth from	594.5	Depth from	413.29	Depth from	341.93
Depth to	282.98	Depth to	441.85	Depth to	595	Depth to	413.67	Depth to	342.86
Interval	3.46	Interval	1.59	Interval	0.5	Interval	0.38	Interval	0.93
Rock type	Serpentinite	Rock type	Serpentinite	Rock type	Serpentinite	Rock type	Serpentinite	Rock type	Serpentinite
Au (ppb)	79	Au (ppb)	3	Au (ppb)	256	Au (ppb)	3	Au (ppb)	85
Cd (ppm)	-	Cd (ppm)	122	Cd (ppm)	_	Cd (ppm)	206	Cd (ppm)	79
Co (ppm)	118	Co (ppm)	100	Co (ppm)	214	Co (ppm)	75	Co (ppm)	55
Cr (ppm)	-	Cr (ppm)	1152	Cr (ppm)	_	Cr (ppm)	3547	Cr (ppm)	1379
Cu(ppm)	943	Cu(ppm)	745	Cu(ppm)	3702	Cu(ppm)	541	Cu(ppm)	401
Mg (ppm)	-	Mg (ppm)	3306	Mg (ppm)	_	Mg (ppm)	4034	Mg (ppm)	2702
Na (ppm)	-	Na (ppm)	0.4983	Na (ppm)	_	Na (ppm)	0.6017	Na (ppm)	0.7611
Ni (ppm)	3165	Ni (ppm)	2500	Ni (ppm)	6074	Ni (ppm)	1882	Ni (ppm)	1265
P (ppm)	-	P (ppm)	-	P (ppm)	_	P (ppm)	_	P (ppm)	_
Pb (ppm)	-	Pb (ppm)	-	Pb (ppm)	_	Pb (ppm)	_	Pb (ppm)	_
S (ppm)	5132	S (ppm)	3535	S (ppm)	1837	S (ppm)	2487	S (ppm)	1702
Sc (ppm)	-	Sc (ppm)	-	Sc (ppm)	_	Sc (ppm)	_	Sc (ppm)	_
Se (ppm)	-	Se (ppm)	116	Se (ppm)	_	Se (ppm)	131	Se (ppm)	89
Sr (ppm)	-	Sr (ppm)	160	Sr (ppm)	_	Sr (ppm)	250	Sr (ppm)	166
Sn (ppm)	-	Sn (ppm)	195	Sn (ppm)	_	Sn (ppm)	362	Sn (ppm)	239
Pd (ppb)	201	Pd (ppb)	195	Pd (ppb)	625	Pd (ppb)	362	Pd (ppb)	239
Pt (ppb)	160	Pt (ppb)	160	Pt (ppb)	444	Pt (ppb)	250	Pt (ppb)	166
2PGE+Au_ppb	440	2PGE+Au_ppb	358	2PGE+Au_ppb	1325	2PGE+Au_ppb	615	2PGE+Au_ppb	490

A total of 8 PGMs were identified in the samples. The samples contain platinum arsenides, palladium bismuthotellurides and palladium antimonides (as summarized below in **Table 6)**. **Figures 30** to **34** show back scattered electron images of the identified PGMs and their adjacent minerals.

Table 6: Identified PGMs, quantitative analyses in weight percentage and their host mineral.

Sample	Fe Wt.%	Ni Wt.%	As Wt. %	Pd Wt.%	Sb Wt. %	Te Wt.%	Pt Wt.%	Bi Wt.%	Pd W.t%	PGM	Chemical Formula	Host mineral
4/2833	0.51	-	38.41	-	0.09		59.9	-	-	Sperrylite	$PtAs_2$	Magnetite
4/4400	0.63	-	44.01	-	0.43		53.88	-	-	Sperrylite	$PtAs_2$	Pyrrhotite
4/4400	0.44	-	40.67	-	0.21		56.9	-	-	Sperrylite	$PtAs_2$	Magnetite
4/4400	-	-	5.75	61.41	6.36	8.92	18.24	-	-	Vincentite	$(Pd, Pt)_3$ (As, Sb, Te)	Pyrrhotite
4/595	0.89	-	40.7	-	9.34		51.94	-	-	Sperrylite	$PtAs_2$	Magnetite
4/595	-	1.23		22.31	20.12	15.08	9.95	29.68		Michenerite	PdBiTe	Pentlandite
4/4135	-	3.24	0.45	-	27.86		0.31	-	68.11	Stibiopalladinite	Pd_5Sb_2	Pentlandite
4/3426	-	-	7.75	16.54	8.36	7.92	59.41	-	-	Vincentite	$(Pd, Pt)_3$ (As, Sb, Te)	Magnetite

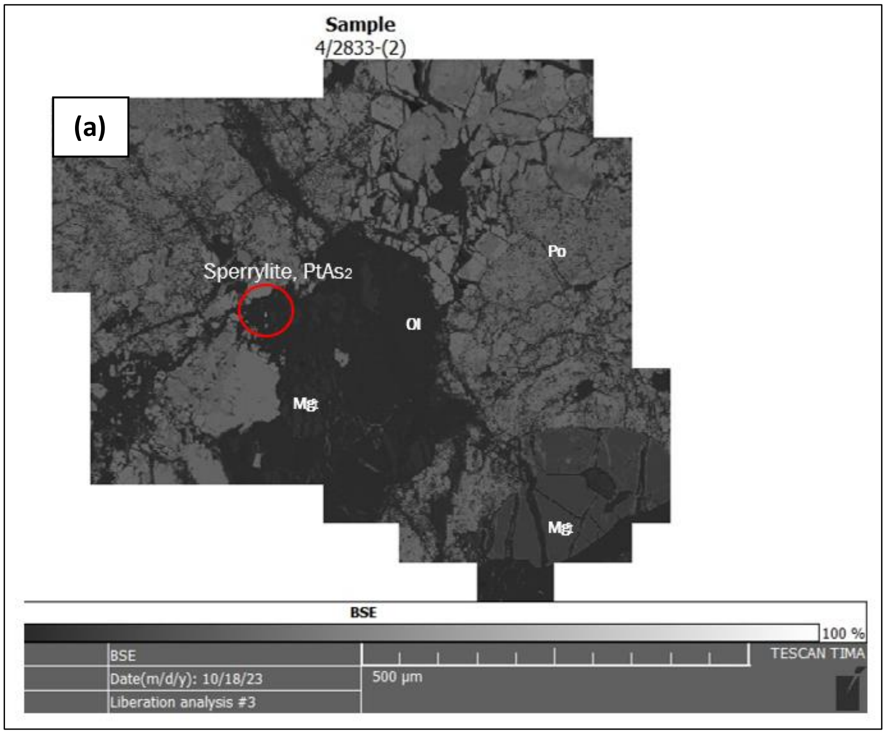

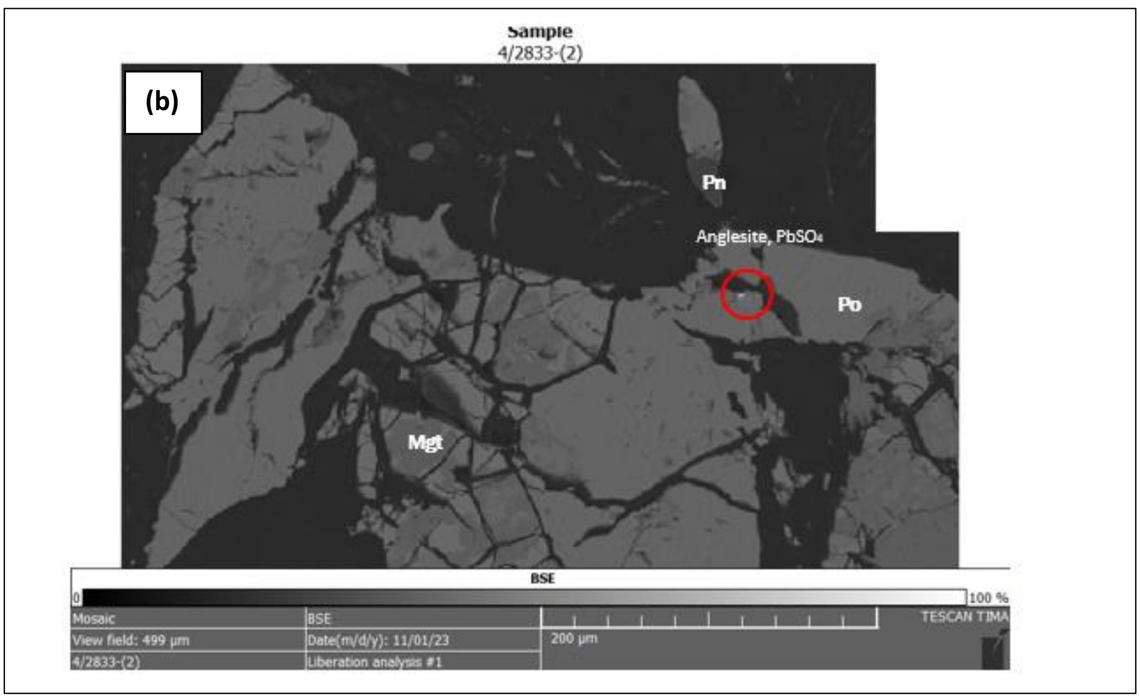

Fig. 30: Back-scattered electron images for sample 4/2833, serpentinite (altered dunite) from borehole KNDB002 (279.52 m to 282.98 m) (**a**) A grain of sperrylite at the grain boundary of Mgt and olivine, (**b**) A grain of anglesite hosted in Po with the silicate matrix minerals in black.

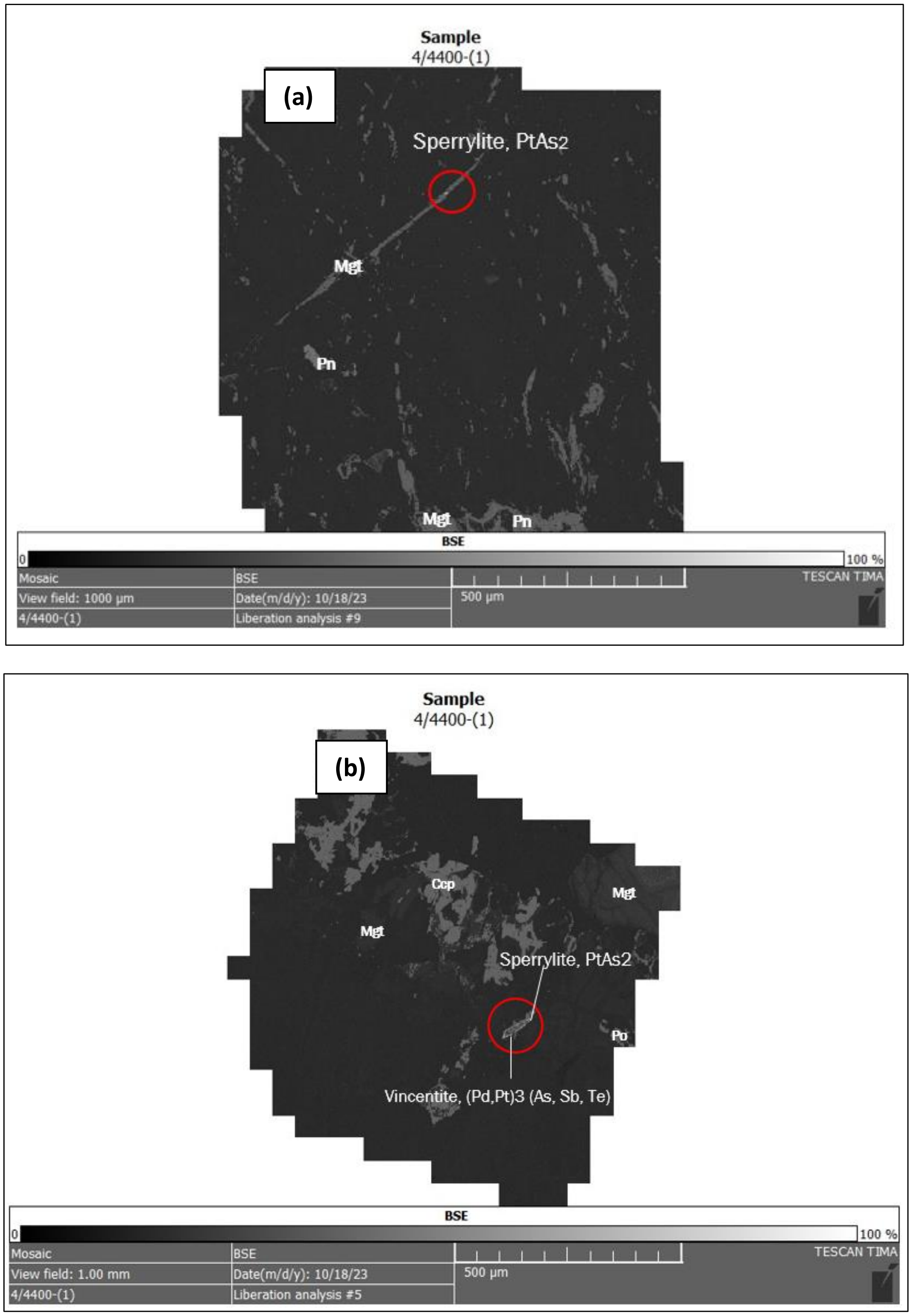

Fig. 31: Back-scattered electron images for sample 4/4400, serpentinite (altered dunite) from borehole KNDB002 (440.26 m to 441.85 m) **(a)** A grain of sperrylite hosted in a thin vein of Mgt, **(b)** Grains of sperrylite and vincentite hosted in a sulphide assemblage with the silicate matrix in black.

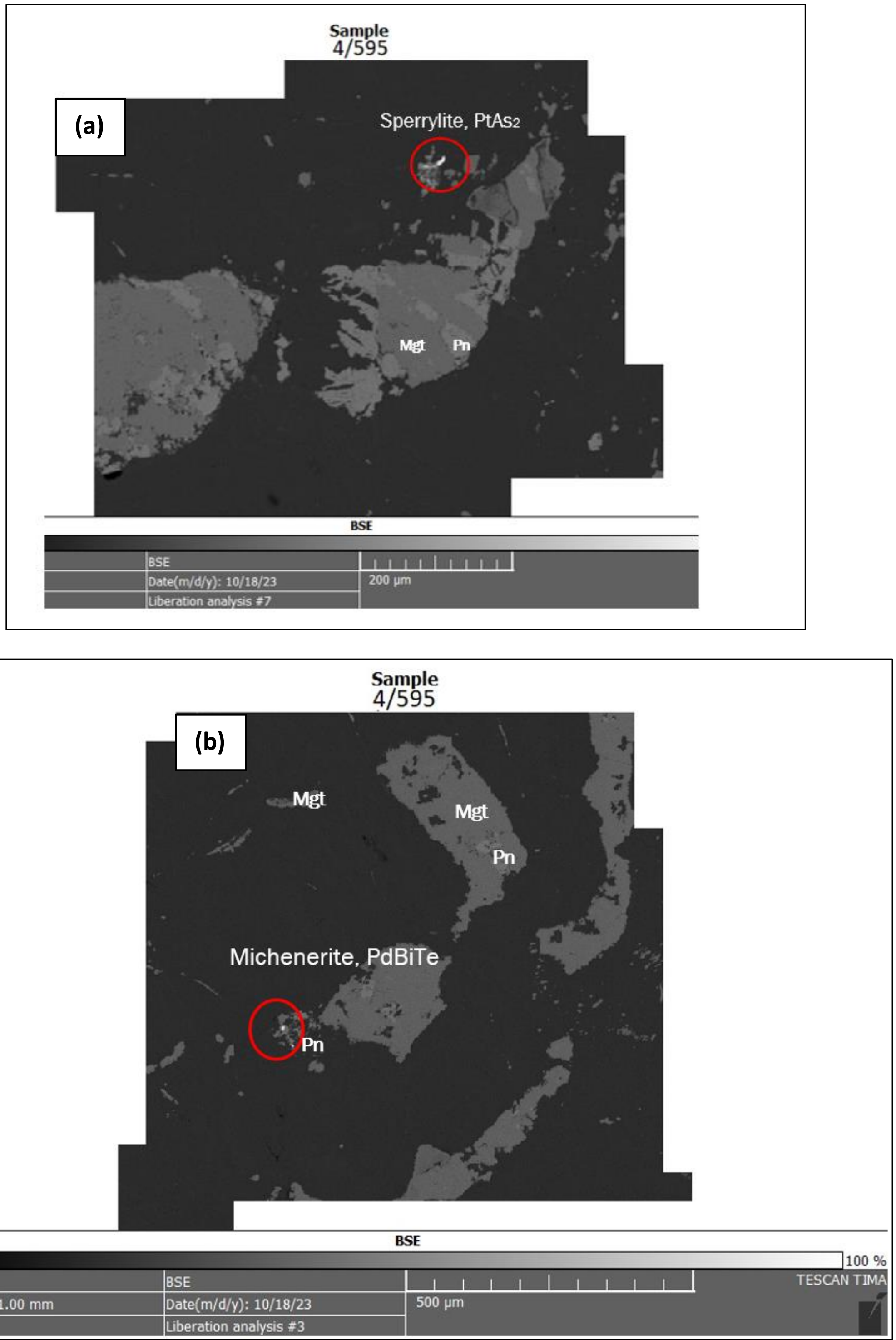

Fig. 32: Back-scattered electron images for sample 4/595, serpentinite (altered dunite) from borehole KNDB004 (594.50 m to 595.00 m) **(a)** A grain of sperrylite hosted in sulphide-oxide (Po-Mgt) assemblage, **(b)** A grain of michenerite hosted in Pn with the silicate matrix in black.

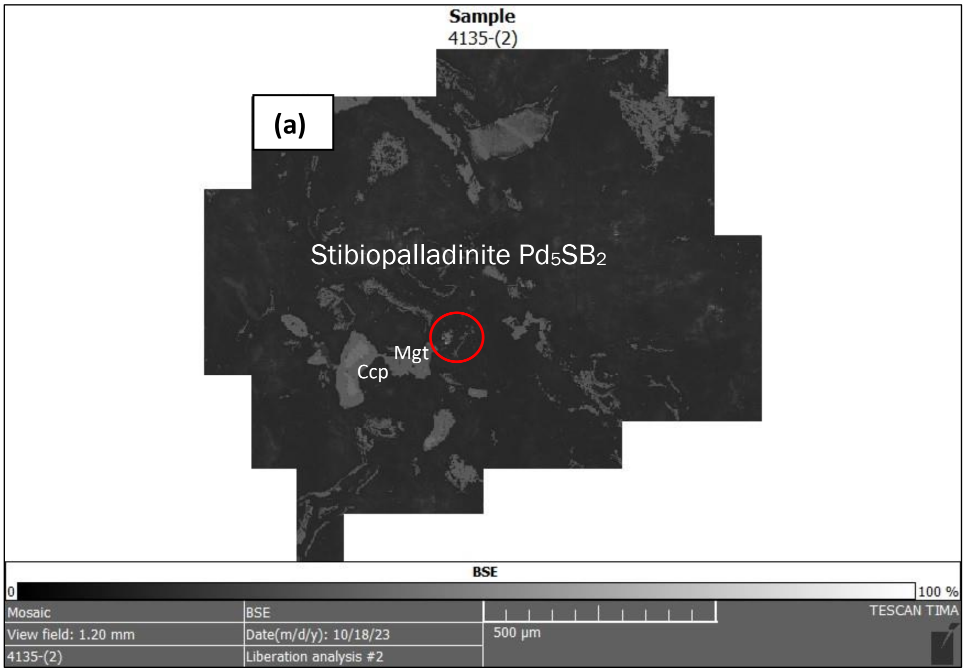

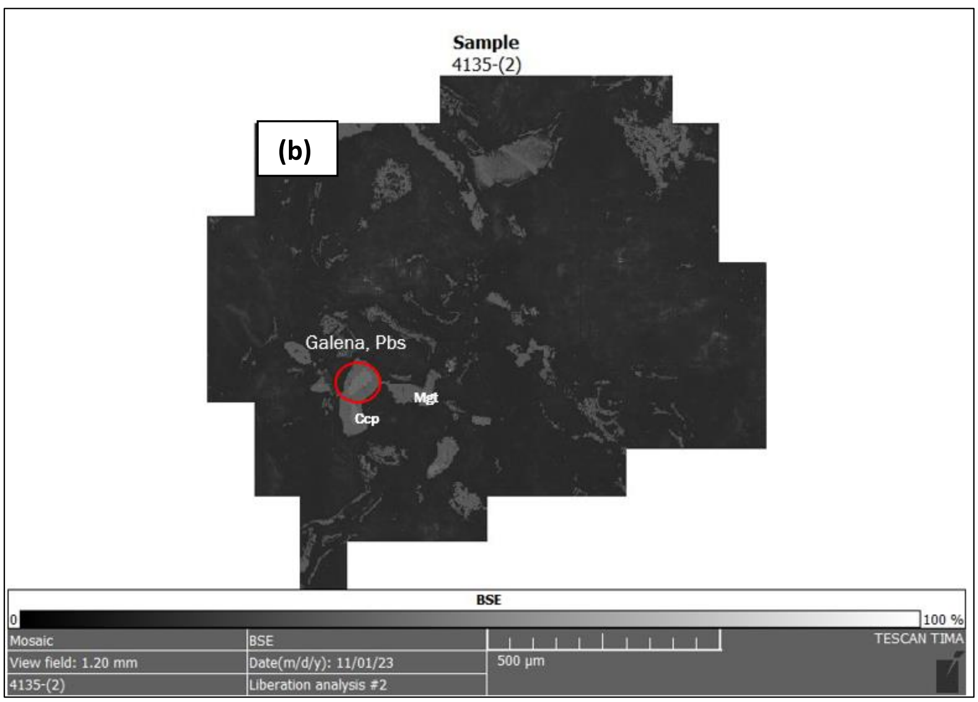

Fig. 33: Back-scattered electron images for sample 4/4135, serpentinite (altered dunite) from borehole KNDB002 (413.29 m to 413.67 m) **(a)** A grain of stibiopalladinite hosted in Pn, **(b)** A grain of galena at the grain boundary between Ccp and Mgt with the silicate matrix in black.

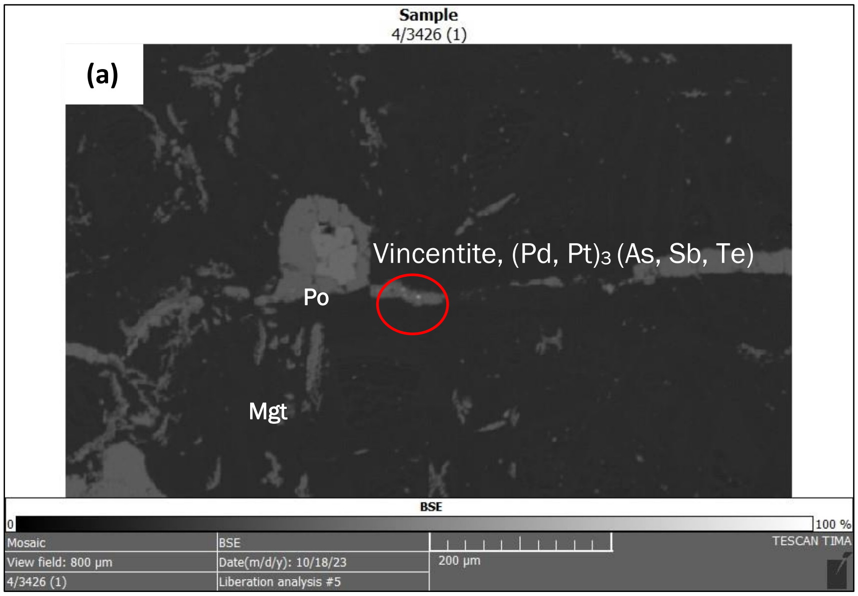

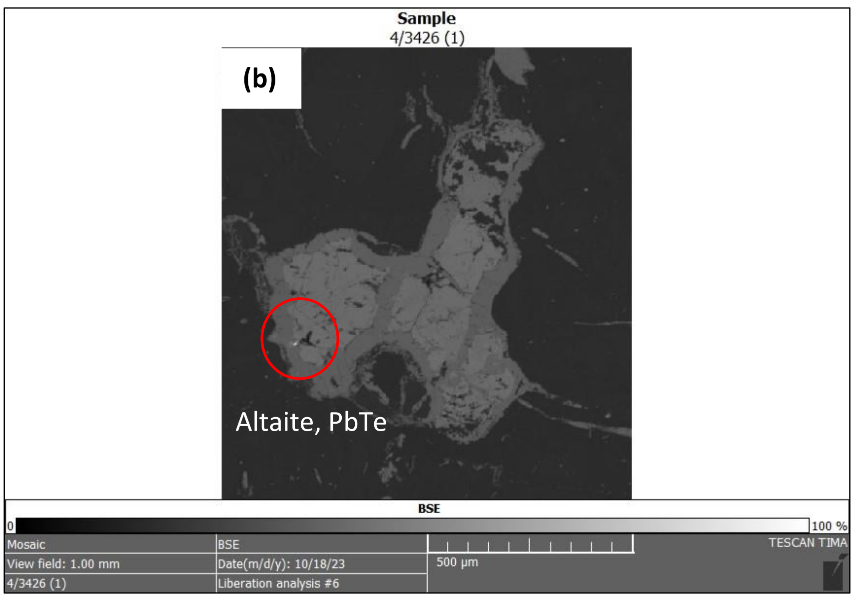

Fig. 34: Back-scattered electron images for sample 4/3426, altered harzburgite from borehole KNDB004 (341.93 m to 342.86 m). **(a)** A grain of vincentite hosted in Pn, **(b)** A grain of altaite at the boundary between Pn and Mgt within the black silicate matrix.

CHAPTER 5: DISCUSSION

5.1. The magmatic sulphide assemblage at Ombuku North

Magmatic sulphide minerals like chalcopyrite, pyrrhotite, and pentlandite, often associated with PGE are present in the mafic-ultramafic intrusions peripheral to the Kunene Complex (KC). These sulphides are found enclosed in silicates and are commonly replaced by secondary magnetite in altered rocks (**Fig. 15**, **Fig. 16**, **Fig. 19**, **Fig. 20**, **Fig. 23**, and **Fig. 24**). Pyrrhotite and pentlandite are predominant as the main primary sulphides phases, occurring as coarse grains, with magnetite frequently overprinting pentlandite. Highly altered rocks are mainly composed of serpentinised olivine with significant secondary magnetite. The PGMs are clearly associated with sulphides and oxides, with this mineralisation significantly influenced by late hydrothermal processes. This significantly contributed to the redistribution of the PGMs.

5.2. Ombuku North intrusion and its platinum group minerals association

PGMs were identified in samples 4/2833, 4/4400, 4/595, 4/4135 and 4/3426 of the Ombuku North intrusion. The analysed samples are characterised by the dominance of platinum arsenides ($PtAs_2$), which appear as single crystals. The second occurrence of sperrylite is found alongside other PGM and is in hydrothermally altered dunite (**Fig. 31**). Sperrylite is present in most of the samples and is commonly observed enclosed in magnetite, within the sulphide assemblage, and at the grain boundary of sulphide-oxide. Palladium bismuthotellurides occur in pentlandite co-existing with olivine. A typical magmatic PGM, unrelated to secondary magnetite is shown in **Fig. 32.** Palladium and platinum are the main PGEs related to base metal sulphides, which implies a high partition coefficient of these two elements into the ISS (Cu-rich residual liquid). The exsolution of ISS and MSS at relatively low temperatures (200 – 700 °C), resulted in Pt and Pd bonding with semi-metals (As, Te, Bi, and Pb) to form PGM (for example sperrylite and michenerite).

Within these rocks, the PGMs are also associated with Sb, As, Bi, Te, Pb, and Au, which indicates that these elements existed before the differentiation of the magmatic sulphide liquid (Zaccarini et al., 2022). Hydrothermal fluids that caused the serpentinisation modified the PGM assemblage by hydrothermal fluids that caused the serpentinisation modified the PGM assemblage in these rocks without changing the whole rock magmatic PGE contents within the mafic and ultramafic rocks. Some of the PGMs are hosted by oxides (**Fig. 30**, **Fig. 31** and **Fig. 34**) and this is attributed to a further intense alteration stage in the low-temperature genesis of the PGMs (Gunn and Shaw, 1991). These PGMs mainly occur in altered ultramafic rocks (serpentinite), indicating that the distribution is attributed to the alteration processes. Tiny and polygonal PGM at the grain boundaries of the sulphides have been identified (**Fig. 30** and **Fig. 34**). The occurrence of metal-rich base metal sulphides indicates that the PGMs were derived from metal-rich sulphide melt (Naldrett et al., 2000) and were later remobilised by hydrothermal fluids.

Lead sulphide (galena), lead sulphate (anglesite), lead telluride (altaite) also occur in Ombuku North (**Fig. 31**, **Fig. 34** and **Fig. 35**). Elements such as Pt, Pd, Ag, As, Bi, Cd, Sb, Sn, Te, Pb and Zn are incompatible in MSS, and they prefer to concentrate in the residual Cu-rich liquid and the amount of these semi-metals in the melt determines if the PGM crystallises at higher temperatures or are hosted by base metal sulphides and later exsolved as PGM (Dare et al., 2010). As observed in this study, PGMs are predominantly hosted by BMS, and they occur at the grain boundary of sulphides and silicates and are included in oxides. According to the schematic model for distribution of the PGM by Dare et al (2010), the PGM that crystallises at high temperatures (e.g., platinum arsenides such as sperrylite) are hosted by sulphides. Sperrylites observed in Ombuku North are hosted either by a sulphide-oxide assemblage or solely oxide, suggesting that they have been remobilised by hydrothermal fluids. Sulphides control the distribution and occurrence of PGEs and related chalcophile elements within the mafic-ultramafic intrusions (Macheyeki et al., 2020, Maier et al., 2023).

Figure 35 illustrates the relationship of chalcophile elements with sulphur. Cu and Au in the mafic-ultramafic intrusions exhibits good correlation with sulphur (**Fig. 35 b**) and most of the samples have high sulphur contents (>1000 ppm) and high Cu, due to presence of Cu-rich sulphides (Dare et al., 2010; Maier et al., 2023). Other chalcophile elements (Au, Bi, As) in **Fig. 35 b**, **c** and **d** also show a good correlation. The combined enrichment of PGE and Bi suggests that the distribution of the PGEs are associated with bismuthides. The identified PGM assemblage of vincentite $(Pd, Pt)_3 (As, Sb, Te)$, sperrylite ($PtAs_2$), michenerite (PdBiTe), stibiopalladinite (Pd_5Sb_2) also confirm that the PGEs are associated with antimonides, tellurides and arsenides phases.

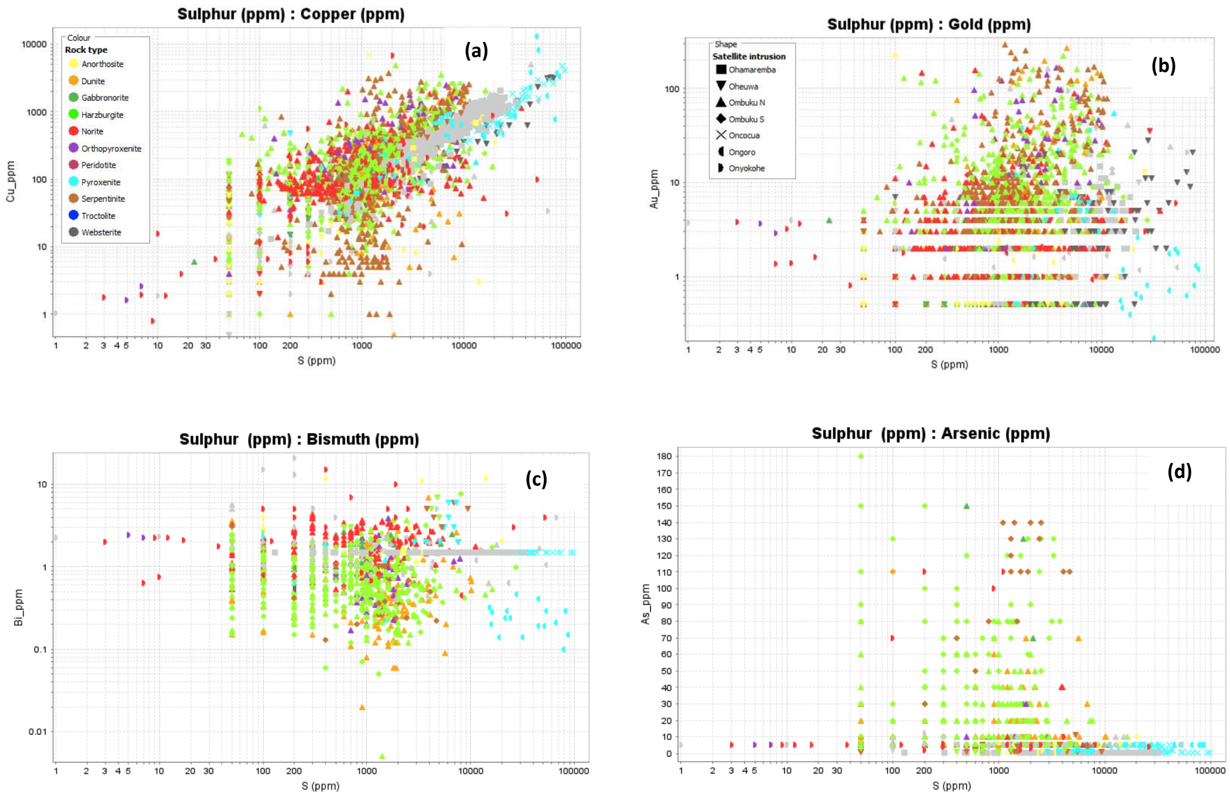

Fig. 35: Binary variation diagrams of chalcophile metals versus sulphur. The correlation of chalcophile elements with sulphur are an important indicator of sulphur contribution for PGE mineralisation.

The presence of PGM mineralisation can be attributed to both its initial formation through magmatic processes and subsequent remobilisation during late-stage hydrothermal activity. The occurrence of PGMs as identified in this study are associated with palladium bismuthotellurides suggesting that the mineralisation is attributed to the magmatic process and implies that the mineralisation was also hydrothermally upgraded. Palladium is more mobile than platinum during secondary hydrothermal process, i.e., hydrothermal fluids tend to remove palladium resulting in positive palladium anomalies over platinum (Mogessie et al., 2000).

The observed PGM mineralisation from the whole rock geochemical data of Ombuku North shows positive palladium concentration, indicating that the mineralisation may have been influenced by the hydrothermal process. Vincentite occurs as an individual grain and co-exists with sperrylite, indicating that vincentite identified in the sample has been hydrothermally mobilised. Palladium bismuthotelluride mineralisation occurs as inclusions in pentlandite and its presence in pentlandite implies that it was primarily concentrated during the cooling of a parental sulphide liquid (Ripley and Chryssoulis, 1994).

However, the association of PGMs with elements such as Bi, Sb, and Te suggests that these PGMs are the products of secondary remobilisation (Rowell and Edgar, 1986; Distler et al., 2000, Augé et al., 2002).

5.3. PGE enrichment and the potential mineral system

The assessment of the PGE economic potential will be locally restricted to Ombuku North. Typically, economic PGE deposits contain an average platinum grade of 5 – 10 gram per ton (Macdonald, 1987). Within these MUM rocks of the KC, the highest PGE values generally correlates with high Ni and Cu values and show a good correlation between Pd and Pt values (> 100 ppb) and Au, which is attributed to the potential hydrothermal redistribution and concentration of the PGE and Au by hydrothermal processes (**Fig. 27 a, b, c, d, g and h**).

The Cu/Pd ratio versus Pd, and the R-factor of the mafic-ultramafic intrusion peripheral to the KC **(Fig. 36)** provides evidence that a sulphide liquid removed the residual chalcophile elements. The "R factor" is a measure of how much silicate magma interacts with sulphide liquid during the formation of magmatic sulphide deposits (Karykowski et al., 2017). It influences the concentration of chalcophile elements like copper (Cu) and palladium (Pd) in the sulphide liquid. A high R factor means that the sulphide liquid efficiently extracts Pd from a large amount of magma, leading to lower Cu/Pd ratios. Conversely, a low R factor results in less efficient extraction, leading to higher Cu/Pd ratios (Karykowski et al., 2017).

The highly serpentinised mafic-ultramafic rocks from the Ombuku North intrusion display high Pd values at low Cu/Pd ratios, suggesting the presence of a relatively PGE-rich magma. PGE-poor samples, predominately harzburgite, norite and websterite of the mafic-ultramafic intrusions plot at a high Cu/Pd ratio, suggesting that the sulphide liquid segregated from a PGE-depleted magma (Liu et al., 2012; Karykowski et al., 2017). The PGE enriched samples plot with a low Cu/Pd ratio (Barnes and Maier, 1999). The samples plotting in the low Cu/Pd region are the highly altered lithologies, mainly from Ombuku North. Most of the samples are within the primitive mantle region (i.e., within the mantle values) with an R-factor between 1000 and 10000, indicating that in the case of this minor group of samples, there was no sulphide segregation before emplacement (Liu et al., 2012). However, the highly altered lithologies of Ombuku North are characterised by higher R-factors, which implies high PGE tenors in sulphide were formed in this intrusion.

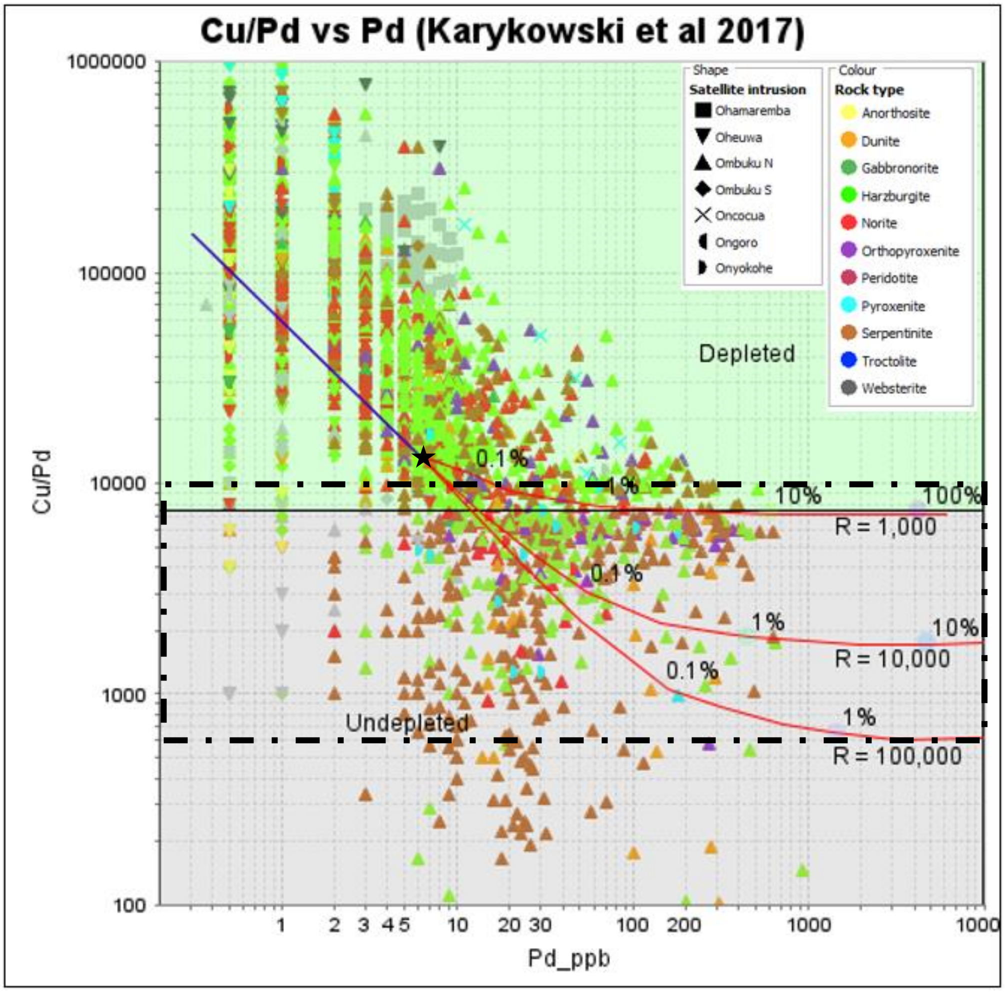

Fig. 36: A plot of Cu/Pd ratio versus Pd (ppb) of the mafic-ultramafic intrusions peripheral to the KC in the Zebra Lobe. The red lines indicate the model sulphides forming from the slightly metal-depleted melt at various R-factors. The diagram is divided into three parts showing the enriched and depleted region, with the primitive mantle region indicated by dashed lines.

The PGE enriched zones are mainly in dunite and serpentinite with some high Pd values within the norite, harzburgite and orthopyroxenite lithologies and there is a quite significant change in the Cu/Pd ratio downhole, through a series of various mafic-ultramafic rocks (**Fig. 37**). Furthermore, PGE enriched lithologies show Cu/Pd below that of primitive mantle values (800 – 10 000), indicating a PGE-fertile magma (Järvinen et al., 2020). Within the ultramafic zones (dunite, harzburgite, serpentinite), the Cu/Pd ratios remain generally low and significant peaks are observed within the mafic zone (norite).

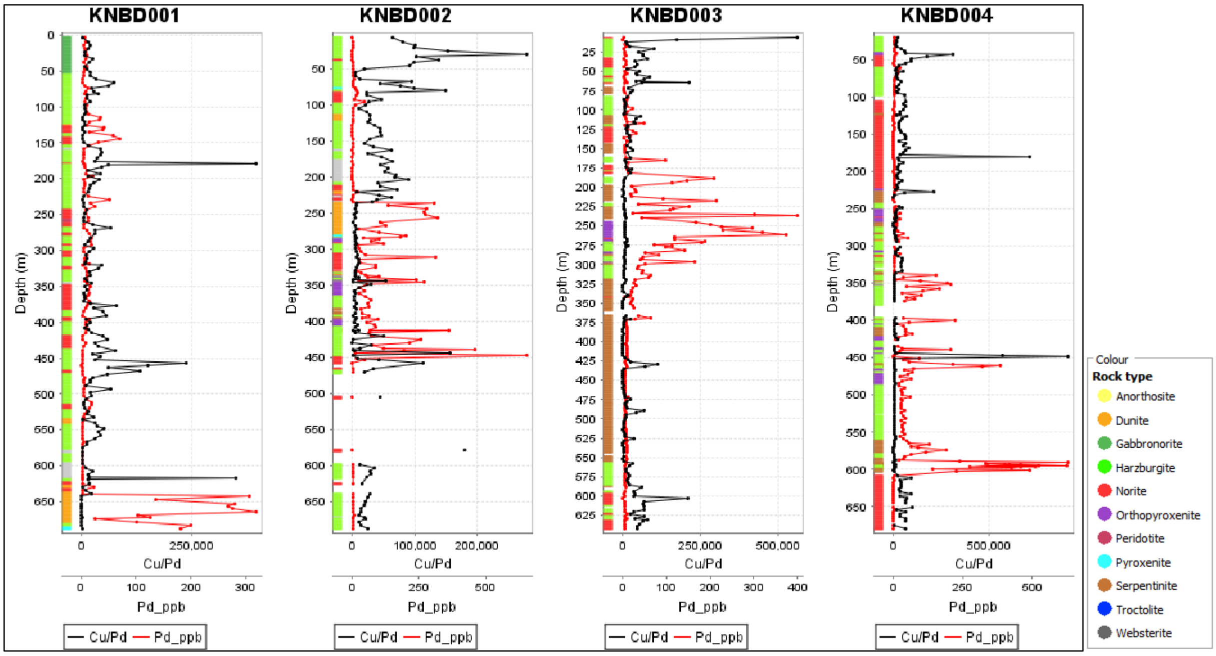

Fig. 37: Downhole plots for Ombuku North illustrating Cu/Pd ratio versus Pd. Columns on the left show lithologies intersected and Cu/Pd ratio in black and the Pd (ppb) is plotted in red. The gaps on the lithological logs represent locations where there was no sampling done.

5.4. A comparison between methods: Using a SEM-EDS and TIMA technique for identifying PGM in mafic-ultramafic rocks

In the previous research conducted by Ntuli (2022), SEM-EDS was used to identify PGMs in samples from the mafic-ultramafic intrusions peripheral to the KC in the Zebra Lobe. A total of seven thin sections (4/595, 4/2360, 4/4135, 4/4400, 4/4489, KSAT 280/159 and KSAT 280/169) were analysed with the SEM-EDS technique. The following samples (4/2833, 4/4400, 4/595, 4/4135, 4/3426, 4/4489, 4/2827 and 4/2802) were analysed in this study using TIMA. The three samples (4/595, 4/4400, and 4/4135) analysed also in Ntuli (2022) yielded similar results in terms of the PGM species. However, SEM-EDS identified PGM (sperrylite, moncheite, irarsite), lead telluride, and electrums in sample 4/4489, whereas the bright phase search method using TIMA on the same sample did not show bright spots which could be attributed to the resolution settings adopted in the TIMA mapping. TIMA is an automated analysis technique, but it also has technical limitations. The accuracy of mineral classification and quantification relies on the quality of the reference library and the settings used. Misclassification can happen if the reference library does not adequately cover the range of mineral species in the sample. Therefore, building a comprehensive mineral library is essential for this technique. Additionally, the size of the pixel affects the scanning and mineral mapping process. Smaller pixels can require more time for bright phase scanning and liberation analysis, and they can generate a large amount of data.

CHAPTER 6: CONCLUSION

The mafic-ultramafic intrusions peripheral to the Kunene AMCG Complex (KC) of southern Angola and northern Namibia are prospective magmatic Ni-Cu-(Co)-PGE sulphide deposits. These intrusions commonly contain magmatic sulphide assemblages including base metal sulphides such as pentlandite, pyrrhotite and chalcopyrite assemblage co-existing with magnetite. These sulphides are often overprinted by secondary magnetite. The majority of the samples with high PGEs values correspond with other metals such Ni, Cu, Co, and sulphur.

The analyses of the drillcore samples from the mafic-ultramafic rocks indicate that they can be relatively enriched in mantle-derived PGEs which were possibly redistributed by hydrothermal fluids. The discussed intrusions contain low PGE values, except for Ombuku North which is characterised by an anomalously high PGE content (> 80 ppb to up to 900 ppb) in whole rock, associated with highly altered lithologies such as serpentinite. This indicates potential PGE fertility for the Ombuku North intrusion. It is worth mentioning that even though there is limited analyses and low PGE values from the other six intrusions, a few anomalous values were obtained from Onyokohe and Oncocua. The concentrations of PGE at Ohamaremba, Ombuku South, Ongoro and Oheuwa are relatively low with the majority of values below 10 ppb. Specifically, the ranges for Pt are between 0.5 ppb and 40 ppb, while for Pd, they range from 0.02 ppb to 53 ppb.

In Ombuku North, three distinct groups of PGM compositions have been identified: platinum arsenides (sperrylite), palladium bismuthotellurides (michenerite, vincentite) and palladium antimonides (stibiopalladinite). The platinum arsenides are mainly hosted in magnetite and in pyrrhotite, the palladium bismuthotellurides and the palladium antimonide are hosted in pentlandite. The different phases of the PGM association are attributed to both magmatic and hydrothermal processes.

We suggest that the mineralisation of platinum arsenides in sulphides formed as result of fractional crystallisation of an immiscible sulphide melt and that sperrylite in magnetite is attributed to a late hydrothermal process that remobilised PGE from sulphide. The other Pd-Bi-Te arsenides associated with silicate phases (serpentinite) and secondary magnetite are evidence of hydrothermal remobilisation. The remobilisation of the PGE may be related to metasomatic processes during a high grade metamorphic event. Further work is recommended to better understand how these fluids could concentrate the PGE, as well as their mechanism of transport and mobilisation to determine the most prospective areas for economic exploration in the region. The evaluation of the PGE potential relies on limited data on Pt-Pd, and mostly from the Ombuku North intrusion. Further analyses of the full range of platinum group elements in all the intrusions are recommended. The ongoing field mapping and exploration in this region by Anglo American Discovery and Geosciences team and Principal investigators will hopefully contribute to a better understanding of metallogenesis in the Kunene Complex.

REFERENCES

Ashwal, L.D. and Twist, D., 1994. The Kunene complex, Angola/Namibia: a composite massif-type anorthosite complex. Geological Magazine, 131(5), pp.579-591.

Augé, T., Salpeteur, I., Bailly, L., Mukherjee, M.M. and Patra, R.N., 2002. Magmatic and hydrothermal platinum-group minerals and base-metal sulfides in the Baula complex, India. The Canadian Mineralogist, 40(2), pp.277-309.

Bai, Y., Tan, W. and Xing, J., 2023. Occurrence and magmatic origin of platinum-group minerals in the Hongge layered intrusion, SW China. Journal of Asian Earth Sciences, 255, p.105776.

Barnes, S.J. and Maier, W.D., 1999. The fractionation of Ni, Cu and the noble metals in silicate and sulphide liquids. Short Course Notes-Geological Association of Canada, 13, pp.69-106.

Barnes, S.J. and Maier, W.D., 2002. Platinum-group element distributions in the Rustenburg layered suite of the Bushveld Complex, South Africa.

Barnes, S.J., Staude, S., Le Vaillant, M., Piña, R. and Lightfoot, P.C., 2018. Sulfide-silicate textures in magmatic Ni-Cu-PGE sulfide ore deposits: Massive, semi-massive and sulfide-matrix breccia ores. Ore Geology Reviews, 101, pp.629-651.

Barnes, S.J. and Ripley, E.M., 2016. Highly siderophile and strongly chalcophile elements in magmatic ore deposits. Reviews in Mineralogy and Geochemistry, 81(1), pp.725-774.

Brandt, S. (2003). Metamorphic evolution of ultrahigh-temperature granulite facies and upper amphibolite facies rocks of the Epupa Complex, NW Namibia. Dr. rer. Nat. thesis, University of Würzburg.

Burlakovs, J., Vincevica-Gaile, Z., Krievans, M., Jani, Y., Horttanainen, M., Pehme, K.M., Dace, E., Setyobudi, R.H., Pilecka, J., Denafas, G. and Grinfelde, I., 2020. Platinum group elements in geosphere and anthroposphere: Interplay among the global reserves, urban ores, markets, and circular economy. Minerals, 10(6), p.558.

Bybee, G.M., Hayes, B., Owen-Smith, T.M., Lehmann, J., Ashwal, L.D., Brower, A.M., Hill, C.M., Corfu, F. and Manga, M., 2019. Proterozoic massif-type anorthosites as the archetypes of long-lived (≥ 100 Myr) magmatic systems—New evidence from the Kunene Anorthosite Complex (Angola). Precambrian Research, 332, p.105393.

Cabri, L.J, 1981. The platinum-group minerals.

Cabri, L.J., 1994. Current status of determination of mineralogical balances for platinum-group element-bearing ores. Transactions of the Institution of Mining and Metallurgy-Section B-Applied Earth Science, 103, p.B3.

Chistyakova, S., Latypov, R., Hunt, E.J. and Barnes, S., 2019. Merensky-type platinum deposits and a reappraisal of magma chamber paradigms. *Scientific Reports*, *9*(1), p.8807.

Dare, S.A., Barnes, S.J. and Prichard, H.M., 2010. The distribution of platinum group elements (PGE) and other chalcophile elements among sulfides from the Creighton Ni–Cu–PGE sulfide deposit, Sudbury, Canada, and the origin of palladium in pentlandite. Mineralium Deposita, 45, pp.765-793.

Distler, V.V., Yudovskaya, M.A., Prokof ev, V.Y., Sluzhenikin, S.F., Mokhov, A.V. and Mun, Y.V., 2000. Hydrothermal platinum mineralization of the Waterberg deposit (Transvaal, South Africa). GEOLOGY OF ORE DEPOSITS C/C OF GEOLOGIIA RUDNYKH MESTOROZHDENII, 42(4), pp.328-339.

Drüppel, K, VON SECKENDORFF, V. and Okrusch, M., 2001. Subsolidus reaction textures in the anorthositic rocks of the southern part of the Kunene Intrusive Complex, NW Namibia. European Journal of Mineralogy, 13(2), pp.289-309.

Drüppel, K., Littmann, S., Romer, R.L. and Okrusch, M., 2007. Petrology and isotope geochemistry of the Mesoproterozoic anorthosite and related rocks of the Kunene Intrusive Complex, NW Namibia. Precambrian Research, 156(1-2), pp.1-31.

Gleißner, P., Drüppel, K. and Taubald, H., 2010. Magmatic evolution of anorthosites of the Kunene Intrusive Complex, NW Namibia: Evidence from oxygen isotope data and trace element zoning. Journal of Petrology, 51(4), pp.897-919.

Gleißner, P., Drüppel, K. and Romer, R.L., 2011. The role of crustal contamination in massif-type anorthosites, new evidence from Sr–Nd–Pb isotopic composition of the Kunene Intrusive Complex, NW Namibia. Precambrian Research, 185(1-2), pp.18-36.

Green, T. and Peck, D., 2005. Platinum group elements exploration: economic considerations and geological criteria.

Gunn, A.G. and Shaw, M.H., 1991. Investigations for Cu-Ni and PGE in the Hill of Barra area, near Oldmeldrum, Aberdeenshire.

Hayes, B., Lehmann, J., Bybee, G.M. and Owen-Smith, T.M., 2022. Crystal transfer from magma to wallrock during syntectonic granite emplacement. Journal of the Geological Society, 179(1).

Helmy, H.M., Ballhaus, C., Berndt, J., Bockrath, C. and Wohlgemuth-Ueberwasser, C., 2007. Formation of Pt, Pd and Ni tellurides: experiments in sulfide–telluride systems. Contributions to Mineralogy and Petrology, 153, pp.577-591.

Holwell, B.D. and McDonald, I., 2010. A review of the behaviour of platinum group elements within natural magmatic sulfide ore systems. Platinum Metals Review, 54(1), pp.26-36.

Hornsey, R., 2020. Overview of Kunene Satellite Intrusions (internal unpublished report).

Hrstka, T., Gottlieb, P., Skala, R., Breiter, K. and Motl, D., 2018. Automated mineralogy and petrology-applications of TESCAN Integrated Mineral Analyzer (TIMA). Journal of Geosciences, 63(1), pp.47-63.

Järvinen, V., Halkoaho, T., Konnunaho, J., Heinonen, J.S. and Rämö, O.T., 2020. Parental magma, magmatic stratigraphy, and reef-type PGE enrichment of the 2.44-Ga mafic-ultramafic Näränkävaara layered intrusion, Northern Finland. Mineralium Deposita, 55(8), pp.1535-1560.

Jelsma, H.A., McCourt, S., Perritt, S.H. and Armstrong, R.A., 2018. The geology and evolution of the Angolan shield, Congo craton. Geology of Southwest Gondwana, pp.217-239.

Junge, M., Wirth, R., Oberthür, T., Melcher, F. and Schreiber, A., 2015. Mineralogical siting of platinum-group elements in pentlandite from the Bushveld Complex, South Africa. Mineralium Deposita, 50, pp.41-54.

Karykowski, B.T., Polito, P.A., Maier, W.D., Gutzmer, J. and Krause, J., 2017. New insights into the petrogenesis of the Jameson Range layered intrusion and associated Fe-Ti-PV-PGE-Au mineralisation, West Musgrave Province, Western Australia. Mineralium Deposita, 52, pp.233-255.

Lehmann, J., Bybee, G.M., Hayes, B., Owen-Smith, T.M. and Belyanin, G., 2020. Emplacement of the giant Kunene AMCG complex into a contractional ductile shear zone and implications for the Mesoproterozoic tectonic evolution of SW Angola. International Journal of Earth Sciences, 109(4), pp.1463-1485.

Liu, Q., Hou, Q., Xie, L., Li, H., Ni, S. and Wu, Y., 2012. Different origins of the fractionation of platinum-group elements in Raobazhai and Bixiling Mafic-ultramafic rocks from the Dabie Orogen, central China. Journal of Geological Research, 2012.

Macdonald, A.J., 1987. Ore deposit models# 12. The platinum group element deposits: classification and genesis. Geoscience Canada.

Macheyeki, Athanas Simon, Xiaohui Li, D. P. Kafumu, and F. Yuan. "Elements of exploration geochemistry." Applied Geochemistry: Advances in Mineral Exploration Techniques (2020): 1-43.

Mansur, E.T., Barnes, S.J., Duran, C.J. and Sluzhenikin, S.F., 2020. Distribution of chalcophile and platinum-group elements among pyrrhotite, pentlandite, chalcopyrite and cubanite from the Noril'sk-Talnakh ores: Implications for the formation of platinum-group minerals. *Mineralium Deposita*, *55*, pp.1215-1232.

Maier, W.D., 2005. Platinum-group element (PGE) deposits and occurrences: Mineralization styles, genetic concepts, and exploration criteria. Journal of African Earth Sciences, 41(3), pp.165-191.

Maier, W.D., Rasmussen, B., Fletcher, I.R., Li, C., Barnes, S.J. and Huhma, H., 2013. The Kunene anorthosite complex, Namibia, and its satellite intrusions: geochemistry, geochronology, and economic potential. Economic Geology, 108(5), pp.953-986.

Maier, W.D., Barnes, S.J. and Smith, W.D., 2023. Petrogenesis of the Mesoarchaean Stella layered intrusion, South Africa: implications for the origin of PGE reefs in the upper portion of layered intrusions. Mineralium Deposita, 58(8), pp.1477-1497.

Mayer, A., Hofmann, A.W., Sinigoi, S. and Morais, E., 2004. Mesoproterozoic Sm–Nd and U–Pb ages for the Kunene anorthosite complex of SW Angola. Precambrian Research, 133(3-4), pp.187-206.

McCourt, S., Armstrong, R.A., Jelsma, H. and Mapeo, R.B.M., 2013. New U–Pb SHRIMP ages from the Lubango region, SW Angola: insights into the Palaeoproterozoic evolution of the Angolan Shield, southern Congo Craton, Africa. Journal of the Geological Society, 170(2), pp.353-363.

Menge, G.F., 1998. The antiformal structure and general aspects of the Kunene Complex, Namibia. Zeitschrift der Deutschen Geologischen Gesellschaft, pp.431-448.

Milani, L., Lehmann, J., Bybee, G.M., Hayes, B., Owen-Smith, T.M., Oosthuizen, L., Delport, P.W. and Ueckermann, H., 2022. Geochemical and geochronological constraints on the Mesoproterozoic Red Granite Suite, Kunene AMCG Complex of Angola, and Namibia. Precambrian Research, 379, p.106821.

Milani, L., Oosthuizen, L., Owen-Smith, T.M., Bybee, G.M., Hayes, B., Lehmann, J., H.A, Jelsma.,2024. Magnetite geochemistry as a proxy for metallogenic processes: A study on sulfde-mineralized mafc–ultramafic intrusions peripheral to the Kunene Complex in Angola and Namibia.

Mogessie, A., Hauzenberger, C.A., Hoinkes, G., Felfernig, A., Stumpfl, E.F., Bjerg, E.A. and Kostadinoff, J., 2000. Genesis of platinum-group minerals in the Las Aguilas mafic-ultramafic rocks, San Luis Province, Argentina: textural, chemical, and mineralogical evidence. Mineralogy and Petrology, 68, pp.85-114.

Mudd, G.M., Jowitt, S.M. and Werner, T.T., 2018. Global platinum group element resources, reserves and mining–A critical assessment. Science of the Total Environment, 622, pp.614-625.

Mungall, J.E., 2005. Magmatic geochemistry of the platinum-group elements.

Naldrett, A.J., Keats, H., Sparkes, K., Moore, R. and McKenzie, C., 1997. Voisey's Bay, Canada: Implications for Exploration. Minerals industry international, (1034), pp.66-70.

Naldrett, A.J., Singh, J., Krstic, S. and Li, C., 2000. The mineralogy of the Voisey's Bay Ni-Cu-Co deposit, northern Labrador, Canada: Influence of oxidation state on textures and mineral compositions. Economic Geology, 95(4), pp.889-900.

Naumov, 2010, A geological profile (W-E direction) through boreholes KNAD001 and KNAD002 of Ohamaremba intrusion (unpublished).

Ntuli, N., 2022 Characterisation of Platinum Group Elements in mafic/ultramafic intrusions peripheral to the Kunene Complex in Angola and Namibia(unpublished).

O'Driscoll, B. and González-Jiménez, J.M., 2016. Petrogenesis of the platinum-group minerals. Reviews in Mineralogy and Geochemistry, 81(1), pp.489-578.

Peregoedova, A.V., 1998. The experimental study of the Pt–Pd–partitioning between monosulphide solid solution and Cu–Ni–sulfide melt at 900–840 C. In The 8th International Platinum Symposium (pp. 325-373).

Rao, C.R.M. and Reddi, G.S., 2000. Platinum group metals (PGM); occurrence, use and recent trends in their determination. TrAC Trends in Analytical Chemistry, 19(9), pp.565-586.

Rey-Moral, C., Mochales, T., Martínez, E.M., Lobón, J.L.G., Bahut, M.T.L., Martín-Banda, R., Feria, M.C., Ballesteros, D., Machadinho, A. and Alves, D., 2022. Recording the largest gabbro-anorthositic complex worldwide: The Kunene Complex (KC), SW Angola. Precambrian Research, 379, p.106790.

Ripley, E.M. and Chryssoulis, S.L., 1994. Ion microprobe analysis of platinum-group elements in sulfide and arsenide minerals from the Babbitt Cu-Ni deposit, Duluth Complex, Minnesota. Economic Geology, 89(1), pp.201-210.

Rowell, W.F. and Edgar, A.D., 1986. Platinum-group element mineralization in a hydrothermal Cu-Ni sulfide occurrence, Rathbun Lake, northeastern Ontario. Economic Geology, 81(5), pp.1272-1277.

Selfe, 2003 Oncocua write up-Oncocua (Angola) Project. unpublished Anglo American internal report.

Smuts, J., 1998. Situation Report – Oncocua (Angola) Project. Unpublished Internal Report, Anglo American Prospecting services (Proprietary) Limited, Southern Africa Business Office, Reference: 13/103/5048a/UNI/98/0317.

Van der Mescht, 2023. ANL+Investor+Presentation+29+March+2023.pdf (squarespace.com)

Van Zyl, A.C., 2022. Geochemistry and geochronology of the peripheral intrusions to the Kunene Anorthosite Complex in southern Angola and northern Namibia. MSc thesis, unpublished.

Zaccarini, F., Economou-Eliopoulos, M., Kiseleva, O., Garuti, G., Tsikouras, B., Pushkarev, E. and Idrus, A., 2022. Platinum Group Elements (PGE) Geochemistry and Mineralogy of Low Economic Potential (Rh-Pt-Pd)-Rich Chromitites from Ophiolite Complexes. Minerals, 12(12), p.1565.

(https://cimera.co.za/kunene-complex/), accessed 1 June 2024

Appendix A: Summary of assay data, including PGE analyses.

Oncocua intrusion							
Sampe ID	ONC-1 0008						
East	333836						
South	8151534						
Depth from	78.75						
Depth to	80.35						
Interval	1.6						
Rock type	Pyroxenite						
Ag (ppm)		**Fe (ppm)**	166261	**Ni (ppm)**	682	**Te (ppm)**	<20
Au(ppb)		**Ga (ppm)**	<20	**P (ppm)**	14686	**Th (ppm)**	<20
Al (ppm)	2558	**Ge (ppm)**	<20	**Pb (ppm)**	12	**Tl (ppm)**	<20
As (ppm)	4	**Hf (ppm)**	<5	**Pd (ppb)**	85	**Ti (ppm)**	553
B (ppm)	11	**In (ppm)**	<10	**Pt (ppb)**	-	**U (ppm)**	<20
Ba (ppm)	27	**K (ppm)**	791	**Rb (ppm)**	<1	**V (ppm)**	70
Be (ppm)	<1	**La (ppm)**	85	**S (ppm)**	34596	**W (ppm)**	24
Bi (ppm)	<10	**Li (ppm)**	<1	**Sb (ppm)**	<10	**Y (ppm)**	100
Ca (ppm)	95907	**Mg (ppm)**	33267	**Sc (ppm)**	4	**Zn (ppm)**	80
Cd (ppm)	<1	**Mn (ppm)**	1246	**Se (ppm)**	<10	**Zr (ppm)**	6
Co (ppm)	223	**Mo (ppm)**	4	**Sr (ppm)**	206	**Cu/Cu+Ni**	683
Cr (ppm)	37	**Na (ppm)**	267	**Sn (ppm)**	<2	**2PGE+Au_ppb**	85
Cu (ppm)	1327	**Nb (ppm)**	<20	**Ta (ppm)**	207	**Pt+Pd (pbb)**	85
Total Pd Analyses	6						
Total Pt Analyses	0						
Total PGE Analyses > 80 ppb	1						

Onyokohe intrusion			
Sampe ID	KNDD001	**Sampe ID**	KNV007
UTM33K East	321976	**UTM33K East**	321470
UTM33K South	8097190	**UTM33K South**	8099580
Depth from	177	**Depth from**	104.2
Depth to	177.7	**Depth to**	106.05
Interval	0.7	**Interval**	1.85
Rock type	Pyroxenite	**Rock type**	Troctolite
Au(ppb)	3	**Au(ppb)**	2
As (ppm)	-	**As (ppm)**	5
Bi (ppm)	-	**Bi (ppm)**	2
Co (ppm)	64	**Co (ppm)**	47
Cr (ppm)		**Cr (ppm)**	390
Cu(ppm)	643	**Cu(ppm)**	701
Ni (ppm)	441	**Ni (ppm)**	39
Pd (ppb)	104	**Pd (ppb)**	-
Pt (ppb)	42	**Pt (ppb)**	710
S (ppm)	9400	**S (ppm)**	1300
Sb (ppm)	-	**Sb (ppm)**	<dl
Te (ppm)	-	**Te (ppm)**	-
2PGE+Au_ppb	149	**2PGE+Au_ppb**	712
Pt+Pd (pbb)	146	**Pt+Pd (pbb)**	710
Total Pd Analyses	70		
Total Pt Analyses	139		
Total PGE Analyses > 80 ppb	2		

Intrusion	Ombuku N	Ombuku N	Ombuku N	Ombuku N	Ombuku N	Ombuku N	Ombuku N	Ombuku N	Ombuku N	Ombuku N	Ombuku N	Ombuku N
Sampe ID	KNBD001	KNBD001	KNBD001	KNBD001	KNBD001	KNBD001	KNBD001	KNBD001	KNBD001	KNBD001	KNBD001	KNBD002
UTM33K East	321337	321337	321337	321337	321337	321337	321337	321337	321337	321337	321337	321337
UTM33K South	8092107	8092107	8092107	8092107	8092107	8092107	8092107	8092107	8092107	8092107	8092107	8092107
Depth from	640.4	644.9	650.19	655.3	656.75	661.45	666	671	676	680	684.85	234.99
Depth to	644.9	650.19	655.3	656.75	661.45	666	671	672.55	680	684.85	689.72	239
Interval	4.01	2.2	5	5	3.13	5.32	5.35	5	4.77	3.46	0.5	4.01
Rock type	Dunite	Dunite	Dunite	Dunite	Dunite	Dunite	Dunite	Dunite	Dunite	Harzburgite	Pyroxenite	Dunite
Au(ppb)	2	1			4	4	1	2	2	2	5	148
As (ppm)	-	-	-	-	-	-	-	-	-	-	-	-
Bi (ppm)	-	-	-	-	-	-	-	-	-	-	-	-
Co (ppm)	28	17	13	1	94	101	95	53	105	108	59	147
Cr (ppm)	1949	868	1564	1834	1044	1387	197	682	339	943	1033	
Cu(ppm)	31	72	24	7	52	31	5	132	18	21	180	1949
Ni (ppm)	77	41	26	4	1348	1506	1489	549	1542	1373	691	4505
Pd (ppb)	306	136	280	268	276	319	104	126	102	201	181	306
Pt (ppb)	253	107	222	233	223	265	90	99	84	160	112	253
S (ppm)	9069	5054	6963	8010	4814	5789	2943	3805	3396	5132	13189	9069
Sb (ppm)	-	-	-	-	-	-	-	-	-	-	-	-
Te (ppm)	-	-	-	-	-	-	-	-	-	-	-	-
2PGE+Au_ppb	561	244	502	501	503	588	195	227	188	363	298	707
Pt+Pd (pbb)	559	243	502	501	499	584	194	225	186	361	293	559

Intrusion	Ombuku N	Ombuku N	Ombuku N	Ombuku N	Ombuku N	Ombuku N	Ombuku N	Ombuku N	Ombuku N	Ombuku N	Ombuku N	Ombuku N	Ombuku N
Sampe ID	KNBD002	KNBD002	KNBD002	KNBD002	KNBD002	KNBD002	KNBD002	KNBD002	KNBD002	KNBD002	KNBD002	KNBD002	KNBD002
UTM33K East	321337	321337	321337	321337	321337	321337	321337	321337	321337	321337	321337	321337	321337
UTM33K South	8092107	8092107	8092107	8092107	8092107	8092107	8092107	8092107	8092107	8092107	8092107	8092107	8092107
Depth from	239	241.2	246.2	251.2	254.33	259.65	265	274.75	279.52	282.98	284.7	291.82	310.1
Depth to	241.2	246.2	251.2	254.33	259.65	265	270	279.52	282.98	283.48	286.95	293.05	312.75
Interval	2.2	5	5	3.13	5.32	5.35	5	4.77	3.46	0.5	2.25	1.23	2.65
Rock type	Dunite	Dunite	Dunite	Dunite	Dunite	Dunite	Dunite	Dunite	Harzburgite	Pyroxenite	Orthopyroxenite	Norite	Norite
Au(ppb)	52	113	130	117	123	33	38	27	79	55	2	4	4
As (ppm)	-	-	-	-	-	-	-	-	-	-	-	-	-
Bi (ppm)	-	-	-	-	-	-	-	-	-	-	-	-	-
Co (ppm)	114	147	138	101	145	98	102	109	118	144	71	45	83
Cr (ppm)	-	-	-	-	-	-	-	-	-	-	592	780	2112
Cu(ppm)	868	1564	1834	1044	1387	197	682	339	943	1033	592	780	2112
Ni (ppm)	2994	3975	4515	3457	3943	2432	2613	2406	3165	4325	1735	1447	3509
Pd (ppb)	136	280	268	276	319	104	126	102	201	181	103	116	313
Pt (ppb)	107	222	233	223	265	90	99	84	160	112	74	78	242
S (ppm)	5054	6963	8010	4814	5789	2943	3805	3396	5132	13189	3162	3024	10303
Sb (ppm)	-	-	-	-	-	-	-	-	-	-	-	-	-
Te (ppm)	-	-	-	-	-	-	-	-	-	-	-	-	-
2PGE+Au_ppb	295	615	631	616	707	227	263	213	440	348	179	198	559
Pt+Pd (pbb)	243	502	501	499	584	194	225	186	361	293	177	194	555

Intrusion	Ombuku N	Ombuku N	Ombuku N	Ombuku N	Ombuku N	Ombuku N	Ombuku N	Ombuku N	Ombuku N	Ombuku N	Ombuku N	Ombuku N	Ombuku N
Sampe ID	KNBD002	KNBD002	KNBD002	KNBD002	KNBD002	KNBD002	KNBD002	KNBD002	KNBD002	KNBD002	KNBD002	KNBD002	KNBD002
UTM33K East	321337	321337	321337	321337	321337	321337	321337	321337	321337	321337	321337	321337	321337
UTM33K South	8092107	8092107	8092107	8092107	8092107	8092107	8092107	8092107	8092107	8092107	8092107	8092107	8092107
Depth from	319.65	323.8	336.89	341.93	344.47	396.55	404	406.4	413.29	422.8	427.1	435.56	439.62
Depth to	323.8	328.3	338	342.86	346.2	399.05	406.4	411.45	413.67	427.1	431.7	439.62	440.26
Interval	4.15	4.5	1.11	0.93	1.73	2.5	2.4	5.05	0.38	4.3	4.6	4.06	0.64
Rock type	Norite	Norite	Harzburgite	Harzburgite	Orthopyroxenite	Orthopyroxenite	Orthopyroxenite	Harzburgite	Harzburgite	Harzburgite	arzburgite	Harzburgite	Harzburgite
Au(ppb)	2	2	6	85	7	4	3	3	3	2	3	3	2
As (ppm)	-	-	-	-	-	-	-	-	-	-	-	-	-
Bi (ppm)	-	-	-	-	-	-	-	-	-	-	-	-	-
Co (ppm)	46	48	37	55	42	98	97	84	75	89	108	137	79
Cr (ppm)	746	665	629	1379	1698	775	664	541	3547	2361	1471	745	2018
Cu(ppm)	746	665	495	401	157	512	775	399	541	287	17	1471	250
Ni (ppm)	1102	1030	691	1265	930	1848	2368	1792	1882	1906	2168	4023	2424
Pd (ppb)	89	88	100	239	269	95	86	89	362	259	216	118	460
Pt (ppb)	62	63	64	166	191	61	60	65	250	311	180	95	337
S (ppm)	3036	1794	1010	1702	905	2488	4083	2207	2487	1841	2082	6347	2865
Sb (ppm)	-	-	-	-	-	-	-	-	-	-	-	-	-
Te (ppm)	-	-	-	-	-	-	-	-	-	-	-	-	-
2PGE+Au_ppb	153	153	170	490	467	160	149	157	615	572	399	216	799
Pt+Pd (pbb)	151	151	164	405	460	156	146	154	612	570	396	213	797

Intrusion	Ombuku N	Ombuku N	Ombuku N	Ombuku N	Ombuku N	Ombuku N	Ombuku N	Ombuku N	Ombuku N	Ombuku N	Ombuku N	Ombuku N	Ombuku N
Sampe ID	KNBD002	KNBD002	KNBD012	KNBD003	KNBD003	KNBD003	KNBD003	KNBD003	KNBD003	KNBD003	KNBD003	KNBD003	KNBD003
UTM33K East	321337	321337	321537	321337	321337	321337	321337	321337	321337	321337	321337	321337	321337
UTM33K South	8092107	8092107	8092406	8092207	8092207	8092207	8092207	8092207	8092207	8092207	8092207	8092207	8092207
Depth from	440.26	445.42	391.55	187.63	189.6	193.1	213.9	216.8	224.24	226.72	227.73	234.51	236
Depth to	441.85	449.33	396.1	189.6	193.1	194.6	216.8	217.88	226.72	227.73	232.2	236	238.3
Interval	1.59	3.91	4.55	1.97	3.5	1.5	2.9	1.08	2.48	1.01	4.47	1.49	2.3
Rock type	Harzburgite	Harzburgite	Dunite	Harzburgite	Harzburgite	Harzburgite	Serpentinite	Serpentinite	Serpentinite	Serpentinite	Serpentinite	Serpentinite	Serpentinite
Au(ppb)	3	8	26	69	40	44	22	73	56	46	49	150	242
As (ppm)	-	-	5	-	-	-	-	-	-	-	-	-	-
Bi (ppm)	-	-	0.64	-	-	-	-	-	-	-	-	-	-
Co (ppm)	100	122	102	126	120	141	152	207	152	148	136	173	188
Cr (ppm)	1152	2022	25										
Cu(ppm)	745	1152	356	1068	443	465	469	1369	665	485	694	1704	2399
Ni (ppm)	2500	3306	2520	3263	2429	2530	2907	4250	3095	2729	2586	4791	5311
Pd (ppb)	195	653	296	209	148	112	92	215	151	115	109	301	399
Pt (ppb)	160	409	132	122	74	79	64	150	99	85	86	273	340
S (ppm)	3535	4983	2700	4084	1381	701	7648	6013	2565	2083	1231	1393	1325
Sb (ppm)	-	-	5	-	-	-	-	-	-	-	1800	-	-
Te (ppm)	-	-	-	-	-	-	-	-	-	-	273	-	-
2PGE+Au_ppb	358	1070	454	400	262	235	178	438	306	246	244	724	981
Pt+Pd (pbb)	355	1062	428	331	222	191	156	365	250	200	195	574	739

Intrusion	Ombuku N	Ombuku N	Ombuku N	Ombuku N	Ombuku N	Ombuku N	Ombuku N	Ombuku N	Ombuku N	Ombuku N	Ombuku N	Ombuku N	Ombuku N
Sampe ID	KNBD003	KNBD003	KNBD003	KNBD003	KNBD003	KNBD003	KNBD003	KNBD003	KNBD003	KNBD003	KNBD003	KNBD003	KNBD003
UTM33K East	321337	321337	321337	321337	321337	321337	321337	321337	321337	321337	321337	321337	321337
UTM33K South	8092207	8092207	8092207	8092207	8092207	8092207	8092207	8092207	8092207	8092207	8092207	8092207	8092207
Depth from	243.79	247.07	250.54	251.05	254	257	260	263	266.05	269.52	270.58	275	276
Depth to	247.07	250.54	251.05	254	257	260	263	266.05	269.52	270.58	273.3	276	279.5
Interval	3.28	3.47	0.51	2.95	3	3	3	3.05	3.47	1.06	2.72	1	3.5
Rock type	Orthopyroxenite	Orthopyroxenite	Orthopyroxenite	Orthopyroxenite	Orthopyroxenite	Orthopyroxenite	Orthopyroxenite	Orthopyroxenite	Norite	Orthopyroxenite	Harzburgite	Harzburgite	Harzburgite
Au(ppb)	75	82	76	122	98	142	166	57	57	41	39	113	64
As (ppm)	-	-	-	-	-	-	-	-	-	-	-	-	-
Bi (ppm)	-	-	-	-	-	-	-	-	-	-	-	-	-
Co (ppm)	92	79	67	90	78	104	119	70	63	145	113	168	103
Cr (ppm)	-	-	-	-	-	-	-	-	-	-	-	-	-
Cu(ppm)	925	1088	1361	1517	1391	1791	2248	804	1573	2430	1152	2117	1002
Ni (ppm)	2444	2309	2462	2847	2376	3547	3968	1621	1788	4920	2462	2783	1980
Pd (ppb)	168	200	226	297	229	320	374	118	119	189	180	112	98
Pt (ppb)	129	146	182	217	165	238	261	84	70	104	114	70	64
S (ppm)	3527	5845	1711	1075	3787	2942	3625	1586	7618	9945	2431	5145	5400
Sb (ppm)	-	-	-	-	-	-	-	-	-	-	-	-	-
Te (ppm)	-	-	-	-	-	-	--	-	-	-	-	-	-
2PGE+Au_ppb	372	428	484	636	492	700	801	259	246	334	333	295	226
Pt+Pd (pbb)	297	346	408	514	394	558	635	202	189	293	294	182	162

Intrusion	Ombuku N	Ombuku N	Ombuku N	Ombuku N	Ombuku N	Ombuku N	Ombuku N	Ombuku N	Ombuku N	Ombuku N	Ombuku N	Ombuku N	Ombuku N
Sampe ID	KNBD003	KNBD003	KNBD003	KNBD004	KNBD004	KNBD004	KNBD004	KNBD004	KNBD004	KNBD004	KNBD004	KNBD004	KNBD004
UTM33K East	321337	321337	321337	321337	321337	321337	321337	321337	321337	321337	321337	321337	321337
UTM33K South	8092207	8092207	8092207	8092007	8092007	8092007	8092007	8092007	8092007	8092007	8092007	8092007	8092007
Depth from	279.5	286.4	295.75	338.9	346.55	349.78	351.05	356.62	358.29	364.39	398.85	439.1	449.86
Depth to	283.33	289.4	297.42	341.35	348.1	351.05	352.88	358.29	361.52	367.54	400.63	439.8	452.01
Interval	3.83	3	1.67	2.45	1.55	1.27	1.83	1.67	3.23	3.15	1.78	0.7	2.15
Rock type	Harzburgite	Serpentinite	Orthopyroxenite	Harzburgite	Serpentinite	Harzburgite	Orthopyroxenite	Harzburgite	Harzburgite	Harzburgite	Serpentinite	Orthopyroxenite	Harzburgite
Au(ppb)	66	44	97	72	23	81	97	71	50	44	93	74	47
As (ppm)	-	-	-	-	-	-	-	-	-	-	-	-	-
Bi (ppm)	-	-	-	-	-	-	-	-	-	-	-	-	-
Co (ppm)	127	111	119	139	127	104	82	143	110	119	142	81	120
Cr (ppm)	-	-	-	-	-	-	-	-	-	-	-	-	-
Cu(ppm)	898	473	1193	822	501	1083	1354	1065	730	686	1363	1464	495
Ni (ppm)	2681	2306	2855	2165	2197	2468	2351	2965	2240	2352	3682	3269	2318
Pd (ppb)	141	83	164	154	99	196	208	168	107	100	222	207	94
Pt (ppb)	100	61	121	114	89	149	139	119	75	71	163	119	68
S (ppm)	5121	8015	3983	1295	1545	4117	586	5545	3457	6093	2498	1499	1337
Sb (ppm)	-	-	-	-	-	-	-	-	-	-	-	-	-
Te (ppm)	-	-	-	-	-	-	-	-	-	-	-	-	-
2PGE+Au_ppb	307	188	382	340	211	426	444	358	232	215	478	400	209
Pt+Pd (pbb)	241	144	285	268	188	345	347	287	182	171	385	326	162

Intrusion	Ombuku N	Ombuku N	Ombuku N	Ombuku N	Ombuku N	Ombuku N	Ombuku N	Ombuku N	Ombuku N	Ombuku N	Ombuku N	Ombuku N	Ombuku N
Sampe ID	KNBD004	KNBD004	KNBD004	KNBD004	KNBD004	KNBD004	KNBD004	KNBD004	KNBD004	KNBD004	KNBD004	KNBD004	KNBD004
UTM33K East	321337	321337	321337	321337	321337	321337	321337	321337	321337	321337	321337	321337	321337
UTM33K South	8092007	8092007	8092007	8092007	8092007	8092007	8092007	8092007	8092007	8092007	8092007	8092007	8092007
Depth from	457.97	459.92	460.49	565.7	569.83	572.95	576	588.7	590	591.8	593	593.5	594
Depth to	459.92	460.49	462.99	567.3	572.95	576	578.57	590	591.8	593	593.5	594	594.5
Interval	1.95	0.57	2.5	1.6	3.12	3.05	2.57	1.3	1.8	1.2	0.5	0.5	0.5
Rock type	Harzburgite	Serpentinite	Harzburgite	Serpentinite	Serpentinite	Serpentinite	Serpentinite	Serpentinite	Serpentinite	Serpentinite	Serpentinite	Serpentinite	Serpentinite
Au(ppb)	84	148	143	57	43	90	51	121	210	143	159	174	161
As (ppm)	-	-	-	-	-	-	-	-	-	-	-	-	-
Bi (ppm)	-	-	-	-	-	-	-	-	-	-	-	-	-
Co (ppm)	150	215	146	186	139	159	135	134	194	151	173	167	180
Cr (ppm)	-	-	-	-	-	-	-	-	-	-	-	-	-
Cu(ppm)	1365	2998	1943	571	48	334	55	945	1173	757	3184	1800	1692
Ni (ppm)	3092	4873	4117	3042	2396	2924	2424	3251	4723	3580	4793	5205	5213
Pd (ppb)	214	384	319	130	89	191	116	239	628	331	401	418	457
Pt (ppb)	133	243	224	70	65	134	86	168	426	238	266	385	332
S (ppm)	726	1366	9791	935	809	860	931	1315	1458	2449	1540	1832	2489
Sb (ppm)	-	-	-	-	-	-	-	-	-	-	-	-	-
Te (ppm)	-	-	-	-	-	-	-	-	-	-	-	-	-
2PGE+Au_ppb	431	775	686	257	197	415	253	528	1264	712	826	977	950
Pt+Pd (pbb)	347	627	543	200	154	325	202	407	1054	569	667	803	789

Intrusion	Ombuku N	Ombuku N	Ombuku N	Ombuku N	Ombuku N	Ombuku N	Ombuku N	Ombuku N	Ombuku N	Ombuku N	Ombuku N	Ombuku N	Ombuku N
Sampe ID	KNBD004	KNBD004	KNBD004	KNBD004	KNBD004	KNBD004	KNBD004	KNBD004	KNBD004	KNBD004	KNBD005	KNBD007	KNBD007
UTM33K East	321337	321337	321337	321337	321337	321337	321337	321337	321337	321337	321636	321136	321136
UTM33K South	8092007	8092007	8092007	8092007	8092007	8092007	8092007	8092007	8092007	8092007	8092906	8092118	8092118
Depth from	594.5	595	595.5	596	596.52	596.97	597.47	597.97	600.55	602.45	176.45	72	79.28
Depth to	595	595.5	596	596.52	596.97	597.47	597.97	600.55	602.45	603.43	178.73	74.4	82.2
Interval	0.5	0.5	0.5	0.52	0.45	0.5	0.5	2.58	1.9	0.98	2.28	2.4	2.92
Rock type	Serpentinite	Serpentinite	Serpentinite	Serpentinite	Harzburgite	Harzburgite	Harzburgite	Serpentinite	Serpentinite	Serpentinite	Serpentinite	Orthopyroxenite	Serpentinite
Au(ppb)	256	293	126	77	161	223	161	42	172	79	23	29	12
As (ppm)	-	-	-	-	-	-	-	-	-	-	-	-	-
Bi (ppm)	-	-	-	-	-	-	-	-	-	-	-	-	-
Co (ppm)	214	204	161	171	238	244	222	130	211	149	222	64	171
Cr (ppm)													
Cu(ppm)	3702	3097	2145	2061	4843	2658	2608	367	507	562	216	1266	787
Ni (ppm)	6074	5488	4425	4234	5402	5522	4967	2632	4291	2971	3375	1683	2690
Pd (ppb)	625	525	342	274	511	460	424	141	492	229	128	99	83
Pt (ppb)	444	352	244	221	333	318	271	100	378	197	79	48	42
S (ppm)	1837	1156	1023	2124	2158	4240	5720	4199	8384	7347	1090	3099	2464
Sb (ppm)	-	-	-	-	-	-	-	-	-	-	-	-	-
Te (ppm)	-	-	-	-	-	-	-	-	-	-	-	-	-
2PGE+Au_ppb	1325	1170	712	572	1005	1001	856	283	1042	505	230	176	137
Pt+Pd (pbb)	1069	877	586	495	844	778	695	241	870	426	207	147	125

Intrusion	Ombuku N	Ombuku N	Ombuku N	Ombuku N	Ombuku N	Ombuku N	Ombuku N	Ombuku N	Ombuku N	Ombuku N	Ombuku N	Ombuku N	Ombuku N
Sampe ID	KNBD007	KNBD007	KNBD007	KNBD007	KNBD007	KNBD007	KNBD007	KNBD007	KNBD007	KNBD007	KNBD007	KNBD007	KNBD007
UTM33K East	321136	321136	321136	321136	321136	321136	321136	321136	321136	321136	321136	321136	321136
UTM33K South	8092118	8092118	8092118	8092118	8092118	8092118	8092118	8092118	8092118	8092118	8092118	8092118	8092118
Depth from	84.4	106.15	107.32	110.35	112.9	119	120.95	123.82	126.7	130.22	131.17	133.28	135.35
Depth to	85.07	107.32	110.35	112.9	115.8	120.95	123.82	126.7	130.22	131.17	133.28	135.35	138.8
Interval	0.67	1.17	3.03	2.55	2.9	1.95	2.87	2.88	3.52	0.95	2.11	2.07	3.45
Rock type	Harzburgite	Harzburgite	Harzburgite	Harzburgite	Harzburgite	Harzburgite	Harzburgite	Harzburgite	Harzburgite	Harzburgite	Harzburgite	Serpentinite	Harzburgite
Au(ppb)	19	34	22	34	27	33	25	39	36	33	27	46	22
As (ppm)	-	-	-	-	-	-	-	-	-	-	-	-	-
Bi (ppm)	-	-	-	-	-	-	-	-	-	-	-	-	-
Co (ppm)	171	141	135	140	133	154	125	153	136	176	134	150	125
Cr (ppm)	-	-	-	-	-	-	-	-	-	-	-	-	-
Cu(ppm)	2270	1253	933	1142	1114	1564	1067	1662	1399	2014	1224	1890	969
Ni (ppm)	2889	2675	2364	2526	2443	2994	2292	3081	2585	3310	2414	3059	2228
Pd (ppb)	120	136	106	115	107	150	95	143	126	158	127	205	81
Pt (ppb)	51	54	44	49	51	66	38	57	49	57	48	84	35
S (ppm)	3637	2692	5459	4213	5013	3631	6653	4345	7206	5330	7850	5170	7300
Sb (ppm)	-	-	-	-	-	-	-	-	-	-	-	-	-
Te (ppm)	-	-	-	-	-	-	-	-	-	-	-	-	-
2PGE+Au_ppb	190	224	172	198	185	249	158	239	211	248	202	335	138
Pt+Pd (pbb)	171	190	150	164	158	216	133	200	175	215	175	289	116

Intrusion	Ombuku N	Ombuku N	Ombuku N	Ombuku N	Ombuku N	Ombuku N	Ombuku N	Ombuku N	Ombuku N	Ombuku N	Ombuku N	Ombuku N	Ombuku N
Sampe ID	KNBD007	KNBD007	KNBD007	KNBD007	KNBD007	KNBD007	KNBD007	KNBD007	KNBD007	KNBD007	KNBD007	KNBD010	KNBD010
UTM33K East	321136	321136	321136	321136	321136	321136	321136	321136	321136	321136	321136	321437	321437
UTM33K South	8092118	8092118	8092118	8092118	8092118	8092118	8092118	8092118	8092118	8092118	8092118	8092207	8092207
Depth from	138.8	141.47	143.26	144.85	145.44	145.95	146.82	149.96	151.32	227.53	260.73	114.08	116.4
Depth to	141.47	143.26	144.85	145.44	145.95	146.82	149.96	151.32	153.06	228.92	262.09	116.4	118.62
Interval	2.67	1.79	1.59	0.59	0.51	0.87	3.14	1.36	1.74	1.39	1.36	2.32	2.22
Rock type	Harzburgite	Harzburgite	Serpentinite	Serpentinite	Serpentinite	Serpentinite	Serpentinite	Serpentinite	Serpentinite	Harzburgite	Harzburgite	Harzburgite	Harzburgite
Au(ppb)	63	78	78	56	57	41	26	39	24	32	143	50	48
As (ppm)	-	-	-	-	-	-	-	-	-	-	-	-	-
Bi (ppm)	-	-	-	-	-	-	-	-	-	-	-	-	-
Co (ppm)	176	193	176	196	167	179	154	162	143	157	149	166	180
Cr (ppm)													
Cu(ppm)	2259	2703	2578	2344	2223	1406	1144	1685	1071	287	2186	1484	1877
Ni (ppm)	3729	4249	3876	4371	3609	3652	2554	2906	2327	2697	6115	3235	3746
Pd (ppb)	185	290	267	253	206	214	119	162	106	155	327	81	117
Pt (ppb)	63	109	99	79	79	84	45	61	41	111	234	45	66
S (ppm)	4101	9151	11305	10010	10227	9002	7201	5337	6988	1854	650	7124	8320
Sb (ppm)	-	-	-	-	-	-	-	-	-	-	-	-	-
Te (ppm)	-	-	-	-	-	-	-	-	-	-	-	-	-
2PGE+Au_ppb	311	477	444	388	342	339	190	262	171	298	704	176	231
Pt+Pd (pbb)	248	399	366	332	285	298	164	223	147	266	561	126	183

Intrusion	Ombuku N	Ombuku N	Ombuku N	Ombuku N	Ombuku N	Ombuku N	Ombuku N	Ombuku N	Ombuku N	Ombuku N	Ombuku N	Ombuku N	Ombuku N
Sampe ID	KNBD010	KNBD010	KNBD010	KNBD010	KNBD010	KNBD010	KNBD010	KNBD010	KNBD010	KNBD010	KNBD010	KNBD010	KNBD010
UTM33K East	321437	321437	321437	321437	321437	321437	321437	321437	321437	321437	321437	321437	321437
UTM33K South	8092207	8092207	8092207	8092207	8092207	8092207	8092207	8092207	8092207	8092207	8092207	8092207	8092207
Depth from	226.3	229.47	233.62	241.62	244.44	245.6	249.7	252.76	256.54	260.16	262.4	266.58	269.25
Depth to	226.97	231.65	234.82	244.44	245.6	246.78	252.76	253.96	257.92	262.4	264.3	269.25	270.74
Interval	0.67	2.18	1.2	2.82	1.16	1.18	3.06	1.2	1.38	2.24	1.9	2.67	1.49
Rock type	Norite	Harzburgite	Serpentinite	Serpentinite	Serpentinite	Serpentinite	Serpentinite	Serpentinite	Serpentinite	Serpentinite	Serpentinite	Orthopyroxenite	Serpentinite
Au(ppb)	48	55	78	43	60	119	78	74	42	44	88	46	168
As (ppm)	-	-	-	-	-	-	-	-	-	-	-	-	-
Bi (ppm)	-	-	-	-	-	-	-	-	-	-	-	-	-
Co (ppm)	62	72	181	168	147	187	161	171	125	165	129	87	179
Cr (ppm)	-	-	-	-	-	-	-	-	-	-	-	-	-
Cu(ppm)	1432	1120	1999	1140	1478	2186	1423	1421	495	695	1368	748	2082
Ni (ppm)	2120	1913	4187	3116	3508	4279	3391	4255	2233	3223	3129	2138	4974
Pd (ppb)	114	114	127	98	155	178	180	208	95	101	182	110	305
Pt (ppb)	91	93	107	80	117	147	150	164	70	78	139	83	249
S (ppm)	6134	6298	10502	5220	9372	10495	6284	6892	3040	4244	6738	9303	3892
Sb (ppm)	-	-	-	-	-	-	-	-	-	-	-	-	-
Te (ppm)	-	-	-	-	-	-	-	-	-	-	-	-	-
2PGE+Au_ppb	253	262	312	221	332	444	408	446	207	223	409	239	722
Pt+Pd (pbb)	205	207	234	178	272	325	330	372	165	179	321	193	554

Intrusion	Ombuku N	Ombuku N	Ombuku N	Ombuku N	Ombuku N	Ombuku N	Ombuku N	Ombuku N
Sampe ID	KNBD010	KNBD010	KNBD010	KNBD010	KNBD010	KNBD010	KNBD010	KNBD010
UTM33K East	321437	321437	321437	321437	321437	321437	321437	321437
UTM33K South	8092207	8092207	8092207	8092207	8092207	8092207	8092207	8092207
Depth from	270.74	278.89	280.45	281.5	282.56	283.88	285.15	286.19
Depth to	272.74	280.45	281.5	282.56	283.88	285.15	286.19	287.94
Interval	2	1.56	1.05	1.06	1.32	1.27	1.04	1.75
Rock type	Serpentinite	Serpentinite	Serpentinite	Serpentinite	Serpentinite	Serpentinite	Serpentinite	Serpentinite
Au(ppb)	119	161	122	108	39	59	137	37
As (ppm)	-	-	-	-	-	-	-	-
Bi (ppm)	-	-	-	-	-	-	-	-
Co (ppm)	147	181	182	194	157	166	201	139
Cr (ppm)	-	-	-	-	-	-	-	-
Cu(ppm)	1335	1917	1870	2017	819	1255	1783	562
Ni (ppm)	3800	4954	4982	5284	3299	4001	5332	3136
Pd (ppb)	216	324	246	279	115	206	350	98
Pt (ppb)	165	251	203	233	75	138	218	68
S (ppm)	10356	7337	5079	2971	10135	10292	9750	5478
Sb (ppm)	-	-	-	-	-	-	-	-
Te (ppm)	-	-	-	-	-	-	-	-
2PGE+Au_ppb	500	736	571	620	229	403	705	203
Pt+Pd (pbb)	381	575	449	512	190	344	568	166

Intrusion	Ombuku N	Ombuku N	Ombuku N	Ombuku N	Ombuku N	Ombuku N	Ombuku N	Ombuku N	Ombuku N
Sampe ID	KNBD010	KNBD010	KNBD010	KNBD010	KNBD010	KNBD010	KNBD010	KNBD010	KNBD010
UTM33K East	321437	321437	321437	321437	321437	321437	321437	321437	321437
UTM33K South	8092207	8092207	8092207	8092207	8092207	8092207	8092207	8092207	8092207
Depth from	287.94	290.75	292.55	301.6	304.91	306	313.6	315.87	318.56
Depth to	290.75	292.55	294.5	304.91	306	310.4	315.87	318.56	319.67
Interval	2.81	1.8	1.95	3.31	1.09	4.4	2.27	2.69	1.11
Rock type	Serpentinite	Serpentinite	Serpentinite	Serpentinite	Serpentinite	Serpentinite	Serpentinite	Serpentinite	Serpentinite
Au(ppb)	98	82	162	44	123	26	68	132	139
As (ppm)	-	-	-	-	-	-	-	-	-
Bi (ppm)	-	-	-	-	-	-	-	-	-
Co (ppm)	179	171	164	152	226	153	179	204	215
Cr (ppm)	-	-	-	-	-	-	-	-	-
Cu(ppm)	1174	1900	1146	598	1492	639	2349	2802	1067
Ni (ppm)	4195	4713	4129	3053	4516	2722	4430	5105	3342
Pd (ppb)	221	302	243	123	328	104	243	287	142
Pt (ppb)	160	215	179	85	192	69	175	240	113
S (ppm)	6983	9278	4073	2896	3023	2638	7074	3821	2421
Sb (ppm)	-	-	-	-	-	-	-	-	-
Te (ppm)	-	-	-	-	-	-	-	-	-
2PGE+Au_ppb	479	599	584	252	643	199	486	659	394
Pt+Pd (pbb)	381	517	422	208	520	173	418	527	255
Total Pd Analyses	**1805**								
Total Pt Analyses	**1800**								
Total PGE Analyses > 80 ppb	**273**								